Dissertation

Continuous Crystallization of Active Pharmaceutical Ingredients via a Tubular Reactor: Simulation and Process Design

to obtain the academic degree of

'Doktor der technischen Wissenschaften'

Graz University of Technology

DI Maximilian Besenhard

Graz, 2014

Institute of Process and Particle Engineering

Graz University of Technology

Graz, Austria

Research Center Pharmaceutical Engineering GmbH

Graz, Austria

Maximilian Besenhard

Continuous Crystallization of Active Pharmaceutical Ingredients via a Tubular Reactor: Simulation and Process Design

Dissertation

First assessor

Univ.-Prof. Dr. Johannes G. Khinast

Institute for Process and Particle Engineering

Graz University of Technology, and

Research Center Pharmaceutical Engineering GmbH

Second assessor

Univ.-Prof. Dr. Robert Schennach

Institute of Solid State Physics

Graz University of Technology, and

CD-Laboratory for surface chemical and physical fundamentals of paper strength

EIDESSTATTLICHE ERKLÄRUNG

AFFIDAVIT

Ich erkläre an Eides statt, dass ich die vorliegende Arbeit selbstständig verfasst, andere als die angegebenen Quellen/Hilfsmittel nicht benutzt, und die den benutzten Quellen wörtlich und inhaltlich entnommenen Stellen als solche kenntlich gemacht habe. Das in TUGRAZonline hochgeladene Textdokument ist mit der vorliegenden Dissertation identisch.

I declare that I have authored this thesis independently, that I have not used other than the declared sources/resources, and that I have explicitly indicated all material which has been quoted either literally or by content from the sources used. The text document uploaded to TUGRAZonline is identical to the present doctoral dissertation.

25.10.2014

Datum / Date

Unterschrift / Signature

Abstract

The scope of this thesis is the development and investigation of tubular reactor designs for continuous crystallization and coating applications. The entire experimental part of this thesis was executed in tubular reactor designs utilizing silicon tubing of $10 - 20\,m$ in length with an inner diameter of $2\,mm$. Beside the experimental process development, the thesis focuses on the mathematical modeling of crystallization processes. A detailed mathematical process model based on population balance equations was developed and validated in order to understand the temporal behavior of the crystal size distribution as it is dependent on all process settings. The proof of concept for continuous coating from solution in such a tubular reactor was demonstrated via an enteric coating application by means of coacervation. The latter provides an opportunity to simultaneously execute both crystallization and a subsequent coating process within the same tubular reactor. Furthermore a feedback control strategy is presented with the goal of tuning and maintaining the mean crystal size during the crystallization process. The realization of a feedback controller became feasible due to the implementation of an online crystal size distribution analyzer and a model free control strategy developed from the results of minor initial experimental studies. This simple control strategy was only possible due to the process design of the presented tubular crystallizer.

Kurzfassung

Diese Arbeit beschäftigt sich mit der Entwicklung und Untersuchung von Rohrreaktoren für kontinuierliche Kristallisations- und Coatingprozesse. Sämtliche experimentelle Arbeiten welche in dieser Doktorarbeit gezeigt werden beschäftigen sich mit Rohrreaktoren, bestehend aus Silikonschläuchen mit einer Länge von $10 - 20\,\mathrm{m}$ und einem inneren Durchmesser von $2\,\mathrm{mm}$. Neben der experimentellen Prozessentwicklung liegt ein Schwerpunkt dieser Arbeit in der Modellierung von Kristallisationsprozessen.

Ein detailliertes mathematisches Prozessmodel auf Basis von „Population Balance Equations“ wurde erstellt welches in der Lage ist das Zeitliche Verhalten von Kristallgrößenverteilungen im Rohrreaktor vorherzusagen. Des Weiteren wird die Anwendbarkeit eines Rohrreaktors für kontinuierliche Coatingprozesse gezeigt. Letzeres wird anhand eines enterischen Coatings aus einer Lösung mittels Coacervation demonstriert. Da gezeigt wurde, dass sowohl Kristallisationsprozesse als auch Coatingprozesse in zwei nahezu baugleichen Reaktoren durchgeführt werden beweist diese Arbeit, dass es möglich ist jene zwei Prozesse in einem Rohrreaktor zu kombinieren. Desweiteren stellt diese Arbeit eine Rückkoppelungsregelung (engl. feedback control) vor, welche es ermöglicht, die mittlere Kristallgröße der im Rohrreaktor erzeugten Kristalle genau zu einzustellen. Diese wurde durch die Implementierung eines Kristallgrößenmessgerätes ermöglicht, welches in der Lage ist die Kristallgrößenverteilung während der gesamten Prozessdauer zu messen. Die Regelung selber erfolgte durch eine „Model freie“ Methode welche einzig und alleine die Resultate ein paar weniger Vorversuche benötigte. Dieses einfache Konzept der Kristallgrößensteuerung wurde nur auf Grund der einfachen aber genauen Prozessführung im Rohrreaktor möglich.

.

Acknowledgement

I am beyond grateful for the scientific supervision of Prof. Johannes Khinast throughout my thesis and my employment at the Research Center of Pharmaceutical Engineering. Our discussions provided valuable insights into and motivation for overcoming even the most challenging obstacles. The perfectly equipped laboratories of our Center facilitated experimental studies that would not have been possible to execute elsewhere. This advantage, as well as constant support from my colleagues and all the master's students I was allowed to supervise, enabled me to work on cutting edge technologies over the past few years.

Furthermore I would like to thank my entire family and my wonderful girlfriend Silvia for their support during the last years.

Contents

List of Abbreviations

Abbreviation	*Meaning*
API	**Active Pharmaceutical Ingredient**
CSSD	**Crystal Size and Shape Distribution**
CSD	**Crystal Size Distribution**
QA	**Quality Attributes**
CQA	**Critical Quality Attributes**
QbT	**Quality by Testing**
FDA	**Food and Drug Administration**
PAT	**Process Analytical Technology**
ATR	**Attenuated Total Reflection**
FTIR	**Fourier Transformation Infrared**
PVM	**Particle Vision and Measurement**
MSMPR	**Mixed Product Suspension Mixed Product Removal**
PBE	**Population Balance Equations**
OBC	**Oscillatory Baffled Crystallizer**

1. Introduction

1.1 Motivation

Crystallization processes have a long history in the food, chemical and pharmaceutical industries. What these industries have in common is a need for highly purified solid organic particles. A common unit operation for the purification of solid particles via phase separation is crystallization from solution. Not least since solution crystallization features an efficient process with relatively low capital and operating costs [1][2]. Its importance for the pharmaceutical industry is apparent since more than 90 percent of all pharmaceutical products contain Active Pharmaceutical Ingredients (API) in a crystalline form [3].

Almost 70 percent of new APIs being pursued are poorly soluble in water [4]. The dissolution and disintegration rates and consequently the bioavailability in the body[5][6], particularly for low-solubility APIs, depend strongly on physical properties like the size and shape of the crystals. The crystal size and shape distribution (CSSD) determines the interfacial surface area and therefore affects the dissolution rate. Different crystal structures of the same molecule (= polymorphs) can exhibit different solubilities [7][8]. While one polymorph dissolves in the digestive system, others might not, which would hamper the therapeutic effect of a drug. All of these physiochemical properties, i.e., crystal sizes, shapes, and solid forms, can and must be controlled via the final API crystallization step [3]. Furthermore, the CSSD affects a powder's flowability [9], segregation phenomena [10][11] and downstream operations like filtration [12], blending [13], capsule filling [14], tabletting [15] and therefore the entire manufacturing process. In this context, the field of "crystal engineering" is increasingly receiving attention and the crystallization process plays a key role in defining the physiochemical properties of solid APIs and their final dosage forms [16].

Traditionally, pharmaceutical manufacturing has always been dominated by batch processing not least because of the regulatory bodies. Nevertheless, regulatory authorities started to support the development and implementation of innovative processing technologies, including continuous manufacturing [17][18]. Within the last decade, significant efforts towards continuous manufacturing have been initiated by universities as well as by pharmaceutical companies in order to replace the pharmaceutical industry's conventional batch systems by continuous manufacturing processes [19]. The most prominent example

is the Novartis-MIT center for continuous manufacturing started in 2007 with a $65 million grant for the development of continuous processes for pharmaceutical manufacturing

Because of its complexity, continuous crystallization is considered one of the bottlenecks towards achieving a fully continuous production of solid dosage forms. The challenge in the design of batch and continuous crystallization processes is to avoid heterogeneities in temperature and concentrations profiles (i.e., inhomogeneous mixing) as well as fluctuating flow patterns, broad residence time distributions, a slow response to changes in the boundary conditions; most importantly, the design should allow for the straightforward control of supersaturation levels. Tubular reactor designs can be used to overcome these obstacles and can serve as a suitable and cost-effective tool for continuous crystallization and further downstream processes as demonstrated within this thesis. Although crystallization has often been viewed more as an art than a science, a systematic approach produces results when art fails [1].

1.2 Solution crystallization

Solution crystallization is based on the phase transition of molecules in a solution into a solid state and is characterized by a well-defined structure dictated by forces acting at the molecular level. This well-defined crystalline structure facilitates impurity rejection from the solid product, making crystallization a highly effective purification process. The driving force for the phase transition is the difference in Gibbs free energy ($\Delta G\ [J]$) between the dissolved and solid state of the molecule (or generally speaking the building blocks of the crystalline material). Below a well-defined temperature, i.e. the melting point, the crystalline structure becomes thermodynamically favored over the dissolved state ($G_{crystal} < G_{dissolved}$). This is because the increased enthalpy ($\Delta H\ [J]$) of the crystalline state overcomes the accompanied reduction in entropy ($\Delta S\ [J/K]$) due to the molecular ordering.

$$\Delta G = \Delta H - T \cdot \Delta S \tag{1}$$

By heating a crystalline material slightly above its melting point, the solid crystalline state collapses. However, cooling below its melting point does not have to be sufficient to form the solid phase again. The latter demonstrates why crystallization processes are not exclusively governed by laws describing the thermodynamic equilibrium. In fact, the final critical quality attributes (CQA) of the product crystals like purity, crystal structures or CSSD, depend strongly on the process kinetics.

In the absence of crystalline material, i.e. all molecules are dissolved, crystallization is initiated by nucleation. Nucleation describes the initial generation of the solid phase, i.e., the formation of "small" solid crystals. The occurrence of nucleation without the involvement of foreign materials (impurities, reactor walls, etc.) is called "homogeneous nucleation" or "primary nucleation". The formation of nuclei facilitated due to the presence of already-formed crystalline material is referred to as secondary nucleation [1][19]. Heterogeneous nucleation describes the nucleation that is catalyzed by interfaces or surfaces other than the crystalline material.

Nucleation is followed by the growth of the generated nuclei to macroscopic dimensions, which is called "crystal growth" [21]. The driving force of nucleation as well as crystal growth is supersaturation. The level of supersaturation quantifies the difference between the thermodynamic equilibrium solubility of the molecules in the solvent and their actual concentration. With regard to solution crystallization, supersaturation can be achieved and controlled via several strategies depending on the chemical and physical properties of the solvent and the material to be crystallized. The most commonly used strategies are:

- Solvent evaporation [19][21]
- Cooling [23][24]
- Antisolvent addition [24][25]
- Chemical reaction (reaction products exceed solubility) [27][28]

Nucleation itself is a stochastic process and therefore barely controllable, which is why crystallization processes are commonly designed to avoid, or at least minimize, further nucleation events after initial nuclei are formed or seed crystals are added. For that reason, supersaturation needs to be restricted to the metastable zone. The latter describes the process domain which is indeed supersaturated but not sufficiently to provoke nucleation. Figure 1 presents the concept for a cooling crystallization process from solution.

With regard to a cooling crystallization, the ideal cooling rate depends not only on current temperatures or concentrations, but also on the properties of the already formed crystalline material. This is because the crystal growth rate and the current amount of the crystalline phase define the maximum crystallization rate, i.e. the gain in crystalline material per time. Hence, the future behavior of a crystallization process depends always on its history. This explains what makes crystallization a challenging unit operation, particularly from a control perspective.

In summary, the road to solid crystalline products from a solution starts with supersaturation generation, subsequent nucleation (if not seeded), crystal growth and stabilization (if necessary), which is then followed by filtration and drying.

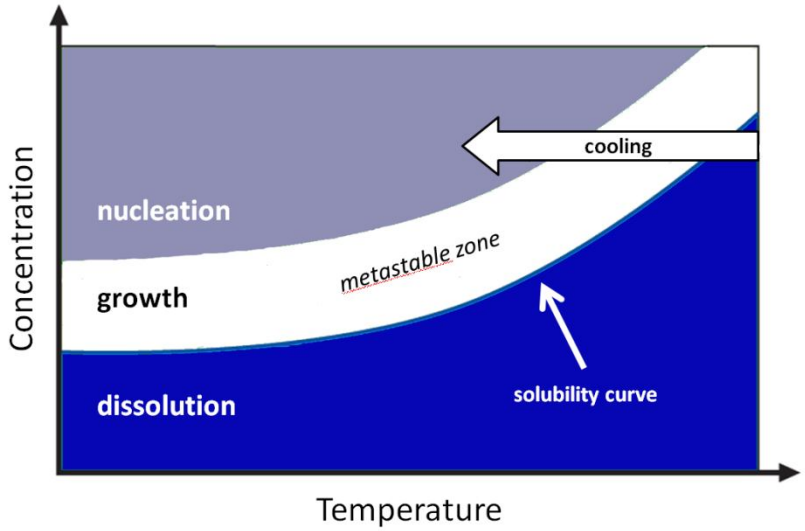

Figure 1: Concept of the metastable zone for solution crystallization via cooling

1.3 Solid forms of APIs

The solid form of the API is a CQA of crystalline pharmaceuticals. APIs can be present in several solid forms of a crystalline structure, including polymorphs, solvates (e.g. hydrates), salts and co-crystals. Furthermore, they can be present in an amorphous form characterized by a disordered arrangement of molecules that lacks a three-dimensional long range order [9][29]. Because of their physiochemical instability relative to corresponding crystals accompanied by higher solubilities, amorphous pharmaceuticals have always been an essential part of research [30]. An overview of the above-mentioned solid forms is presented in figure 2.

During the selection of the most suitable solid form of the API for drug development, its most thermodynamically stable form is generally desired [31]. However, the most stable crystal form might have insufficient solubility resulting in a poor bioavailability of the drug product. In that case, alternative solid forms may be of interest. The formation of a salt by means of pharmaceutically accepted acids or bases is a universal approach to optimizing the physiochemical properties of ionizable compounds [32][33].

In the recent years, co-crystals have become of great interest in pharmaceutical research. The difference between co-crystals and salts is the interaction mechanisms in the crystal lattice. In a salt, the proton transfer can be seen as completed (ionic bonding) whereas there is no proton transfer in the case of co-crystals [34][35]. It should be noted that there is no unique definition of co-crystals and some definitions even include solvates. A restrictive definition is presented by Aakeröy and Salmon [36]: *Co-crystals are structurally homogeneous crystalline materials containing two or more components present in definite stoichiometric amounts. The co-crystals components are discrete neutral molecular reactants which are solids at ambient temperature*. In addition to possible improvement of solubility (accompanied with bioavailability) and stability, co-crystals have the potential to improve a variety of essential properties, including hygroscopicity, compressability and flowability [9][37].

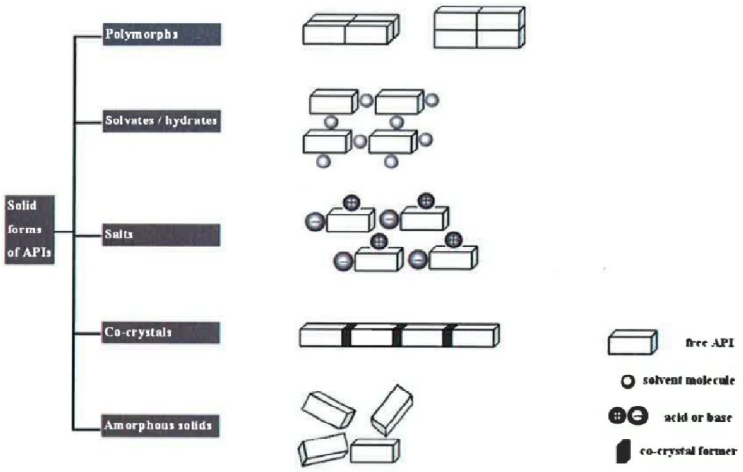

Figure 2: Schematic representation of the structure of solid forms of APIs. Modified from: J. Lu and S. Rohani, "Polymorphism and crystallization of active pharmaceutical ingredients (APIs).," Curr. Med. Chem., vol. 16, no. 7, pp. 884–905, Jan. 2009.

As opposed to salts and co-crystals, polymorphs are characterized by identical chemical compositions. Polymorphism describes the phenomenon whereby molecules can crystallize into numerous crystal structures. Hence, polymorphs are different crystalline forms of the same pure substance in which the molecules have different arrangements. Polymorphs have different physiochemical properties resulting in different stability and bioavailability of drug products [16]. By virtue of these different physiochemical properties, polymorphs are highly crucial for drug manufacturing processes. A prominent example of how the occurrence of a "new" polymorphic form can affect the CQA of pharmaceutics is Ritonavir (Novir®, Abbot Laboratories) [38]. It had to be launched in a second formulation

since a more thermodynamically stable polymorph was discovered that exhibited a much lower solubility in the initial formulation.

More than 50 % of API compounds are reported to be polymorphic [7] which highlights the importance of polymorphism control during crystallization processes. A solid form screening for polymorphs of drug substances is essential and is initially carried out at the drug discovery-development interface [39]. It is of great importance to understand the polymorphic behavior of a drug and to judiciously select the optimal solid form for development [7]. The appearance of polymorphisms depends on the solute concentrations, temperatures, flows rates, and especially, the solvent. Based on the crystallization medium, a metastable polymorph might be generated first if its activation barrier (defining the onset of nucleation) is lower, as shown in figure 3. Figure 3 presents a schematic diagram of Gibbs free energy during the phase transition of the dissolved molecule into the two different crystalline forms. Following Ostwald's rule of stages, a metastable polymorph can be transformed into the most stable form at the end. It can be solvent-mediated, meaning that is likely to happen during solution crystallization processes.

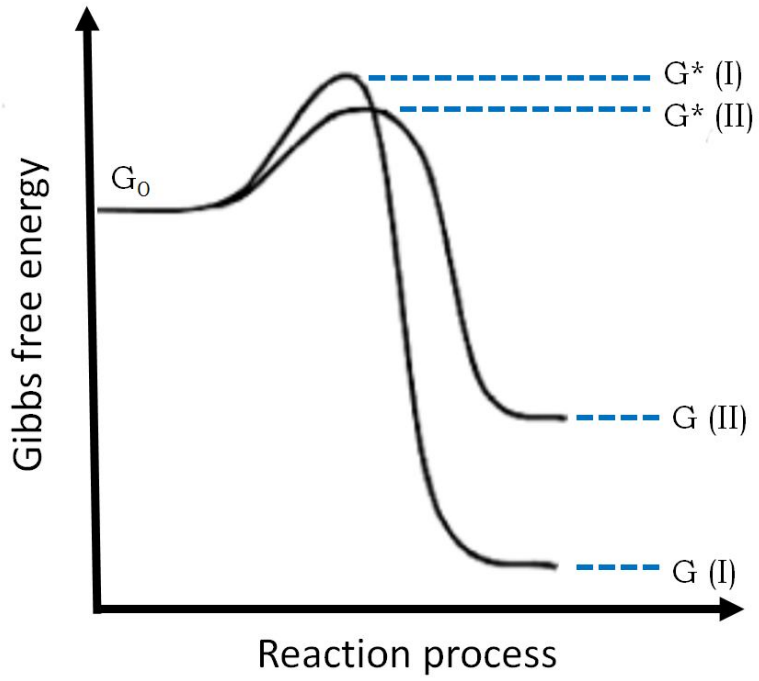

Figure 3: Schematic diagram of Gibbs free energy during the phase transition, showing the activation barriers (*) for the formation of two polymorphic forms (I) and (II)

Crystalline solids that involve the inclusion or incorporation of solvent molecules in the crystal lattice are known as solvates (or hydrates if the solvent is water) [7][40]. The crys-

tal lattice of solvates exhibits a different unit cell compared to the anhydrate form, i.e., the parent compound. This is why the physiochemical properties of solvates may also differ from their anhydrates, as is the case for polymorphs. Therefore solvates/hydrates are also referred to as “pseudo polymorphs” [16], although they are strictly molecular adducts [40]. Special care has to be taken during downstream processes of solvates, since they are likely to undergo phase transitions into other crystal structures (e.g. their anhydrates) or amorphization [41][42]. Nevertheless, several well known drug products containing the API in a hydrate form are available on the market (e.g. Fosamax, Amoxil, Lipitor) [7].

1.4 PAT for crystallization processes

As is common in pharmaceutical manufacturing, crystallization has traditionally been a recipe-bases operation. This means that the crystallization process is controlled such that the trajectories follow the specifications submitted for regular filings [43]. The quality of the product is only determined by testing at the end. This quality-by-testing (QbT) approach often leads to failed batches accompanied by a loss of profit for the company [44][43]. The Food and Drug Administration’s (FDA) process analytical technology (PAT) initiative is a collaborative effort with industry to introduce new and efficient manufacturing technologies into the pharmaceutical industry. The aim of PAT is to design, analyze and control the manufacturing process such that erroneous processing can be detected in time to initiate appropriate counteractions if possible. The globally accepted PAT initiative [18][45] defines PAT as “*a system for designing, analyzing, and controlling manufacturing through timely measurements (i.e., during processing) of critical quality and performance attributes of raw and in-process materials and processes, with the goal of ensuring final product quality*“ [17]. According to Yu et al. [46], the tools of PAT can be summarized as:

- Multivariate data acquisition and analysis tools
- Modern process analyzers or process analytical chemistry tools
- Endpoint monitoring and process control tools
- Knowledge management tools

Crystallizations of APIs, particularly of those possessing multiple solid forms, are among the most critical and least understood pharmaceutical manufacturing processes [46]. The selection of analyzers for process control in the PAT framework depends on the CQA of the final products. With respect to solution crystallization processes, the analysis of concentration (or even the supersaturation), CSD, CSSD, the amount of crystalline material and its polymorphic form in real-time are frequently required.

Probably the most accepted technique for accurately determining the concentration of the dissolved species is attenuated total reflection (ATR) Fourier-transformed infrared (FTIR) spectroscopy [47][48]. Fujiwara et al. reported accuracies of $0.00014\ (g\ dissolved/g\ solvent)$ using ATR–FTIR spectroscopy coupled with chemometrics [49]. However, an accuracy of the solution concentration measurement some orders of magnitude lower is typical [46] and depends on the equipment (e.g., infrared spectrometer, the ATR–FTIR probe [47]), solutes and solvents, as well as operator skills [48].

The real time analysis of the CSD or even the CSSD during crystallization processes is highly complex [50][51]. The accuracy and applicability of common CSD analyzers depend on the solutes, solvents, optical properties of the solid phase, the solid mass fraction ($g\ solid/g\ solvent$) and the crystals' shape. Beside the fact that most analyzers record only univariate CSDs (i.e., a single value determining the size is assigned to the three dimensional crystals), the accuracy of CSD measurements may alter significantly during the crystallization process, since the solid mass fraction can change by several orders of magnitude [48]. Focused beam reflectance measurements are very popular for in-situ characterization particularly for slurries with a solid mass fraction. Nevertheless, due to the complicated relationship between chord length distribution, i.e. the signal recorded by the FBRM probe, and the CSD, FBRM data are mostly used for qualitatively monitoring of process [46]; for instance, in detecting the onset of primary nucleation, attrition and agglomeration [52]. Nevertheless, several new sensor concepts have become available in the recent years that hold a lot of promise in overcoming these difficulties. For example, in-situ video camera systems such as the particle vision and measurement (PVM®, Mettler & Toledo) offer the opportunity for real-time monitoring of crystal shapes and sizes during a crystallization process [46].

The real time monitoring of polymorphism is challenging since traditionally-applied techniques like x-ray powder diffraction, differential scanning calorimetry, solid state nuclear magnetic resonance as well as infrared spectroscopy (of dry material) can hardly deliver data during a process. Raman spectroscopy has been successfully used to monitor polymorphic transitions (and solute concentrations) in-situ [53]–[55] and seems to be the most promising technique for real-time data acquisition. However, quantitative polymorph detection remains challenging.

In order to quantify solid mass fraction during a crystallization process, turbidity probes to analyze optical density are frequently applied. Recently, an ultrasonic monitoring technique for crystallization processes was demonstrated to quantify the solid mass fraction together with mean crystal size and the solution's concentration [56] using one device.

1.5 Batch vs. continuous crystallization

On the grounds of tradition and regulatory issues, batch processing is still the prevalent process form in pharmaceutical manufacturing and hence for API crystallization unit operations.

Batch processes provide some significant advantages because of existing process know-how and experience as well as the well-understood process equipment. Furthermore, single batches can be accepted or rejected with respect to quality assurance (QbT approach). Therefore, batch processing remains at times business driven, not the least because of limited time for developing new process structures. Moreover, batch processes with multi-purpose equipment have been shown to be more profitable than a continuous one for high and even for low capacities [57].

Despite this, batch processes have several drawbacks mostly originating from the large reactor vessels required for high production rates. The scale-up from small equipment, as is used during early stage process development, is highly complex and frequently associated with complications. Furthermore, extensive validation is required by regulating authorities when a process needs to be up scaled [17].The design of larger equipment solely based on geometrical similarity is not sufficient [58]–[60]. The bigger the apertures the more prone the process is to inhomogeneous process conditions hindering process control as well as reproducible processes. Additionally, long throughput times, low production rates and output quantities owed to fixed batch sizes are a consequence of batch production. This is why the pharmaceutical industry started to encourage the development and implementation of innovative processing technologies, of which the most important is continuous manufacturing. This trend towards continuous processing is also supported by regulatory bodies [17][18].

Continuous processes are capable of overcoming several of the drawbacks associated with batch processes. Depending on the reactor design used, there might be no need for scale-up, which is probably one of the most persuasive arguments for continuous manufacturing. Besides the costs associated with scale-up, its redundancy greatly reduces the production-to-market time, which yields a tremendous economic advantage since the patent life of a drug starts immediately upon approval. Even small scale continuous systems may be able to produce large quantities since there is no limit in operating time. If this is not sufficient, scale-up can be realized simply by increasing the number of continuous reactors [61]. Continuous processes deal with smaller reaction vessels which results in

more homogeneous process conditions, meaning that they are able to eliminate batch-to-batch variability and facilitate a tight control of process conditions [62]. In addition, continuous processes are commonly characterized by reduced equipment costs.

Prevalent batch reactors are generally not the optimal equipment for continuous processes. In the case of crystallization, continuous operation is frequently realized using the mixed product suspension mixed product removal (MSMPR) concept [63][64]. Examples include the continuously operable draft tube baffle crystallizers, the force induced circulation crystallizer and the Oslo type crystallizer [65]. Although these crystallizers can be operated operate continuously, MSMPR process designs still require relatively large reaction vessels for large-scale products. Besides the already-mentioned disadvantages associated with large reaction vessels, the MSMPR concept yields extremely broad residence time distributions. This inhibits the production of product crystals with a narrow CSD as commonly desired in pharmaceutical manufacturing.

Therefore continuous crystallization processes require new reactor designs as well. One of the most promising design concepts for high-end continuous crystallization processes are tubular crystallizers.

1.5.1 Tubular Crystallizers

Tubular reactors (including micro-reactors) are gaining increasing interest in pharmaceutical research and industry [65][66]. Their capability has been demonstrated for nano- and micro particle generation [61][67]–[71] as well as for chemical synthesis [73]–[79].

Tubular reactors benefit from a high surface-to-volume ratio that facilitates rapid heat exchange, which means that the temperature of the processed medium can be controlled accurately, even for highly endo- or exothermic reactions [80][66]. Tubular reactor designs are capable of overcoming obstacles like inhomogeneous mixing, high shear rates (which may induce nucleation events or attrition) and a slow response to changes in the outer process parameters. Furthermore a steady state (properties like temperature, concentrations etc. vary spatially but not temporally) is reached quickly and residence times can be accurately tuned via the tube length. These are desirable conditions when dealing with temperature-dependent phase separation processes, such as cooling crystallization. Hence, tubular reactors allow for the straightforward control of the super saturation profile.

Although the mean residence time distribution can be adjusted via the tube length, the residence time distribution of tubular reactors operated in the laminar flow regime can be rather broad [81]. Figure 3 shows the temporal fraction of a tracer induced at the inlet, exiting a tubular reactor of $1\ m$ (and three different diameters) and a throughput of $10\ ml/min$. Other issues with tubular crystallizers are pipe plugging which is likely to occur if the crystal diameters are in the order of magnitude of the tubing's diameter and sedimentation (particularly in the laminar flow regime).

Several continuously operable tubular crystallizers have been proposed in recent years. They can be distinguished into seeded [82] or self-seeded [83], laminar [61][84][85][86] or plug flow [87][62] crystallizers. Plug-flow is most likely realized by segmenting the slurry into liquid slugs via the addition of an immiscible fluid [71][83]. Due to the plug-flow behavior, the crystallizers are less prone to clogging and provide narrow residence time distributions [71] With regard to tubular crystallizers, the continuous oscillatory baffled crystallizer (OBC) its particularly worth mentioning. The OBC employs a piston to agitate the crystal slurry in a long pipe with baffles [88][89][90] and has already been demonstrated for industrial scale crystallization processes.

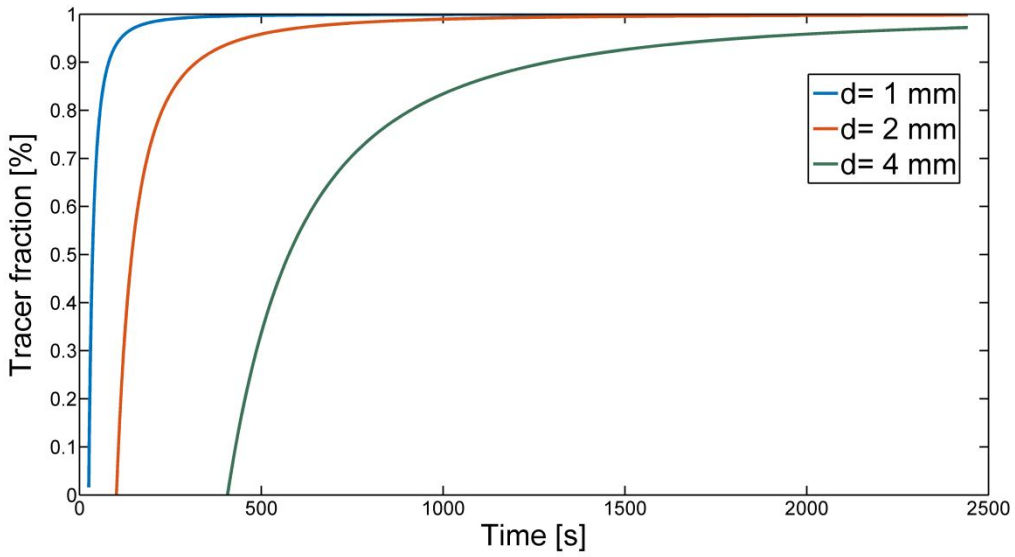

Figure 4: Temporal fraction of a tracer induced at the inlet, exiting a tubular reactor. The reactor length is $1\ m$ *and its throughput is 10 ml/min.*

1.6 Simulation of solution crystallization processes [1]

Crystallization has been studied for more than a hundred years by a broad scientific community. However, the modeling of crystallization processes is still somewhat complicated by the fact that the crystal properties, such as size, shape, morphology, habit or purity, are typically distributed. Nevertheless, many approaches have been reported in the literature [50][91]. Models are frequently used in the design, optimization and scale-up of a crystallization process [12][77]. In addition, the increasing demand for model-based control algorithms requires the development of accurate, yet fast models that can predict the impact of system and processing conditions on the quality attributes of the crystals, such as particle size distribution and shape[78][79]. Moreover, with increasing global competition there has been a demand to implement "optimal" process systems engineering approaches to pharmaceutical manufacturing [62][80]. This also is in line with the Quality by Design approach, introduced by the International Conference on Harmonization (ICH) and increasingly adopted by national or international agencies such as the FDA or EMA.

Owing to the discrete nature of crystals, each crystal being unique in some sense, models that can account for the distribution of properties are required. The ability of population balance equations (PBEs) to capture the discrete and distributed nature of crystals makes their use an appropriate choice for prediction, control and optimization purposes. PBEs date back to the 1970s [81][82][97] and have since become established in many fields of chemical engineering. Hyperbolic partial differential equations describe how the populations of specific properties evolve over time. The generalized PBE for spatially homogenous (well-mixed) processes as previously proposed by [12] can be written as:

$$\frac{\partial}{\partial t} n(x,t) + \frac{\partial}{\partial x}\left(n(x,t) \frac{\partial x}{\partial t} \right) = h(x,t) \tag{2}$$

where n denotes the population of particles, e.g. the number density distribution of property x, at the time t. x is the internal coordinate (typically the size) of interest and its derivative with respect to time defines the growth rate $G = dx/dt$. This means that ndL gives the number of particles per reactor volume with sizes between x and $x + dx$. If x is the

[1] This section is to some extent based on the introduction presented in: **M. O. Besenhard, A. Chaudhury, T. Vetter, R. Ramachandran, and J. G. Khinast**, "Evaluation of Parameter Estimation Methods for Crystallization Processes Modeled via Population Balance Equations," *Chem. Eng. Res. Des.*, Aug. 2014.

size, G is a given function of supersaturation and other physicochemical properties. The right side of Equation 1 comprises the source terms, i.e., describing aggregation, breakage and nucleation. Nucleation can be implemented using a Dirac delta function accounting for the generation of new crystals just at the boundary.

The use of PBEs for the modeling of crystallization processes is well-established in the literature [98]–[100]. Significant work involving 1-D models is attributed to [101]–[104]. Multi-dimensional PBEs involving the implementation of multidimensional equations have also been reported with respect to different length scales [91][92] or volume and surface area as the internal coordinates [93][94]. Various solution techniques have been reported including the method of moments [95][96], method of classes [111], high-resolution algorithms [105] and Monte Carlo techniques [112]. In the modeling of crystallization processes, the PBE is coupled with a mass and energy balance providing information about the level of supersaturation and temperature.

For the aggregation and breakage terms, typically empirical kernels with multiple tunable parameters are used [99][100]. Mechanistic models for defining the kernels are rarely applied. Instead, kernel parameters are optimized to provide the best fit for experimental data. This highlights the need for developing effective parameter estimation (PE) techniques for the accurate representation of crystallization processes via PBEs.

1.7 Thesis content

This thesis deals with the application of tubular reactor designs to pharmaceutical manufacturing of solid dosage forms. The focus of this thesis is on continuous crystallization applications as well as their modeling via PBE. A detailed mathematical process model is presented as well as the application of a feedback controller to tune crystal sizes and the proof of concept of a continuous coating strategy. The entire experimental part was executed in tubular reactor designs using silicon tubing with an inner diameter of 2 mm.

Chapter one introduces basic concepts of solution crystallization, continuous crystallization as well as modeling and control of crystallization processes.

Chapter two describes a mathematical process model based on PBE for the simulation of a solution crystallization process. The model was validated and calibrated via experimental data obtained for several cooling strategies and solution concentrations. Further-

more, the process model was used to identify which settings most affect the mean crystal size and the maximum level of supersaturation during the process.

Chapter three encompasses the proof of concept of continuous coating from solution in tubular reactors, demonstrating enteric coating of API crystals via coacervation. The work presented in chapter three shows that combined crystallization and coating applications are possible with the use of the presented tubular reactors.

Chapter four deals with a feedback control strategy with the goal of tuning and maintaining the mean crystal size during the crystallization process. Feedback control became feasible due to the implementation of an online CSD analyzer and a model-free control strategy based solely on minor initial experimental studies.

1.8 References

[1] D. J. Kirwan and C. J. Orella, *Handbook of Industrial Crystallization*. Elsevier, 2002, pp. 249–266.

[2] J. Ulrich, "Solution Crystallization– Developments and New Trends," *Chem. Eng. Technol.*, vol. 26, no. 8, pp. 832–835, Aug. 2003.

[3] N. Variankaval, A. S. Cote, and M. F. Doherty, "From form to function: Crystallization of active pharmaceutical ingredients," *AIChE J.*, vol. 54, no. 7, pp. 1682–1688, Jul. 2008.

[4] Y. Kawabata, K. Wada, M. Nakatani, S. Yamada, and S. Onoue, "Formulation design for poorly water-soluble drugs based on biopharmaceutics classification system: basic approaches and practical applications.," *Int. J. Pharm.*, vol. 420, no. 1, pp. 1–10, Nov. 2011.

[5] A. Nokhodchi, O. Amire, and M. Jelvehgari, "Physico-mechanical and dissolution behaviours of ibuprofen crystals crystallized in the presence of various additives.," *Daru*, vol. 18, no. 2, pp. 74–83, Jan. 2010.

[6] R. Rowe, P. Sheskey, and S. Owen, *Handbook of pharmaceutical excipients.*, Fifth. London: Pharmaceutical Press, 2006.

[7] A. Y. Lee, D. Erdemir, and A. S. Myerson, "Crystal polymorphism in chemical process development.," *Annu. Rev. Chem. Biomol. Eng.*, vol. 2, pp. 259–80, Jan. 2011.

[8] H. Rolf, *Polymorphism: In the Pharmaceutical Industry*. Wiley-VCH Verlag GmbH & Co. KGaA, 2006.

[9] L. X. Liu, I. Marziano, A. C. Bentham, J. D. Litster, E. T. White, and T. Howes, "Effect of particle properties on the flowability of ibuprofen powders.," *Int. J. Pharm.*, vol. 362, no. 1–2, pp. 109–17, Oct. 2008.

[10] M. Combarros, H. J. Feise, H. Zetzener, and A. Kwade, "Segregation of particulate solids: Experiments and DEM simulations," *Particuology*, vol. 12, pp. 25–32, Feb. 2014.

[11] S. Adam, D. Suzzi, C. Radeke, and J. G. Khinast, "An integrated Quality by Design (QbD) approach towards design space definition of a blending unit operation by Discrete Element Method (DEM) simulation.," *Eur. J. Pharm. Sci.*, vol. 42, no. 1–2, pp. 106–15, Jan. 2011.

[12] R. Wakeman, "The influence of particle properties on filtration," *Sep. Purif. Technol.*, vol. 58, no. 2, pp. 234–241, Dec. 2007.

[13] M. Sen, A. Rogers, R. Singh, A. Chaudhury, J. John, M. G. Ierapetritou, and R. Ramachandran, "Flowsheet optimization of an integrated continuous purification-processing pharmaceutical manufacturing operation," *Chem. Eng. Sci.*, vol. 102, pp. 56–66, Oct. 2013.

[14] E. Faulhammer, M. Llusa, C. Radeke, O. Scheibelhofer, S. Lawrence, S. Biserni, V. Calzolari, and J. G. Khinast, "The effects of material attributes on capsule fill weight and weight variability in dosator nozzle machines.," *Int. J. Pharm.*, vol. 471, no. 1–2, pp. 332–8, Aug. 2014.

[15] S. Mirza, I. Miroshnyk, J. Heinämäki, O. Antikainen, J. Rantanen, P. Vuorela, H. Vuorela, and J. Yliruusi, "Crystal morphology engineering of pharmaceutical solids: tabletting performance enhancement.," *AAPS PharmSciTech*, vol. 10, no. 1, pp. 113–9, Jan. 2009.

[16] J. Lu and S. Rohani, "Polymorphism and crystallization of active pharmaceutical ingredients (APIs).," *Curr. Med. Chem.*, vol. 16, no. 7, pp. 884–905, Jan. 2009.

[17] FDA, "Guidance for Industry: PAT—A Framework for Innovative Pharmaceutical Development, Manufacturing, and Quality Assurance. Pharmaceutical CGMPs," 2004.

[18] International Conference on Harmonization, "Guidance for Industry: Q8(R2) Pharmaceutical Developement." 2004.

[19] J. Markarian, "University Research Centers Transfer Continuous Manufacturing Technology to Industry." Advanstar, 20-Feb-2013.

[20] A. Mersmann, *Crystallization Technology Handbook*, 2nd ed. CRC Press, 2001.

[21] J. A. Kalb, *Phase Change Materials*. Boston, MA: Springer US, 2009.

[22] K. L. Choong and R. Smith, "Novel strategies for optimization of batch, semi-batch and heating/cooling evaporative crystallization," *Chem. Eng. Sci.*, vol. 59, no. 2, pp. 329–343, Jan. 2004.

[23] M. R. A. Bakar, Z. K. Nagy, and C. D. Rielly, "Seeded Batch Cooling Crystallization with Temperature Cycling for the Control of Size Uniformity and Polymorphic Purity of Sulfathiazole Crystals," *Org. Process Res. Dev.*, vol. 13, no. 6, pp. 1343–1356, Nov. 2009.

[24] G. P. Zhang and S. Rohani, "On-line optimal control of a seeded batch cooling crystallizer," *Chem. Eng. Sci.*, vol. 58, no. 9, pp. 1887–1896, May 2003.

[25] N. Nonoyama, K. Hanaki, and Y. Yabuki, "Constant Supersaturation Control of Antisolvent-Addition Batch Crystallization," *Org. Process Res. Dev.*, vol. 10, no. 4, pp. 727–732, Jul. 2006.

[26] D. Duffy, M. Barrett, and B. Glennon, "Novel, Calibration-Free Strategies for Supersaturation Control in Antisolvent Crystallization Processes," *Cryst. Growth Des.*, vol. 13, no. 8, pp. 3321–3332, Aug. 2013.

[27] N. Rodríguez-Hornedo, S. J. Nehm, K. F. Seefeldt, Y. Pagan-Torres, and C. J. Falkiewicz, "Reaction crystallization of pharmaceutical molecular complexes.," *Mol. Pharm.*, vol. 3, no. 3, pp. 362–7, Jan. 2006.

[28] M. Ståhl, B. L. Åslund, and Å. C. Rasmuson, "Reaction crystallization kinetics of benzoic acid," *AIChE J.*, vol. 47, no. 7, pp. 1544–1560, Jul. 2001.

[29] B. C. Hancock and G. Zografi, "Characteristics and significance of the amorphous state in pharmaceutical systems.," *J. Pharm. Sci.*, vol. 86, no. 1, pp. 1–12, Jan. 1997.

[30] L. Yu, "Amorphous pharmaceutical solids: preparation, characterization and stabilization," *Adv. Drug Deliv. Rev.*, vol. 48, no. 1, pp. 27–42, May 2001.

[31] S. R. Byrn, R. R. Pfeiffer, and J. G. Stowell, *Solid-state chemistry of drugs*, 2nd ed. SSCO: West Lafayette, 1999.

[32] C. Saal and A. Becker, "Pharmaceutical salts: a summary on doses of salt formers from the Orange Book.," *Eur. J. Pharm. Sci.*, vol. 49, no. 4, pp. 614–23, Jul. 2013.

[33] D. P. Elder, R. Holm, and H. L. de Diego, "Use of pharmaceutical salts and cocrystals to address the issue of poor solubility.," *Int. J. Pharm.*, vol. 453, no. 1, pp. 88–100, Aug. 2013.

[34] G. P. Stahly, "Diversity in Single- and Multiple-Component Crystals. The Search for and Prevalence of Polymorphs and Cocrystals," *Cryst. Growth Des.*, vol. 7, no. 6, pp. 1007–1026, Jun. 2007.

[35] C. B. Aakeröy, M. E. Fasulo, and J. Desper, "Cocrystal or salt: does it really matter?," *Mol. Pharm.*, vol. 4, no. 3, pp. 317–22, Jan. 2007.

[36] C. B. Aakeröy and D. J. Salmon, "Building co-crystals with molecular sense and supramolecular sensibility," *CrystEngComm*, vol. 7, no. 72, p. 439, Jul. 2005.

[37] A. V Trask, "An overview of pharmaceutical cocrystals as intellectual property.," *Mol. Pharm.*, vol. 4, no. 3, pp. 301–9, Jan. 2007.

[38] J. Bauer, S. Spanton, R. Henry, J. Quick, W. Dziki, W. Porter, and J. Morris, "Ritonavir: An Extraordinary Example of Conformational Polymorphism," *Pharm. Res.*, vol. 18, no. 6, pp. 859–866, Jun. 2001.

[39] M. Palucki, J. D. Higgins, E. Kwong, and A. C. Templeton, "Strategies at the interface of drug discovery and development: early optimization of the solid state phase and preclinical toxicology formulation for potential drug candidates.," *J. Med. Chem.*, vol. 53, no. 16, pp. 5897–905, Aug. 2010.

[40] R. K. Khankari and D. J. W. Grant, "Pharmaceutical hydrates," *Thermochim. Acta*, vol. 248, pp. 61–79, Jan. 1995.

[41] M. P. Feth, N. Nagel, B. Baumgartner, M. Bröckelmann, D. Rigal, B. Otto, M. Spitzenberg, M. Schulz, B. Becker, F. Fischer, and C. Petzoldt, "Challenges in the development of hydrate phases as active pharmaceutical ingredients--an example.," *Eur. J. Pharm. Sci.*, vol. 42, no. 1–2, pp. 116–29, Jan. 2011.

[42] T. Kojima, Y. Yamauchi, S. Onoue, and Y. Tsuda, "Evaluation of hydrate formation of a pharmaceutical solid by using diffuse reflectance infrared Fourier-transform spectroscopy.," *J. Pharm. Biomed. Anal.*, vol. 46, no. 4, pp. 788–91, Mar. 2008.

[43] Z. Q. Yu, J. W. Chew, P. S. Chow, and R. B. H. Tan, "Recent Advances in Crystallization control," *Chem. Eng. Res. Des.*, vol. 85, no. 7, pp. 893–905, Jan. 2007.

[44] A. S. Rathore, "QbD/PAT for bioprocessing: moving from theory to implementation," *Curr. Opin. Chem. Eng.*, vol. 6, pp. 1–8, Nov. 2014.

[45] International Conference on Harmonization, "Guidance for Industry: Q9 Quality Risk Management." 2009.

[46] L. X. Yu, R. A. Lionberger, A. S. Raw, R. D'Costa, H. Wu, and A. S. Hussain, "Applications of process analytical technology to crystallization processes.," *Adv. Drug Deliv. Rev.*, vol. 56, no. 3, pp. 349–69, Feb. 2004.

[47] Z. K. Nagy and R. D. Braatz, "Advances and new directions in crystallization control.," *Annu. Rev. Chem. Biomol. Eng.*, vol. 3, pp. 55–75, Jan. 2012.

[48] M. O. Besenhard, A. Chaudhury, T. Vetter, R. Ramachandran, and J. G. Khinast, "Evaluation of Parameter Estimation Methods for Crystallization Processes Modeled via Population Balance Equations," *Chem. Eng. Res. Des.*, Aug. 2014.

[49] M. Fujiwara, P. S. Chow, D. L. Ma, and R. D. Braatz, "Paracetamol Crystallization Using Laser Backscattering and ATR-FTIR Spectroscopy: Metastability, Agglomeration, and Control," *Cryst. Growth Des.*, vol. 2, no. 5, pp. 363–370, Sep. 2002.

[50] Z. K. Nagy, G. Fevotte, H. Kramer, and L. L. Simon, "Recent advances in the monitoring, modelling and control of crystallization systems," *Chem. Eng. Res. Des.*, vol. 91, no. 10, pp. 1903–1922, Oct. 2013.

[51] N. Gherras, E. Serris, and G. Fevotte, "Monitoring industrial pharmaceutical crystallization processes using acoustic emission in pure and impure media.," *Int. J. Pharm.*, vol. 439, no. 1–2, pp. 109–19, Dec. 2012.

[52] S. H. Chung, D. L. Ma, and R. D. Braatz, "Optimal seeding in batch crystallization," *Can. J. Chem. Eng.*, vol. 77, no. 3, pp. 590–596, Jun. 1999.

[53] E. Simone, A. N. Saleemi, and Z. K. Nagy, "Application of quantitative Raman spectroscopy for the monitoring of polymorphic transformation in crystallization processes using a good calibration practice procedure," *Chem. Eng. Res. Des.*, vol. 92, no. 4, pp. 594–611, Apr. 2014.

[54] H. Qu, H. Alatalo, H. Hatakka, J. Kohonen, M. Louhi-Kultanen, S.-P. Reinikainen, and J. Kallas, "Raman and ATR FTIR spectroscopy in reactive crystallization: Simultaneous monitoring of solute concentration and polymorphic state of the crystals," *J. Cryst. Growth*, vol. 311, no. 13, pp. 3466–3475, Jun. 2009.

[55] G. Févotte, "In Situ Raman Spectroscopy for In-Line Control of Pharmaceutical Crystallization and Solids Elaboration Processes: A Review," *Chem. Eng. Res. Des.*, vol. 85, no. 7, pp. 906–920, Jan. 2007.

[56] T. Stelzer, D. Pertig, and J. Ulrich, "Ultrasonic crystallization monitoring technique for simultaneous in-line measurement of liquid and solid phase," *J. Cryst. Growth*, vol. 362, pp. 71–76, Jan. 2013.

[57] A. Goršek and P. Glavič, "Design of Batch Versus Continuous Processes," *Chem. Eng. Res. Des.*, vol. 75, no. 7, pp. 718–723, 1997.

[58] G. Montante, D. Pinelli, and F. Magelli, "Scale-up criteria for the solids distribution in slurry reactors stirred with multiple impellers," *Chem. Eng. Sci.*, vol. 58, no. 23, pp. 5363–5372, 2003.

[59] H. Leuenberger, "New trends in the production of pharmaceutical granules: batch versus continuous processing," *Eur. J. Pharm. Biopharm.*, vol. 52, no. 3, pp. 289–296, 2001.

[60] G. Klinzing and T. A. Bell, "Challenges in the scale-up of particulate processes—an industrial perspective," *Powder Technol.*, vol. 150, no. 2, pp. 60–71, 2005.

[61] R. J. P. Eder, S. Radl, E. Schmitt, S. Innerhofer, M. Maier, H. Gruber-Woelfler, and J. G. Khinast, "Continuously Seeded, Continuously Operated Tubular Crystallizer for the Production of Active Pharmaceutical Ingredients," *Cryst. Growth Des.*, vol. 10, no. 5, pp. 2247–2257, May 2010.

[62] A. J. Alvarez and A. S. Myerson, "Continuous Plug Flow Crystallization of Pharmaceutical Compounds." American Chemical Society, 01-Mar-2010.

[63] S. Ferguson, F. Ortner, J. Quon, L. Peeva, A. Livingston, B. L. Trout, and A. S. Myerson, "Use of Continuous MSMPR Crystallization with Integrated Nanofiltration Membrane Recycle for Enhanced Yield and Purity in API Crystallization," *Cryst. Growth Des.*, vol. 14, no. 2, pp. 617–627, Feb. 2014.

[64] M. A. Larson, E. T. White, K. A. Ramanarayanan, and K. A. Berglund, "Growth rate dispersion in MSMPR crystallizers," *AIChE J.*, vol. 31, no. 1, pp. 90–94, Jan. 1985.

[65] M. K. Bennett and S. Rohani, "Design of a software application for the simulation and control of continuous and batch crystallizer circuits," *Adv. Eng. Softw.*, vol. 33, no. 6, pp. 365–374, Jun. 2002.

[66] D. M. Roberge, N. Bieler, M. Mathier, M. Eyholzer, B. Zimmermann, P. Barthe, C. Guermeur, O. Lobet, M. Moreno, and P. Woehl, "Development of an Industrial Multi-Injection Microreactor for Fast and Exothermic Reactions - Part II," *Chem. Eng. Technol.*, vol. 31, no. 8, pp. 1155–1161, Aug. 2008.

[67] S. Mascia, P. L. Heider, H. Zhang, R. Lakerveld, B. Benyahia, P. I. Barton, R. D. Braatz, C. L. Cooney, J. M. B. Evans, T. F. Jamison, K. F. Jensen, A. S. Myerson, and B. L. Trout, "End-to-end continuous manufacturing of pharmaceuticals: integrated synthesis, purification, and final dosage formation.," *Angew. Chem. Int. Ed. Engl.*, vol. 52, no. 47, pp. 12359–63, Nov. 2013.

[68] M. Kawase and K. Miura, "Fine particle synthesis by continuous precipitation using a tubular reactor," *Adv. Powder Technol.*, vol. 18, no. 6, pp. 725–738, 2007.

[69] A. K. Yadav, M. J. Barandiaran, and J. C. de la Cal, "Synthesis of water-borne polymer nanoparticles in a continuous microreactor," *Chem. Eng. J.*, vol. 198, pp. 191–200, 2012.

[70] C. Petschacher, A. Eitzlmayr, M. Besenhard, J. Wagner, J. Barthelmes, A. Bernkop-Schnürch, J. G. Khinast, and A. Zimmer, "Thinking continuously: a

microreactor for the production and scale-up of biodegradable, self-assembled nanoparticles," *Polym. Chem.*, vol. 4, no. 7, p. 2342, 2013.

[71] M. Jiang, Z. Zhu, E. Jimenez, C. D. Papageorgiou, J. Waetzig, A. Hardy, M. Langston, and R. D. Braatz, "Continuous-Flow Tubular Crystallization in Slugs Spontaneously Induced by Hydrodynamics," *Cryst. Growth Des.*, vol. 14, no. 2, pp. 851–860, Feb. 2014.

[72] H. W. Kang, J. Leem, S. Y. Yoon, and H. J. Sung, "Continuous synthesis of zinc oxide nanoparticles in a microfluidic system for photovoltaic application.," *Nanoscale*, vol. 6, no. 5, pp. 2840–6, Mar. 2014.

[73] D. Kopetzki, F. Lévesque, and P. H. Seeberger, "A continuous-flow process for the synthesis of artemisinin.," *Chemistry*, vol. 19, no. 17, pp. 5450–6, Apr. 2013.

[74] F. Lévesque and P. H. Seeberger, "Highly efficient continuous flow reactions using singlet oxygen as a 'green' reagent.," *Org. Lett.*, vol. 13, no. 19, pp. 5008–11, Oct. 2011.

[75] B. Wahab, G. Ellames, S. Passey, and P. Watts, "Synthesis of substituted indoles using continuous flow micro reactors," *Tetrahedron*, vol. 66, no. 21, pp. 3861–3865, 2010.

[76] B. Michel and M. F. Greaney, "Continuous-flow synthesis of trimethylsilylphenyl perfluorosulfonate benzyne precursors.," *Org. Lett.*, vol. 16, no. 10, pp. 2684–7, May 2014.

[77] L. Malet-Sanz and F. Susanne, "Continuous flow synthesis. A pharma perspective.," *J. Med. Chem.*, vol. 55, no. 9, pp. 4062–98, May 2012.

[78] Z. He and T. F. Jamison, "Continuous-flow synthesis of functionalized phenols by aerobic oxidation of Grignard reagents.," *Angew. Chem. Int. Ed. Engl.*, vol. 53, no. 13, pp. 3353–7, Mar. 2014.

[79] J. Wu, J. A. Kozak, F. Simeon, T. A. Hatton, and T. F. Jamison, "Mechanism-guided design of flow systems for multicomponent reactions: conversion of CO2 and olefins to cyclic carbonates," *Chem. Sci.*, vol. 5, no. 3, p. 1227, Feb. 2014.

[80] P. Tabeling, *Introduction to Microfluidics*, 2nd ed. Oxford University Press, USA, 2006.

[81] P. V. Danckwerts, "Continuous flow systems," *Chem. Eng. Sci.*, vol. 2, no. 1, pp. 1–13, Feb. 1953.

[82] M. O. Besenhard, A. Hodzic, R. J. P. Eder, and J. G. Khinast, "Modeling a seeded continuous crystallizer for the production of active pharmaceutical ingredients," *Cryst. Res. Technol.*, 2014.

[83] R. J. P. Eder, S. Schrank, M. O. Besenhard, E. Roblegg, H. Gruber-Woelfler, and J. G. Khinast, "Continuous Sonocrystallization of Acetylsalicylic Acid (ASA): Control of Crystal Size," *Cryst. Growth Des.*, vol. 12, no. 10, pp. 4733–4738, Oct. 2012.

[84] O. Prymak, V. Sokolova, T. Peitsch, and M. Epple, "The Crystallization of Fluoroapatite Dumbbells from Supersaturated Aqueous Solution," *Cryst. Growth Des.*, vol. 6, no. 2, pp. 498–506, Feb. 2006.

[85] J. R. Méndez del Río and R. W. Rousseau, "Batch and Tubular-Batch Crystallization of Paracetamol: Crystal Size Distribution and Polymorph Formation," *Cryst. Growth Des.*, vol. 6, no. 6, pp. 1407–1414, Jun. 2006.

[86] S. Ferguson, G. Morris, H. Hao, M. Barrett, and B. Glennon, "In-situ monitoring and characterization of plug flow crystallizers," *Chem. Eng. Sci.*, vol. 77, pp. 105–111, Jul. 2012.

[87] J. Sang-Il Kwon, M. Nayhouse, G. Orkoulas, and P. D. Christofides, "Crystal shape and size control using a plug flow crystallization configuration," *Chem. Eng. Sci.*, vol. 119, pp. 30–39, Nov. 2014.

[88] S. Lawton, G. Steele, P. Shering, L. Zhao, I. Laird, and X.-W. Ni, "Continuous Crystallization of Pharmaceuticals Using a Continuous Oscillatory Baffled Crystallizer," *Org. Process Res. Dev.*, vol. 13, no. 6, pp. 1357–1363, Nov. 2009.

[89] X. Ni and A. Liao, "Effects of mixing, seeding, material of baffles and final temperature on solution crystallization of l-glutamic acid in an oscillatory baffled crystallizer," *Chem. Eng. J.*, vol. 156, no. 1, pp. 226–233, Jan. 2010.

[90] C. J. Brown and X. Ni, "Online Evaluation of Paracetamol Antisolvent Crystallization Growth Rate with Video Imaging in an Oscillatory Baffled Crystallizer," *Cryst. Growth Des.*, vol. 11, no. 3, pp. 719–725, Mar. 2011.

[91] J. Ulrich and M. J. Jones, "Industrial Crystallization," *Chem. Eng. Res. Des.*, vol. 82, no. 12, pp. 1567–1570, Dec. 2004.

[92] G. M. Westhoff and H. J. M. Kramer, "Scale-up of suspension crystallisers using a predictive model framework," *Chem. Eng. Sci.*, vol. 77, pp. 26–34, Jul. 2012.

[93] G. V. Reklaitis, J. Khinast, and F. Muzzio, "Pharmaceutical engineering science—New approaches to pharmaceutical development and manufacturing," *Chem. Eng. Sci.*, vol. 65, no. 21, pp. iv–vii, Nov. 2010.

[94] S. Buchholz, "Future manufacturing approaches in the chemical and pharmaceutical industry," *Chem. Eng. Process. Process Intensif.*, vol. 49, no. 10, pp. 993–995, Oct. 2010.

[95] D. Ramkrishna and J. D. Borwanker, "A puristic analysis of population balance - I," *Chem. Eng. Sci.*, vol. 28, no. 7, pp. 1423–1435, Jul. 1973.

[96] D. Ramkrishna and J. D. Borwanker, "A puristic analysis of population balance—II.," *Chem. Eng. Sci.*, vol. 29, no. 8, pp. 1711–1721, Aug. 1974.

[97] H. M. Hulburt and S. Katz, "Some problems in particle technology," *Chem. Eng. Sci.*, vol. 19, no. 8, pp. 555–574, Aug. 1964.

[98] D. Ramkrishna, *Population Balances: Theory and Applications to Particulate Systems in Engineering*. London: Academic Press, 2000.

[99] D. L. Ma, D. K. Tafti, and R. D. Braatz, "Optimal control and simulation of multidimensional crystallization processes," *Comput. Chem. Eng.*, vol. 26, no. 7–8, pp. 1103–1116, Aug. 2002.

[100] P. Marchal, R. David, J. P. Klein, and J. Villermaux, "Crystallization and precipitation engineering—I. An efficient method for solving population balance in crystallization with agglomeration," *Chem. Eng. Sci.*, vol. 43, no. 1, pp. 59–67, Jan. 1988.

[101] A. Abbas and J. A. Romagnoli, "Multiscale modeling, simulation and validation of batch cooling crystallization," *Sep. Purif. Technol.*, vol. 53, no. 2, pp. 153–163, Feb. 2007.

[102] Z. K. Nagy, J. W. Chew, M. Fujiwara, and R. D. Braatz, "Comparative performance of concentration and temperature controlled batch crystallizations," *J. Process Control*, vol. 18, no. 3–4, pp. 399–407, Mar. 2008.

[103] K. L. Choong and R. Smith, "Optimization of batch cooling crystallization," *Chem. Eng. Sci.*, vol. 59, no. 2, pp. 313–327, Jan. 2004.

[104] C. Lindenberg, M. Krättli, J. Cornel, M. Mazzotti, and J. Brozio, "Design and Optimization of a Combined Cooling/Antisolvent Crystallization Process," *Cryst. Growth Des.*, vol. 9, no. 2, pp. 1124–1136, Feb. 2009.

[105] R. Gunawan, I. Fusman, and R. D. Braatz, "High resolution algorithms for multidimensional population balance equations," *AIChE J.*, vol. 50, no. 11, pp. 2738–2749, Nov. 2004.

[106] M. Oullion, F. Puel, G. Févotte, S. Righini, and P. Carvin, "Industrial batch crystallization of a plate-like organic product. In situ monitoring and 2D-CSD modelling: Part 1: Experimental study," *Chem. Eng. Sci.*, vol. 62, no. 3, pp. 820–832, Feb. 2007.

[107] W. Koch and S. . Friedlander, "The effect of particle coalescence on the surface area of a coagulating aerosol," *J. Colloid Interface Sci.*, vol. 140, no. 2, pp. 419–427, Dec. 1990.

[108] D. E. Rosner, R. McGraw, and P. Tandon, "Multivariate Population Balances via Moment and Monte Carlo Simulation Methods," *Ind. Eng. Chem. Res.*, vol. 42, no. 12, pp. 2699–2711, Jun. 2003.

[109] S. Qamar, S. Noor, and A. Seidel-Morgenstern, "An Efficient Numerical Method for Solving a Model Describing Crystallization of Polymorphs," *Ind. Eng. Chem. Res.*, vol. 49, no. 10, pp. 4940–4947, May 2010.

[110] D. L. Marchisio and R. O. Fox, "Solution of population balance equations using the direct quadrature method of moments," *J. Aerosol Sci.*, vol. 36, no. 1, pp. 43–73, Jan. 2005.

[111] C. B. B. Costa, A. C. da Costa, and R. M. Filho, "Mathematical modeling and optimal control strategy development for an adipic acid crystallization process," *Chem. Eng. Process. Process Intensif.*, vol. 44, no. 7, pp. 737–753, Jul. 2005.

[112] Y. Lin, K. Lee, and T. Matsoukas, "Solution of the population balance equation using constant-number Monte Carlo," *Chem. Eng. Sci.*, vol. 57, no. 12, pp. 2241–2252, Jun. 2002.

[113] M. Vanni, "Approximate Population Balance Equations for Aggregation-Breakage Processes.," *J. Colloid Interface Sci.*, vol. 221, no. 2, pp. 143–160, Jan. 2000.

[114] A. Mersmann, B. Braun, and M. Löffelmann, "Prediction of crystallization coefficients of the population balance," *Chem. Eng. Sci.*, vol. 57, no. 20, pp. 4267–4275, Oct. 2002.

[115] M. O. Besenhard, A. Thurnberger, R. Hohl, E. Faulhammer, J. Rattenberger, and J. G. Khinast, "Continuous API-crystal coating via coacervation in a tubular reactor.," *Int. J. Pharm.*, vol. 475, no. 1–2, pp. 198–207, Aug. 2014.

2. Modeling a Seeded Continuous Crystallizer for the Production of Active Pharmaceutical Ingredients

M. O. Besenhard, R. Hohl, A. Hodzic, R. J. P. Eder, and J. G. Khinast
Cryst. Res. Technol., vol. 49, no. 2–3, pp. 92–108, Mar. 2014

Cryst. Res. Technol. 49, No. 2–3, 92–108 (2014) / DOI 10.1002/crat.201300305

CRYSTAL Research&Technology

Original Paper

Modeling a seeded continuous crystallizer for the production of active pharmaceutical ingredients

M. O. Besenhard[1,2], R. Hohl[1], A. Hodzic[1], R. J. P. Eder[3], and J. G. Khinast[1,3,]*

Received 25 September 2013, revised 23 December 2013, accepted 6 January 2014
Published online 21 February 2014

The approximation of a well mixed reactor is prevalent when it comes to the modeling of a crystallization process. Since temperature, concentration, and mass content vary due to inhomogeneous mixing, this approximation is a very loose one. The continuously operated seeded tubular crystallizer system developed in our group overcomes obstacles like a slow response to changes in the outer parameters and inhomogeneous mixing. Therefore the applicable well mixed assumption facilitates detailed modeling of the crystallization process by means of population balance equations (PBE) coupled with mass and energy balances. Modeled results were validated by means of experiments. The amount of aggregation events during the crystallization could be quantified and it was proven that the growth of seeded crystals is almost exclusively responsible for solid mass uptake if the reactor is operated appropriately. The performed sensitivity analysis exposed which process settings should be maintained most accurately to avoid fluctuations in the product crystals' quality attributes and to limit undesired nucleation events.

1 Introduction

More than 70% of all active pharmaceutical ingredients are small organic molecules, typically delivered in a solid crystalline form [1, 2]. Amorphous solid forms (despite certain advantages, such as higher apparent solubility) are typically avoided due to stability concerns. Thus, separation and purification via crystallization from mother liquor is an essential process in the pharmaceutical manufacturing industry [3, 4]. In this context, crystallization from a solution is a well-established technology with decades of experience gained by process scientists. Nevertheless, purity and polymorphism control are not trivial at times. Aside from crystal purity and polymorphism, the shape and size of the crystals are crucial for the subsequent downstream processes and the final product's quality. The crystal size distribution (CSD) and the shape of the final crystals affect filtration, washing, drying, milling [5], powder flowability and hence feeding, tableting, capsuling and related processes [5]. Also the bioavailability of the final drug depends on the CSD and shape (crystal habit). For example, the dissolution rate varies for different crystal faces [6] and depends not only on the specific surface area [7] but on the crystals' shape. As such, CSD and crystal habit are critical quality parameters in crystallization processes, which must be controlled in order to manufacture products of consistent quality. Most importantly, the polymorphic form of the crystal, which is critically influenced by crystallization conditions, determines the dissolution rate, wettability and stability of a drug crystal and the product. Thus, polymorphism control is one of the most important goals of a robust process design.

Most small-scale crystallization processes in pharmaceutical and fine-chemicals manufacturing are carried out in batch mode. However, significant interest in continuous process design has developed over the last years [1, 3, 8–14]. Continuous crystallization is a complex process and is often viewed as one of the bottlenecks of a fully continuous API production. Reactor designs related to the mixed suspension mixed product removal (MSMPR) ideal crystallizer concept, like the continuously operable draft tube baffle crystallizers, the forced or induced circulation crystallizer and the Oslo type

* Corresponding author: Johannes Khinast; Inffeldgasse 13; A-8010 Graz; Tel.: +43 316 873 30400; Fax: +43 316 873 1030400; E-mail: khinast@tugraz.at www.ippt.tugraz.at
[1] Research Center Pharmaceutical Engineering (RCPE) GmbH, 8010, Graz, Austria
[2] Siemens AG, Corporate Technology, 8054, Graz, Austria
[3] Graz University of Technology, Institute for Process and Particle Engineering, 8010, Graz, Austria

Cryst. Res. Technol. 49, No. 2–3, 92–108 (2014)

CRYSTAL Research&Technology

Original Paper

crystallizer, have been used for continuous crystallization of large-scale products [15].

Generic tubular reactor designs, e.g. the plug flow tubular reactor (PFTR), are frequently applied for the preparation of particles in micro reactors [16, 17]. Also other reactor designs like the continuous oscillatory baffled crystallizers are currently developed [11].

The continuous tubular crystallizer that was developed earlier by us [3, 12] allows continuous crystallization, while tightly controlling the supersaturation profile. Implementation of a segmented flow (i.e., via the introduction of air bubbles) ensures a narrow residence time distributions. However, since the growth kinetics of individual crystals strongly depend on the level of supersaturation, special attention has to be paid to the supersaturation profile (either spatially in the presented design of a PFTR or spatio-temporal in the case of a MSMPR cascade) during the crystallization process. Controlling the supersaturation profile is challenging and thus size, shape and polymorphism control is not a straightforward task. Therefore, the continuous reactor design and control must ensure the ability to monitoring the crystal size and shape distribution (CSSD) and to accurately control the temperature and concentration profiles.

Detailed mathematical models are powerful tools for the design, optimization and model-predictive control of such systems, as they provide information that cannot be obtained experimentally. In this work a model based on population balance equations (PBE) was developed describing the temporal and spatial evolution of the CSD. This process model makes it possible to provide a detailed insight into the process characteristics and may be used for future control applications. In addition, a sensitivity analysis was performed, supporting the optimization of the experimental procedure.

2 Methods and materials

2.1 Reactor design

The reactor design for this study was similar to the one described in previous work [3, 12] of our group. A schematic is given in figure 1. As before, acetylsalicylic acid (ASA) in ethanol (EtOH) was chosen as a model system. The operating principle of the tubular reactor is as follows: A seed suspension of ASA crystals in an ASA-EtOH solution (*Susp*) with temperature T_{susp} was mixed with an undersaturated ASA-EtOH solution (*Sol*) with temperature T_{sol}. The mixing of the suspension and the solution was realized in a Y-fitting. The resulting slurry stream was supersaturated by decreasing the temperature of the tubular crystallizer in consecutive thermostatic baths $T_{Bath\,1} > T_{Bath\,2} > T_{Bath\,3}$ to ensure a relatively constant supersaturation profile. To guarantee a complete dissolution of the starting material, the solution was stored in a stirred vessel at temperatures slightly higher than temperature $T_{sol,\,vessel}$. The solution was tempered to the desired temperature T_{sol} by placing a section of the tubing L_{temp} in an additional thermostatic bath. Thereby also supersaturated solutions can be fed. Two peristaltic pumps (P I and P II), were used to feed the solution and suspension with a flow rate of $\dot{V}_{Sol}$ and $\dot{V}_{Susp}$ into the crystallizer. The residence time of all materials in each thermostatic bath was determined based on flow rates and the respective tube lengths $L_{temp.}$, $L_{Bath\ 1}$, $L_{Bath\ 1}$, and $L_{Bath\ 1}$.To guarantee a constant and identical residence time of each crystal in the tubular reactor and to avoid sedimentation at the bottom of the tubing, the reactor was operated in the slug flow mode. Therefore heated ethanolic air was supplied to the product stream via a third peristaltic pump (P III). Due to the small inner diameter of the tubing, a pronounced slug flow developed. The slug flow concept is shown in figure 2.

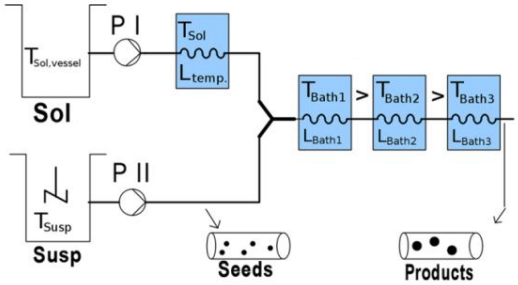

Fig. 1 Schematic drawing of the experimental set up for the continuous cooling crystallization process executed in a tubular reactor.

2.2 Materials

ASA (Rhodine 3020, pharmaceutical grade 100%, monoclinic) was provided by GL-Pharma. EtOH (>96%, ≈3% water, denaturized with 1% metyl ethyl ketone) was purchased from Roth (Lactan). Polysiloxane tubing with an inner diameter (d_{in}) of 2.0 mm and an outer diameter (d_{out}) of 4.0 mm of varying lengths (l) was used in the precooling section of the solutions and the crystallizer (l = 7, 5–27 m). Two peristaltic pumps, P I (Ismatec Reglo MS 2/6V 1.13C; tubing: PHARMED d_{in} = 1.6 mm, d_{out} = 4.8 mm) and P II (Reglo Digital MS-2/6V 1.13C;

CRYSTAL Research & Technology
Original Paper

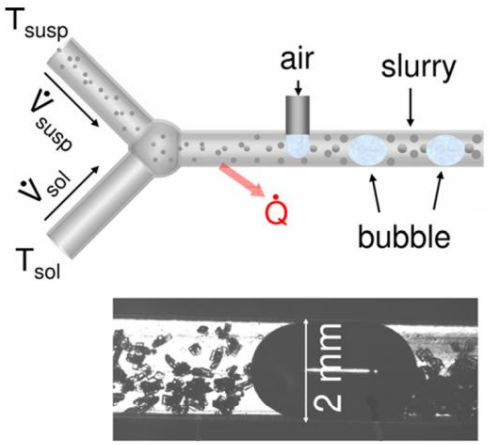

Fig. 2 Principle of the implemented slug (segmented) flow. *Above*: Schematic of the slug-flow system. *Below*: a high-speed camera picture of the slurry in the tubular reactor operated using the slug flow.

tubing: PHARMED din = 2.8 mm, d_{out} = 5.0 mm), were used to pump the solution and the suspension through the tubular crystallizer. The third pump, P III (BVP-Process IP 65 – 3/6; tubing: PHARMED d_{in} = 1.6 mm, d_{out} = 4.8 mm), provided air supply for the segmented flow. The air was saturated with the solvent at room temperature and was obtained from a heated vessel with an ethanol-covered bottom. Straight and Y-fittings (PTFE, d_{in} = 2.0 mm) were used to connect the polysiloxane tubings (straight) to mix the solution with the seed suspension and to introduce air bubbles. Filtration was performed using filter cycles with pore sizes of $>4\mu m$ (Carl Roth–MN 616).

2.3 Particle size measurements and image analysis

Samples were collected via filtration, followed by drying in a vacuum system at approximately 45 mbar for several hours. The solid mass ratio (i.e., the amount of solid material per volume of slurry, denoted as $m_{ASA-solid}$ /V_{slurry} [g/ml] throughout this work), was obtained by the weighing of the dried filter cake, filtered for a specific time, and normalization by the flow rate.

Characterization of the CSD was performed using the QicPic system (Sympatec) and microscope images. The QicPic system is based on an optical method to quantify particle size distribution and shapes. High-speed images of bypassing particles dispersed in the focus of the camera are captured, and the particle size is obtained by evaluating the shadow of each particle. The particle size is then evaluated via the diameter of the equal projected area of a circle (EQPC). As such, obtained particle sizes are valid only for spherical particles, since the applied technique may not yield the same results for particles with the same volume but a different shape [18].

The EQPC evaluation algorithm was adapted to reflect particle shapes that resemble the crystals observed during experiments. Based on our microscope photographs, the shape of each crystal was assumed to be cuboidal (figure 3). Pictures of the crystals were taken with a Leica DM 4000 microscope equipped with a DFC 290 camera.

Under the assumption of a cuboidal shape each crystal has a surface area and volume of

$$A_{cryst} = 2 \cdot L^2 \cdot (k_1 \cdot k_2 + k_1 + k_2) \quad (1)$$

$$V_{cryst} = k_1 \cdot k_2 \cdot L^3 = k_v \cdot L^3 \quad (2)$$

k_v is defined as shown in equation (2), i.e. k_v equals $k_1 \cdot k_2$ [19]. Jennings et al. [20], described that randomly oriented, smooth and convex particles project in average a fourth of their total surface. Therefore, the ECPC values were recalculated by comparing the surface area of the presumed shape to the surface of a circle with a diameter d_{circle}

$$\frac{1}{4} \cdot A_{cryst} \overset{def}{=} A_{circle} = \frac{1}{4} \cdot \pi \cdot d_{circle}^2 \Rightarrow d_{circle} = \sqrt{\frac{2}{\pi}(k_1 \cdot k_2 + k_1 + k_2)} \cdot L \quad (3)$$

Based on microscope images of the crystals grown in the tubular reactor, values of $k_1 = 2/3$ and $k_2 = 1/4$ were selected to best represent the crystals' shape. The particle size determined via the QicPic system was converted into the characteristic length L of a crystal (figure 3) by multiplying the measured particle size by a factor of $\sqrt{(6 \cdot \pi/13)}$. Note that this approach is only applicable if all crystals have the same shape.

For the study of the segmented flow system, pictures were recorded with an IDT-M3 high-speed camera equipped with a 12X objective from Invitar.

2.4 X-Ray analysis

SWAX measurements were performed with a Hecus X-ray System operated in the point focus mode with a Hecus S3-Micropix camera. The micro-beam delivery system operated at 50 kV and 1 mV. The powder samples were placed into a sealed glass capillary (2 mm internal

Cryst. Res. Technol. 49, No. 2–3, 92–108 (2014)

CRYSTAL Research&Technology

Original Paper

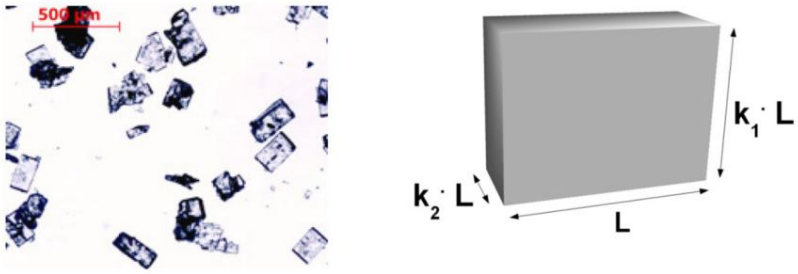

Fig. 3 *Left*: microscope pictures of product crystals (i.e., crystals at the outlet of the reactor); *right:* assumed crystal shape.

diameter), which rotated during the exposure to an X-ray beam with a diameter of 200 μm and a wavelength of $\lambda = 1.54$ Å for 1000 s. Triplicate measurements were performed at room temperature.

2.5 Raman spectroscopy

Raman measurements were performed with a RamanStation 400 F spectrometer (Perkin Elmer, Waltham, Massachusetts) in backscattering mode. The instrument was equipped with a 350 mW near-infrared (785 nm) laser as a source (100 μm diameter) and an echell spectrograph with a cooled (–50 °C) 256 × 1024 CCD detector. The resolution was 2 cm^{-1} from 200 to 3.278 cm^{-1}. The exposure time was 1 s and the number of exposures was 10. For scanning the sample area the mapping mode was chosen: the sample was automatically moved under the laser source to defined positions, and at least one hundred spectra were collected and later averaged such that one sample is represented by one average spectrum. The sample was placed on a brazen sample holder. For data analysis Unscrambler v 10.2 was used (CAMO Software AS, Oslo, Norway).

2.6 Solubility measurement

To prepare saturated solutions the solvent and a sufficiently large amount of ASA (to guarantee the presence of a solid phase) were placed into a flask at various temperatures. The suspension was stirred for approximately 40 minutes at the desired temperature, using a magnetic stirrer that was switched off for at least 30 minutes before taking a sample of the supernatant to measure density. Densitometry was used to determine amount of dissolved ASA using a DSA 5000M densitometer (Anton Paar). Different amounts of ASA were dissolved in EtOH 96%, i.e. the solvent used in this work. To obtain a calibration the density of these solutions was measured at 40 °C. The solubility curve was determined by identifying the concentrations of the dissolved ASA in the saturated solutions.

3 Mathematical process modeling

In this section the process model based on population balance equations is presented, describing the spatiotemporal changes of the CSD. Moreover, the temperature profile in the crystallizer and the rate of mass transfer from the solution to the solid phase are modeled.

3.1 PBE model

PBE modeling is an established method for the description of crystallization processes [21–25], i.e., to describe the temporal change of a population density distribution (i.e., the CSD within this work). However, expressions for particle growth, nucleation, aggregation and breakage must be determined and the kernels used in these expressions may be somewhat empirical. Moreover, the complex fluid dynamics in stirred crystallizers make a simulation of these systems challenging, as a coupling of methods such as computational fluid dynamics (CFD) or Lagrangian particle tracking are required. Nevertheless, current computational capabilities and sophisticated solution techniques for partial differential-integral equations [26, 27] make it possible to couple CFD with PBE [28–30].

A general PBE model for a spatially inhomogeneous process [31] is given by

$$\frac{\partial f(\xi, t, x)}{\partial t} + \frac{\partial (G(\xi, t, x) \cdot f(\xi, t, x))}{\partial \xi} + \frac{\partial (v(\xi, t, x) \cdot f(\xi, t, x))}{\partial x} = B(\xi, t, x) - D(\xi, t, x) \quad (4)$$

CRYSTAL Research & Technology

Original Paper

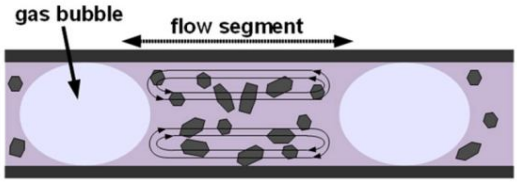

Fig. 4 Schematic of the particle movement in the segmented flow, inducing good mixing and heat exchange in the present work we referred to a single flow segment as a slug.

Here f is the number of particles with the internal coordinate ξ at time t and the spatial coordinates x. In this work f stands for the number density of particles per ml slurry and the characteristic particle length L serves as internal coordinate. G is the crystal growth rate, v is the particle velocity in the tubular crystallizer and B and D are the birth and death terms, describing the change in f due to aggregation and/or breakage or nucleation of particles.

Due to the small size of each slug ($\approx$0.05 cm^3) and the re-circulating flow field (see figure 4) it can be assumed that each flow segment is perfectly mixed. Assuming that no crystals can be transferred from one flow segment to another, each segment can be modeled as a well-mixed crystallizer and all crystals have an identical residence time. Therefore, the third term in equation (4) can be dropped, and the PBE model can be written for a single slug element moving through the tube x_{tube} at a speed of $u_{fs} = \frac{x_{tube}}{t}$, i.e.,

$$\frac{\partial f(L,t)}{\partial t} + \frac{\partial (G(L,t)\cdot f(L,t))}{\partial L} = B(L,t) - D(L,t) \tag{5}$$

Since the linear growth rate $G = \partial L/\partial t$ depends on the temperature T and the concentration of dissolved ASA, the PBE is coupled with material and energy balances (see below).

3.2 Particle growth

The overall growth rate and the final shape of the crystals depend on whether the growth occurs via diffusion or surface integration [6, 22]. In this work we used a semi-empirical expression for G [32], i.e.

$$G = k_{G1}\cdot \exp\left(-\frac{k_{G2}}{R\cdot T}\right)\cdot (c_{ASA}{}^{*} - c_{ASA,diss})^{k_{G3}} \tag{6}$$

Here c_{ASA} is the solubility of ASA and $c_{ASA,diss}$ is the actual concentration of the dissolved ASA in the solvent.

Table 1 Growth rate parameters [22]

Parameter	Value
k_{G1} =	$(3.21 \pm 0.18)\times 10^{-4}\left[\frac{m}{s}\right]$
k_{G2} =	$(2.58 \pm 0.14)\times 10^{-4}\left[\frac{J}{mol}\right]$
k_{G3} =	(1.00 ± 0.01)

The empirical parameters were taken from Lindenberg et al. [22] who performed cooling/antisolvent crystallization experiments with ASA in an ethanol-water mixtures (see Table 1).

3.3 Aggregation

Aggregation of crystals is frequently reported to be a function of the particle size, the level of supersaturation (or the growth rate), the crystals' shape and the local flow field [33–36]. In PBE models, this complex dependence is expressed via an aggregation kernel [37], which describes the likelihood that particles of various sizes collide and aggregate. Only binary aggregation was considered for the present work, determined by a time-invariant aggregation kernel β_{agg}. The terms B(L,t) and D(L,t) accounting for birth and death of particles due to aggregation are defined in equation (5) (see for example Marchisio et al. [27]):

$$B(L,t) = \frac{L^2}{2}\cdot \int_{\lambda=0}^{L} \frac{\beta_{agg}(\lambda, \sqrt[3]{L^3-\lambda^3})\cdot f(\lambda,t)\cdot f(\sqrt[3]{L^3-\lambda^3},t)}{\sqrt[3]{(L^3-\lambda^3)^2}} d\lambda \tag{7}$$

$$D(L,t) = f(L,t)\cdot \int_{\lambda=0}^{L} \beta_{agg}(L,\lambda)\cdot f(\lambda,t) d\lambda \tag{8}$$

β_{agg} is typically reported as the product of the collision frequency and the sticking probability [25, 27, 38, 39]. The former depends only on the flow characteristics and the latter on repulsive and attractive forces between the particles, which are determined by the particle sizes (inertia, etc.) and the conditions in the slurry (level of supersaturation, etc.).

Detailed models based on the DLVO-Theory (named after Derjagin, Landau, Verwey, Overbeek) [40, 41] describing the sticking probability are only applicable to small particles ($<1\ \mu$m) [33] and are commonly used for nano-particles [38, 42]. For larger particles, a general approach involves the flow and particle-size-dependent collision frequency and a phenomenological method for the sticking possibility.

Cryst. Res. Technol. 49, No. 2–3, 92–108 (2014)

CRYSTAL Research&Technology

Original Paper

A large variety of aggregation kernels for crystallization processes exist in literature [25, 32, 34, 43]. In the present work we consider a collision frequency proportional to $\sim(L_1 + L_2)^2$ [34, 44, 45] and to the velocities of the slugs u_{fs} as we assume that higher velocities of the latter promote the collision of particles. The sticking probability is often described to be proportional to the growth rate or a power thereof [34, 36, 46]. Hence, the simple aggregation kernel used this work is

$$\beta_{agg}(L_1, L_2) = C_{agg} \cdot G \cdot u_{fs} \cdot (L_1 + L_2)^2. \tag{9}$$

The linear constant C_{agg} was quantified from the product crystals' CSD as described in the results section.

Throughout this work we do not distinguish between aggregation (week Van-der Waals forces) and agglomeration (stronger solid state necks). Both terms are used diversely in literature.

3.4 Breakage

Experiments were performed, which indicated that breakage-related effects with regard to the CSD seem to be negligible (see below). Therefore, breakage was not considered in the PBE.

3.5 Energy balance equation

The energy balance used to model the temperature trajectory in the crystallizer is similar to the one reported in our previous work [3]. Each flow segment is assumed to have a uniform temperature. However, the temperature changes as the slug passes through the tubular crystallizer. Neglecting the heat of crystallization, the one-dimensional energy balance becomes

$$\frac{\partial T}{\partial x} = \frac{\partial T}{\partial (u_{fs} \cdot t)} = \frac{d_{outer} \cdot \pi}{\dot{m}_{tot} \cdot c_{p,slurry}} \cdot k \cdot (T(u_{fs} \cdot t) - T_{amb}). \tag{10}$$

The heat transfer coefficient k is given by

$$k = \frac{1}{r_{outer} \cdot \left(\frac{1}{r_{inner} \cdot \alpha_{inner}} + \frac{\ln(r_{outer}/r_{inner})}{\lambda_{tubing}} + \frac{1}{r_{outer} \cdot \alpha_{outer}}\right)}. \tag{11}$$

r_{outer} and r_{inner} are the outer and inner diameter of the tubing and λ_{tubing} the thermal heat conductivity of the tubing. Using an expression for the Nusselt number by Qunwu et al. [47] for slugs with a length of 2 cm, the inner heat transfer coefficient can be approximated as follows:

$$\alpha_{inner} = \frac{\lambda_{slurry}}{d_{inner} \cdot Nu} \tag{12}$$

$$Nu = 24.2 + 0.54 \cdot Pe_l^{0.45} \cdot \left(\frac{L_{slug}}{d_{inner}}\right)^{-1.34} \tag{13}$$

Here, Pe_l stands for the thermal Peclet number which is defined as

$$Pe_l = \frac{u_{fs} \cdot c_{p,slurry} \cdot d_{inner} \cdot \varrho_{slurry}}{\lambda_{slurry}}. \tag{14}$$

The used density, heat capacity and conductivity values are listed in Table 2.

Table 2 Model parameters

Parameter	Value	Definition
d_{out}	0.002 [m]	outer diameter of the tubing
d_{in}	0.001 [m]	inner diameter of the tubing
α_{outer}	1494 $\left[\frac{W}{m^2 \cdot K}\right]$	outer heat transfer coefficient of the tubing
λ_{tubing}	0.3 $\left[\frac{W}{m \cdot K}\right]$	heat conductivity of the tubing
λ_{slurry}	0.168 $\left[\frac{W}{m \cdot K}\right]$	heat conductivity of the slurry
ν_{slurry}	1.121 $\left[\frac{10^{-5} m^2}{s}\right]$	kinematic viscosity of the slurry [3]
$c_{p,sat}$	2934 $\left[\frac{J}{g \cdot K}\right]$	heat capacity of the saturated solution at 25°C
$c_{p,ASA}$	1260 $\left[\frac{J}{kg \cdot K}\right]$	heat capacity of ASA
$c_{p,slurry}$	2600 $\left[\frac{J}{kg \cdot K}\right]$	heat capacity of the slurry
M_{ASA}	180.16 $\left[\frac{g}{mol}\right]$	molar mass of ASA

3.6 Mass balance equation

In the present work concentrations are denoted in mol/ml. Changes in the concentration of the dissolved ASA were calculated using the material balance:

$$\frac{\partial c_{ASA.diss}}{\partial t} = \frac{\partial c_{ASA.diss}}{\partial (x/u_{fs})} = -\frac{3}{M_{ASA}} \cdot k_v \cdot G \times \varrho_{ASA} \cdot \int_0^\infty f(L, t) \cdot L^2 \cdot dL \cdot \left(\frac{1}{1 - \epsilon_{solid,0}}\right) \tag{15}$$

$\epsilon_{solid,0}$ is the volume fraction of the slug volume occupied by the solid phase at the initial conditions (i.e., the first Y-fitting). Although the factor on the right is

CRYSTAL Research & Technology

Original Paper

negligible for small seed loadings, it becomes more significant if the solid mass ratio of the seed suspension increases. It accounts for the decrease in the percentage of the solution in the slurry at higher seed loadings. Therefore, the total amount of moles of the dissolved species that can be consumed decreases at a higher seed loading. Equation (15) is derived in the Appendix.

3.7 Conditions after mixing at the first Y-Fitting (initial conditions)

Assuming that solvent and slurry have similar heat capacities, after the first Y-fitting the temperature is:

$$T_{inlet} = \frac{\dot{V}_{susp}}{\dot{V}_{susp} + \dot{V}_{sol}} \cdot T_{susp} + \frac{\dot{V}_{sol}}{\dot{V}_{susp} + \dot{V}_{sol}} \cdot T_{sol}. \quad (16)$$

Similarly, the amount of dissolved ASA in the slurry after the first Y-fitting can be calculated based on the amount of dissolved ASA in the seed suspension and the concentration of the feed solution:

$$c_{ASA.diss\ inlet} = \frac{\dot{V}_{susp}}{\dot{V}_{susp} + \dot{V}_{sol}} \cdot c^*(T_{susp}) + \frac{\dot{V}_{sol}}{\dot{V}_{susp} + \dot{V}_{sol}} \cdot c_{ASA.diss\ sol} \quad (17)$$

It is worth noticing that equation (17) is only valid if the level of supersaturation $S_{inlet} = \frac{c^*(T_{inlet})}{c_{ASA.diss\ inlet}} \geq 1$ because the dissolution of particles is not considered in the process model. The total number of particles of various sizes per volume of the slurry fed into the tubular reactor f(L, 0) was determined based on the solid mass ratio $m_{ASA-solid}/V_{slurry}$ and the seed crystals CSD, obtained as:

$$\left(\frac{m_{ASA-solid}}{V_{slurry}}\right)_{inlet} = \sum_{L=0}^{\infty} f(L, 0) \cdot k_v \cdot L^3 \cdot \varrho_{ASA} \quad (18)$$

3.8 Numerical solution of the process model

Different approaches exist for the solution of PBE models (see Ramkrishna [39], Marchisio et al. [27] and Qamar et. al. [48]). For the present work the "classes method" (CM) [49, 50] was applied. The discretization and the implementation of aggregation for the CM were performed as described in previous studies of our group [38]. The code was mass-conservative, even when using few classes. 300 classes were used for the simulations involving particle growth only. In order to reduce computational time, 150 classes were used when aggregation was considered.

The PBEs (equations 5–9) were solved together with the material balance equation (equation 15) using the MATLAB ode45 solver. The temperature profile was calculated separately via the energy mass balance equation (equations 10–14) and the same solver.

4 Results

4.1 Solubility curve

The results of the density measurements as a function of the ASA mass fraction are shown in figure 5a. The regression curve that fit the experimental calibration values $w_{ASA}(\rho)$ was a straight line determined via the least square fitting. Based on this calibration curve, the density of the saturated solution at various temperatures (figure 5b) was evaluated, as described previously. Because of the almost linear relationship, a linear approximation of the solubility curve was used in the mathematical process model. The measurements are shown together with the solubility curve for ASA in EtOH 99.9% computed via the Nyvlt model [51].

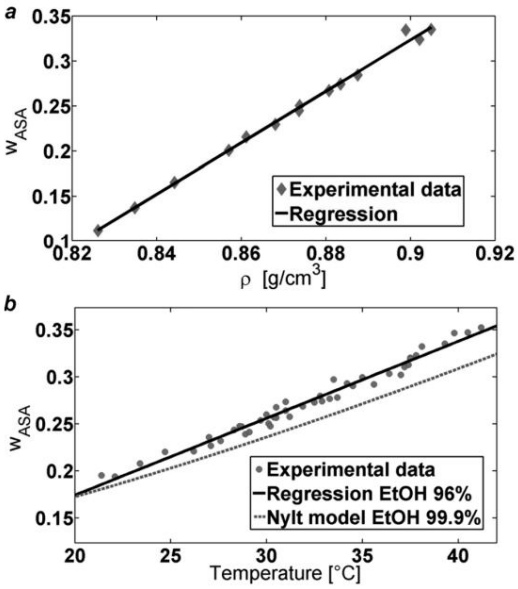

Fig. 5 (a) concentration vs. density calibration curve, (b) solubility curves for EtOH 99.9% and EtOH 96%.

Cryst. Res. Technol. 49, No. 2–3, 92–108 (2014)

CRYSTAL Research&Technology

Original Paper

Table 3 Process parameters used for the breakage experiment (no temperature treatment)

Parameter	Value
$\dot{V}_{susp.}$	40$[\frac{ml}{min}]$
$\dot{V}_{Air}$	15$[\frac{ml}{min}]$
T_{slurry}	22[°C]
$T_{Bath\,1} = T_{Bath\,2} = T_{Bath\,3}$	22[°C]
$L_{Bath\,1} = L_{Bath\,2} = L_{Bath\,3}$	5[m]
$m_{ASA-solid}$ / V_{slurry}	0.3 $[\frac{g}{ml}]$

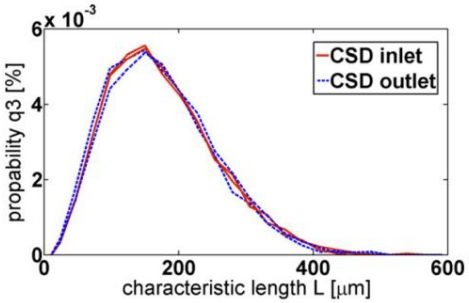

Fig. 6 CSD at the inlet and outlet of the tubular reactor operated using the settings listen in Table 3.

Compared to pure ethanol, the solubility of ASA in water is very low. Nevertheless, EtOH 96% (≈3% water, 1% metyl ethyl ketone) seems to have higher solubility for ASA than EtOH 99.9% which was used for previous studies [3, 12]. This is in agreement with the experimental findings of Lindenberg et al. [22] who showed that ASA's solubility in ethanol-water mixtures increased with alcohol contents at small weight fractions of water (≈0−13%) before decreasing at higher weight fractions.

4.2 Quantification of breakage in the reactor

To investigate the existence of breakage, a suspension with a high solid-mass ratio was pumped through the tubular reactor with a high velocity (high compared to the settings of the crystallization processes, see Table 4). Used tubular reactor settings are listed in Table 3. These settings were selected in order to promote breakage events. As we wanted to exclude aggregation or crystal growth, these experiments were performed without cooling, i.e., no supersaturation occurred.

The experiment was executed twice and the seed and product crystals were sampled at the inlet and outlet of the tubing. The measured CSDs are shown in Figure 6. No difference between the CSDs of the seed and product crystals was observed. Still the generation of small crystals $<4\ \mu$m could not be excluded based on the limited sensitivity of the analyzer.

4.3 Investigation of the CSD and solid mass ratio in the reactor

The tubular crystallizer operates in the slug flow mode, which facilitates sampling at defined residence times due to the inherent narrow residence time distribution. Thus, the local CSD can be accurately determined and its spatio-temporal evolution can be measured. To correlate the CSD and the solid mass ratio sampling was performed as described above. For each experiment the product and seed crystals were sampled twice to determine the CSD and the solid mass ratio as described

Table 4 Experimental settings used for crystallization experiments

Process Parameters:	Settings 1:	Settings 2:	Settings 3:
$T_{sol,\,vessel}$ [°C]	38	38	36
T_{sol} [°C]	35	35	33
T_{susp} [°C]	25	22	22
$\dot{V}_{susp}$ $[\frac{ml}{min}]$	6	6	6
$\dot{V}_{sol}$ $[\frac{ml}{min}]$	25	25	20
$\dot{V}_{Air}$ $[\frac{ml}{min}]$	12	6	6
ASA / EtOH mass $ratio_{susp}$ $[\frac{g}{g}]$	0.30	0.30	0.30
ASA / EtOH mass $ratio_{sol}$ $[\frac{g}{g}]$	0.40	0.45	0.40
$T_{Bath\,1}$ [°C]	30	29	29
$T_{Bath\,2}$ [°C]	25	27	27
$T_{Bath\,3}$ [°C]	22	25	25
$T_{Bath\,4}$ [°C]	-	22	22
L_{temp} [m]	7	7	7
$L_{Bath\,1}$ [m]	5	5	5
$L_{Bath\,2}$ [m]	5	5	5
$L_{Bath\,3}$ [m]	5	5	5
$L_{Bath\,4}$ [m]	-	5	5

CRYSTAL Research & Technology

Original Paper

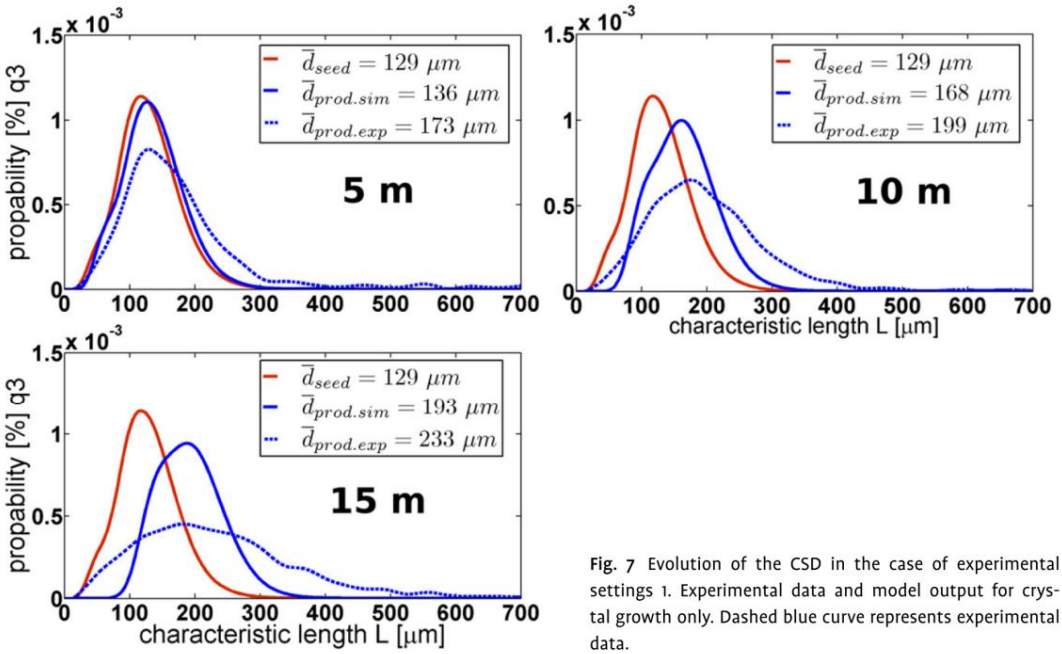

Fig. 7 Evolution of the CSD in the case of experimental settings 1. Experimental data and model output for crystal growth only. Dashed blue curve represents experimental data.

above. As in our previous works [3, 12], the CSDs of the two respective samples were almost identical, proving the reproducibility of the experiments. Thus, the average CSD was used.

For the modeling f(L, 0) was determined from the initial CSD and the solid mass ratio $m_{ASA-solid}/V_{slurry}$ of the seed stream according to equation (18). Experiments were performed using three different settings, listed in Table 4. Note that we always applied settings such that a supersaturation of $S \approx 1$ was achieved at the inlet, according to equations (16) and (17). Avoiding higher levels of supersaturation at the first Y-fitting prevented the tubing from plugging.

In the case of experimental settings 1, the CSD was measured after 5, 10 and 15 m. Figure 7 shows the seed and product CSDs together with the process model output, considering only growth of crystals (i.e., no aggregation). The solid mass ratios determined experimentally and those according to the process model are in acceptable agreement (see Table 5). As can be seen in figure 7, a process model taking into account crystal growth only cannot explain the evolution of the CSD for experimental settings 1. Especially the existence of large crystals (>250 μm) is not predicted with the model results. In order to quantify the influence of aggregation which apparently causes the deviation between the experimental and model results, we used the aggregation model described above. The linear constant in the aggregation kernel C_{agg} (see equation (9)) was determined by matching the volumetric mean diameter of the final product crystals (i.e., after 15 m of tubing). The constant was tuned to obtain the same value for the experimentally determined CSD and the one calculated from the process model taking into account aggregation.

A value of $C_{agg} = 1.4 \times 10^{-11}$ $[1/(particles per ml\ slurry \cdot s)]$ was determined, which implies a decrease in the number of particles of approximately 30%. Figure 8 shows the CSDs obtained by the process model taking into account aggregation. The incorporation of aggregation into the PBE resulted in slight changes of the calculated solid mass ratio as can be seen in Table 5. These variations originate from the effect that aggregation reduces the total surface area of crystals in the slurry and therefore the crystallization rate of dissolved species.

Accounting for aggregation in the process model gives a much better agreement between the modeled and experimental data despite some differences for small crystals (<100 μm). From the comparison of figure 7 and 8 we conclude, that crystals bigger than 250 μm are aggregates rather than crystals which increased their size due to growth only.

Cryst. Res. Technol. 49, No. 2–3, 92–108 (2014)

CRYSTAL Research&Technology

Original Paper

Table 5 Experimentally determined and modeled solid mass ratios

		$\frac{m_{ASA-solid}}{V_{slurry}}\left[\frac{g}{ml}\right]$			
				Model output (growth only)	Model output (growth + aggregation)
Experimental settings 1					
15 m	*seed sample*	0.009			
	prod sample 1	0.046	*average* = 0.050	0.063	0.061
	prod sample 2	0.053			
10 m	*seed sample*	0.010			
	prod sample 1	0.025	*average* = 0.025	0.035	0.034
	prod sample 2	0.024			
5 m	*seed sample*	0.010			
	prod sample 1	0.013	*average* = 0.013	0.013	0.013
	prod sample 2	0.013			
Experimental settings 2					
20 m	*seed sample*	0.008			
	prod sample 1	0.060	*average* = 0.064	0.071	0.067
	prod sample 2	0.068			
Experimental settings 3					
20 m	*seed sample*	0.008			
	prod sample 1	0.071	*average* = 0.066	0.070	0.068
	prod sample 2	0.064			

Sieving of the product crystals was performed for further analysis, to confirm this conclusion. Four size fractions of the product crystals were generated by means of sieving (1: $d_p < 100\ \mu m$; 2: $100 < d_p < 160\ \mu m$; 3: $160 < d_p < 250\ \mu m$; 4: $d_p > 250\ \mu m$). Here the size ranges refer to sieve-mesh widths. Microscope pictures of the sieved crystal fractions are shown in figure 9. The images show that the largest crystals, especially in classes 3 and 4 consist of aggregates, which is in agreement with the model's predictions.

Because of the above mentioned difference between the modeled and measured CSD in the regime of small crystals, X-ray diffraction and Raman spectroscopy were performed to analyze whether the small crystal differ in morphology or composition. X-ray diffraction patterns were recorded for the smallest particles of class 1 ($<160\ \mu m$ and larger ones of class 3 (160–250 μm). Since the spectra show no differences in the reflection pattern, we conclude that all product crystals have the same crystal lattice. Both samples revealed the characteristic pattern of pure ASA [52]. Other stable polymorphs of ASA are only reported for pressures and temperatures that exceed the conditions occurring in the presented experiments [53]. Raman spectra were recorded to investigate if the chemical composition of the crystals varied between the sieved samples. Since the Raman spectra reveal no difference between the sieved samples, which all exhibit the characteristics of pure ASA [54], we conclude that the small and large product crystals have the identical chemical composition. The X-ray diffraction patterns and the Raman spectra are shown in the Appendix (figure A1). In order to prove that aggregates are already present in the crystallizer and not formed during the filtration step, the process was monitored (using experimental settings 1) with a high-speed camera (see figure 10). Recorded pictures demonstrated the occurrence of aggregates ($> 250\ \mu m$) within the tubular reactor.

In the case of experiments executed using experimental settings 2 and 3, the CSD and the solid mass ratio were analyzed at the reactor's inlet (seeds) and outlet after

CRYSTAL Research & Technology

Original Paper

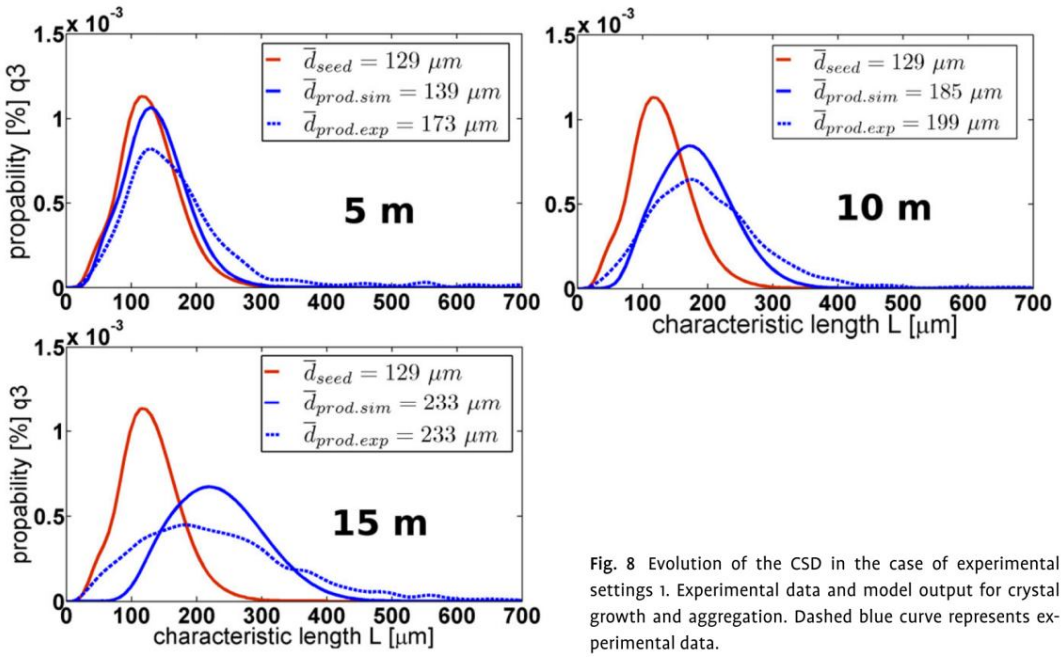

Fig. 8 Evolution of the CSD in the case of experimental settings 1. Experimental data and model output for crystal growth and aggregation. Dashed blue curve represents experimental data.

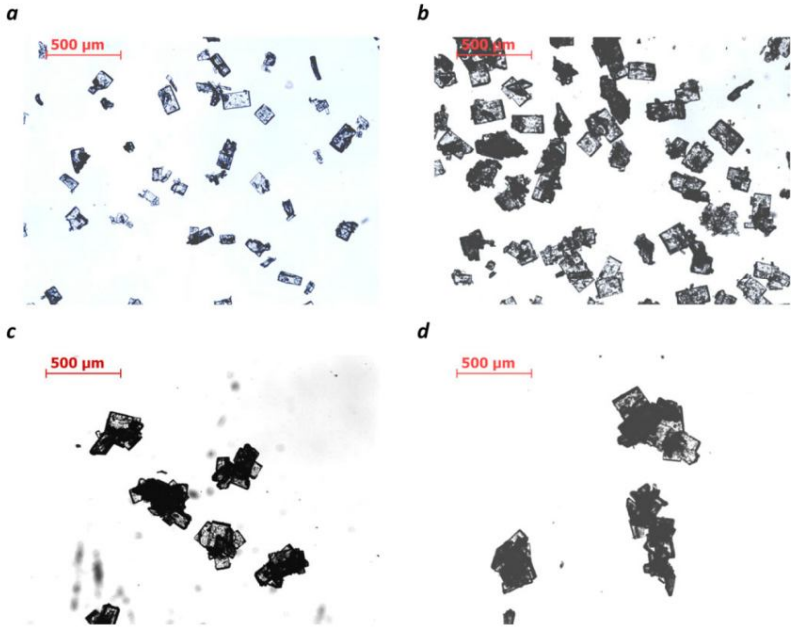

Fig. 9 Microscope pictures of the product crystals after sieving. a: Class 1 $<100\ \mu$m; b: Class 2 with $100 < d_p < 160\ \mu$m; c: Class 3 with $160 < d_p < 250\ \mu$m; and d: Class 4 with $d_p > 250\ \mu$m.

Cryst. Res. Technol. 49, No. 2–3, 92–108 (2014)

CRYSTAL Research&Technology

Original Paper

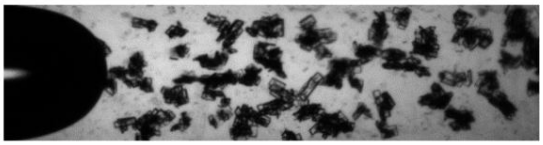

Fig. 10 High-speed camera image recorded during a crystallization process in the tubular reactor close to the outlet, using the experimental settings 1. Evidently aggregated crystals are already present in the reactor.

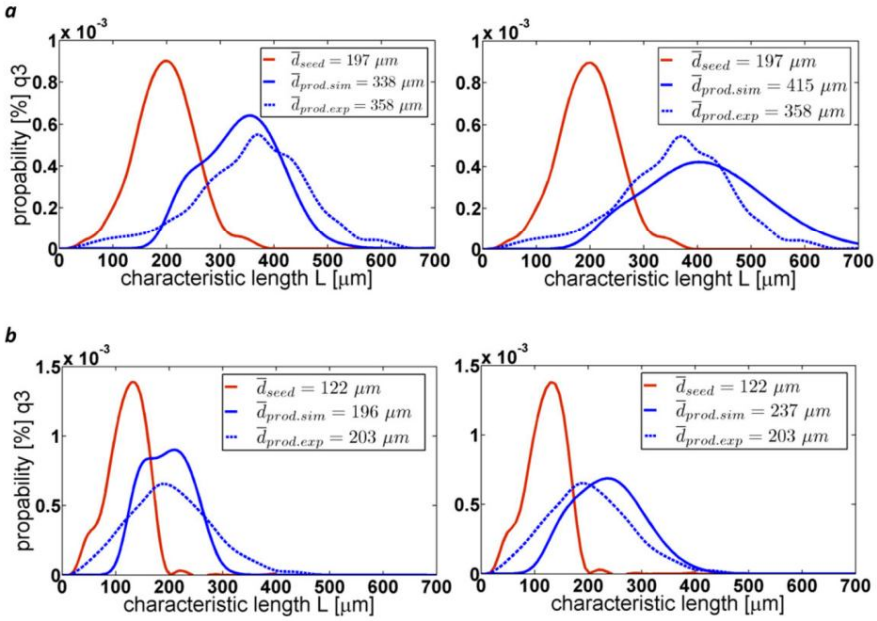

Fig. 11 Evolution of the CSD in the case of experimental settings 2(*a*) and 3(*b*). Experimental data and model output for crystal growth only (left) and including aggregation (*right*).

20 m (product crystals) only. In figure 11 we compare the experimentally determined product CSDs to those computed by means of the process model covering growth only and that covering growth and aggregation for these settings. The same C_{agg} was used in the aggregation kernel as estimated from experimental settings 1, as described above.

For the experimental settings 2 (figure 11a) the CSD computed from the process model considering aggregation still seems to match the experimental data slightly better than the one calculated from the growth only model. In the case of experimental settings 3, the experimental data are represented most adequately by the growth only model (figure 11b *left*). Hence the "growth only" assumption is appropriate in the case of these settings, although minor aggregation cannot be excluded. Apparently, the aggregation model used is not able to account for varying process settings. However, to the best of our knowledge an accurate PBE crystallizer model including aggregation for a broad range of experimental settings has not been reported so far.

The solid mass ratios determined experimentally and according to the process model, listed in Table 5, are in acceptable agreement. The residence time in the tubular reactor and therefore the cooling rate of the slurry, increases with the overall tube length $L_{Bath\,1} + L_{Bath\,2} + L_{Bath\,3} + L_{Bath\,4}$ and decreases with the total flow rate $\dot{V}_{susp} + \dot{V}_{sol} + \dot{V}_{Air}$. Hence, the slurry is cooled at a lower rate using experimental settings 2 than in the case of experiments executed by means of experimental settings 1. Experimental settings 3 yield the slowest cooling. The concentration of ASA in the feed solution ASA/EtOH mass ratio sol. was also lowest in the case of experimental settings 3. On that account,

CRYSTAL Research & Technology
Original Paper

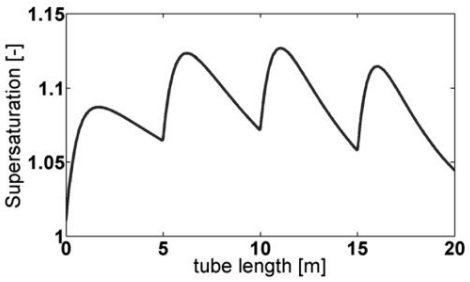

Fig. 12 Computed supersaturation profile using experimental settings 3. The profile exhibits that these settings prevent high supersaturation levels, although cooling was performed in four discrete steps.

experimental settings 3 should provide the lowest level of supersaturation throughout the process. This is in agreement with simulation results; the computed maximum levels of supersaturation during the crystallization process are $S_{max} = 1.28$ using experimental settings 1, $S_{max} = 1.19$ for settings 2 and $S_{max} = 1.14$ for settings 3. The supersaturation profile calculated by the process model (growth only) for experimental settings 3 is shown in figure 12.

The effect of supersaturation on aggregation has already been described above. Therefore, one would expect that product crystals produced with a lower level of supersaturation show less aggregation. This is in agreement with results of the process model and microscope images of (non-sieved) seed and product crystals for experimental settings 1 and 3, as shown in figure 13.

4.4 Sensitivity analysis

In this section the impact of the variation of the model process parameters on the product crystal's mean diameter and the maximum level of supersaturation are presented for experimental settings 3 with the growth only model. Specifically, the process was studied varying the (1) initial mass loadings ASA_{solid}/ml_{slurry} (i.e., the solid mass ratio of seeded crystals), (2–3) flow rates $\dot{V}_{susp.}$&$\dot{V}_{sol.}$, (4) the concentration of the feed solution ASA/EtOH mass ratio insolution and (5–6) seed suspension and feed solution temperatures T_{susp} and T_{sol} by ±10%. Note that the effects of the changes in T_{susp} and T_{sol}, as well as ASA/EtOH mass ratio insolution could only be tested in the case of lower temperatures ($-10 \rightarrow 0\%$) and higher concentrations($0 \rightarrow +10\%$), since variations in the opposite direction would have led to initial levels of supersaturation at the reactors inlet lower than one. In this case the developed process model is invalid, since it does not account for dissolution of the crystals. The results of the sensitivity analysis are shown in figure 14.

The sensitivity analysis showed that the product crystal size and the maximum level of supersaturation are highly sensitive with respect to the ASA concentration dissolved in the feed solution and the initial mass loading. Lower initial temperatures of the seed suspension have almost no impact on the maximum level of supersaturation but a rather strong impact on the product crystal size. The latter results from the minor amount of ASA dissolved in the seed suspension at a lower temperature. However, the product crystal sizes does not depend on the feed solution temperature, as the latter only affects the cooling profile within the first meter of the reactor. The process model assumes a flow-rate independent initial mass loading which explains the insensitivity on changes in $\dot{V}_{susp}$ and $\dot{V}_{sol.}$, i.e., an increase in $\dot{V}_{susp}$ does entail a higher initial mass loading.

Furthermore, note that variations in the flow rates have almost no influence on the initial value of supersaturation at the reactor inlet (i.e., after the first Y-fitting). This originates from the following effect: on the one hand, variations in the flow rates induce variations in the initial concentration of dissolved ASA (see equation 17). On the other hand variations in the flow rates induce variations in the slurry's temperature at the reactor inlet (see equation 16), and therefore affects the solubility concentration.

5 Summary and conclusion

The reactor design presented within this work facilitated the formulation of spatially independent PBEs due the segmented flow. A process model that predicts the temporal behavior of the CSD, the concentration of the dissolved species and the temperature profile during a continuous, seeded cooling-crystallization process in a tubular crystallizer was developed. The process model was used to quantify aggregation. Furthermore it was possible to investigate which process setting lead to a crystallization process for which the CSD is determined exclusively by crystal growth. Finally, the critical process parameters were identified by means of a sensitivity analysis.

The quantitative modeling of the CSD's spatio-temporal behavior during a crystallization process still

Cryst. Res. Technol. 49, No. 2–3, 92–108 (2014)

CRYSTAL Research&Technology

Original Paper

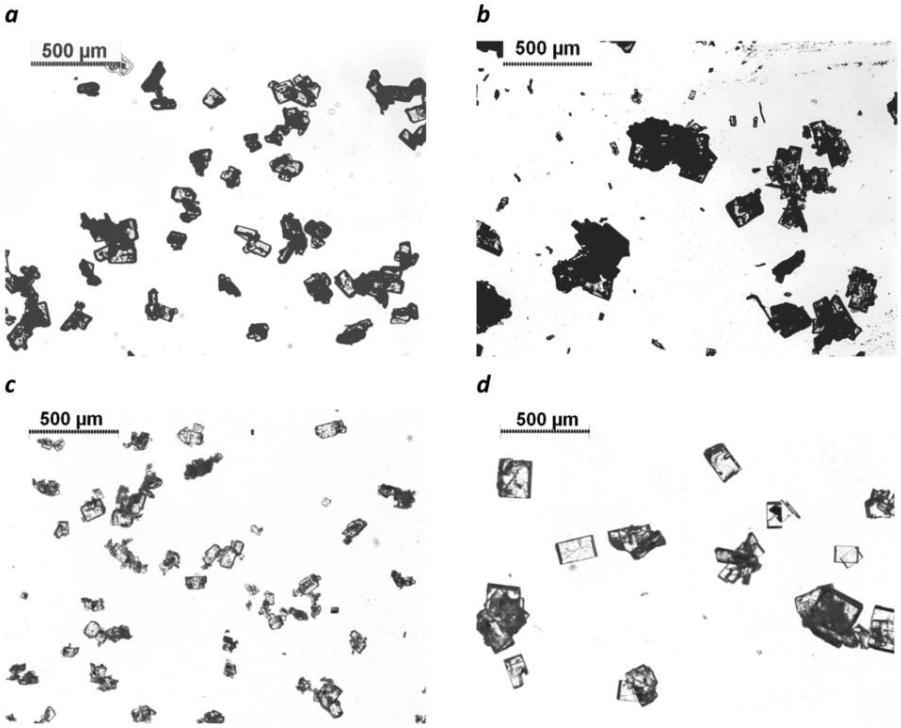

Fig. 13 Microscope pictures of the seed (a,c) and product (b,d) crystals obtained using experimental settings 1(a,b) and 3(c,d)

remains a challenge due to the difficulty in quantifying growth, aggregation, breakage and nucleation. Although these effects can be addressed within the phenomenological framework of PBEs, the identification of adequate mathematical expressions for aggregation, breakage and nucleation rates is challenging. Nevertheless, the combination of experimental results and PBEs comprising various effects (growth, nucleation, aggregation, breakage, etc.) is a powerful method to identify process characteristics and quantify effects determining the product CSD. This is especially important for the development of control models of the process.

With the process model, we could demonstrate that growth of seeded crystals is primarily determining the size of product. Furthermore it was possible to demonstrate that the crystallizer operated with experimental settings 3 (slowest cooling, lowest concentration of initially dissolved ASA), yields product crystals containing only a minor amount of fines and aggregates. The source of fines of experimental settings 1 (fastest cooling, medium initial concentration of initially dissolved ASA), was analyzed in detail. Neither X-ray diffraction pattern nor Raman spectra revealed any difference in the crystal structure or chemical composition between these fines and the residual product crystals. Since breakage was negligible, the occurrence of these fines originates from nucleation events during the process. Thus, the lowest amount of fines was found in crystals produced using the lowest supersaturation profile (i.e., experimental settings 3).

A critical value of $S \approx 1.4$ is reported for the occurrence of primary nucleation during a batch crystallization process of ASA in ethanol-water mixtures [22]. However, this value may vary for different reactor designs especially for a tubular reactor with a high surface-to-volume ratio that could promote heterogeneous nucleation at lower levels of supersaturation, even in the absence of a crystalline phase. The onset of secondary nucleation is reported at much lower supersaturation values than in the case of primary nucleation [32]. In

CRYSTAL Research & Technology

Original Paper

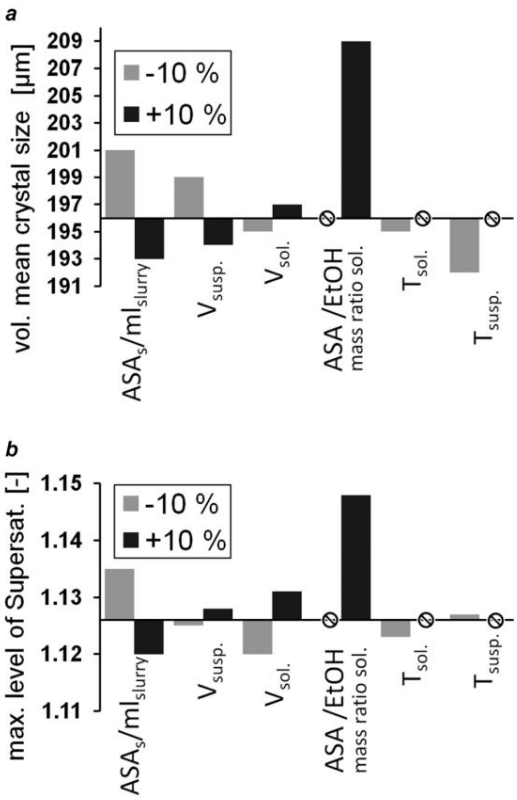

Fig. 14 Computed mean crystal size of product crystals (a) and maximum level of supersaturation (b) for relative variations in the process settings applying the growth only model in the case of experimental settings 3.

general, secondary nucleation cannot be avoided entirely beside crystal growth [32, 33, 56], which might explain discrepancies in the experimentally determined CSD and the one obtained from the process model, since nucleation was not included in the model.

The sensitivity analysis showed that the concentration of the feed solution, the temperature of the suspension and the initial mass loading with seed crystals are sensitive process parameters for the product crystal size and the maximum level of supersaturation. Especially the latter is important to limit nucleation, as discussed above. For the presented reactor design we consider the initial mass loading with seed crystals as the most critical process parameter, as variations might occur due to heterogeneous mass distributions in the flow segments. Moreover, the sensitivity analysis indicates how particle size depends on the operating parameters. This knowledge is particularly beneficial for tuning the CSD or maintaining the CSD in the case of fluctuating process conditions, e.g., seed CSD, in an automated process design.

Acknowledgements. The authors thank Eva-Maria Saurugger and Michael Piller for their support and advice in performing the X-ray diffraction & CSD measurements and Otto Scheibelhofer for assistance with the data evaluation.

Appendix

Derivation of the Mass Balance Equation

The volume of a crystal is given by equation (2). The change in volume V_{cryst} of a single crystal due to an increase in crystal size L is:

$$\frac{dV_{cryst}}{dL} = 3 \cdot k_v \cdot L^2. \quad (A.1)$$

In this work $c_{ASA.diss}$ is denoted in [mol/ml] and the number of moles per volume is given by:

$$\frac{mol}{V_{cryst}} = \frac{\varrho_{ASA}}{M_{ASA}} \quad (A.2)$$

G describes the change in length of a crystal per time unit and f(L,t) stands for the number of particles with a size L at the time t per volume slurry. Therefore, the change in concentration of the dissolved species is calculated by summing up the total increase in volume for all particles per volume slurry.

$$\frac{\partial c_{ASA.diss}}{\partial t} = \frac{\partial c_{ASA.diss}}{\partial (x/u_{fs})} = -\frac{3}{M_{ASA}} \cdot k_v \cdot G \cdot \varrho_{ASA} \cdot \int_0^\infty f(L, t) \cdot L^2 \cdot dL \quad (A.3)$$

Because the particulate phase (i.e., the seeded crystals) requires space, at the expense of space available for the solution and therefore the total amount of dissolved molecules in the flow segments we need to correct equation (A.3) This is usually neglected when it comes to the modeling of seeded crystallization processes which is only valid in the case of low seed loadings. To account for this effect we multiply equation (A.3) with the ratio of the relative space accessible for the solution in the absence of a crystalline phase divided by the relative

Cryst. Res. Technol. 49, No. 2–3, 92–108 (2014)

CRYSTAL Research&Technology

Original Paper

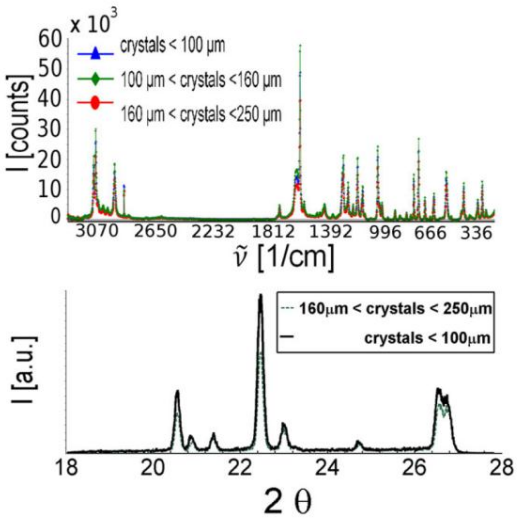

Fig. A1 Raman spectra (up) and X-ray diffraction patterns (down) of sieved crystals

space accessible for the solution in the presence of a crystalline phase at the initial point of the crystallization process (see equation (A.4)).

$$\left(\frac{1}{1-\epsilon_{\text{solid},0}}\right) \tag{A.4}$$

X-ray diffraction pattern and Raman spectra

Recorded Raman spectra and x-ray diffraction patterns of sieved ASA crystals are shown in figure A1. The small product crystals ($<100\ \mu$m) exhibit equal characteristics as the bigger ones using both methods.

Key words. continuous crystallization, PBE modeling, sensitivity analysis, aggregation, supersaturation control.

References

[1] A. J. Alvarez and A. S. Myerson, Cryst. Growth Des. **10**, 2219 (2010).
[2] B. Y. Shekunov and P. York, J. Cryst. Growth **211**, 122 (2000).
[3] R. J. P. Eder, S. Radl, E. Schmitt, S. Innerhofer, M. Maier, H. Gruber-Woelfler, and J. G. Khinast, Cryst. Growth Des. **10**, 2247 (2010).
[4] E. L. Paul, H. H. Tung, and M. Midler, Powder Technol. **150**, 133 (2005).
[5] K. Chow, H. H. Y. Tong, S. Lum, and A. H. L. Chow, J. Pharm. Sci. **97**, 2855 (2008).
[6] R. C. Snyder and M. F. Doherty, Aiche J. **53**, 1337 (2007).
[7] N. Blagden, M. de Matas, P. T. Gavan, and P. York, Adv. Drug Deliv. Rev. **59**, 617 (2007).
[8] H. Gros, T. Kilpio, and J. Nurmi, Powder Technol. **121** (2001).
[9] S. Qamar, M. P. Elsner, I. Hussain, and A. Seidel-Morgenstern, Chem. Eng. Sci. **71**, 5 (2012).
[10] Y. F. Su, H. Kim, S. Kovenklioglu, and W. Y. Lee, J. Solid State Chem. **180** (2007).
[11] S. Lawton, G. Steele, P. Shering, L. Zhao, I. Laird, and X.-W. Ni, Org. Process Res. Dev. **13**, 1357 (2009).
[12] R. J. P. Eder, E. K. Schmitt, J. Grill, S. Radl, H. Gruber-Woelfler, and J. G. Khinast, Cryst. Res. Technol. **46**, 227 (2011).
[13] R. J. P. Eder, S. Schrank, M. O. Besenhard, E. Roblegg, H. Gruber-Woelfler, and J. G. Khinast, Cryst. Growth Des. **12**, 4733 (2012).
[14] S. Y. Wong, A. P. Tatusko, B. L. Trout, and A. S. Myerson, Cryst. Growth Des. **12**, 5701 (2012).
[15] B. Wierzbowska, N. Hutnik, K. Piotrowski, and A. Matynia, Cryst. Growth Des. **11**, 1557 (2011).
[16] Z. Chun-Xia, H. Lizhong, Q. Shi Zhang, and A. P. J. Middelberg, Chem. Eng. Sci. **66**, 1463 (2011).
[17] C. H. Chang, B. K. Paul, V. T. Remcho, S. Atre, and J. E. Hutchison, J. Nanopart. Res. **10**, 965 (2008).
[18] W. Yu and B. C. Hancock, Int. J. Pharm. **361**, 150 (2008).
[19] J. M. D. Valle and F. H. Goldman, Ind. Eng. Chem.-Anal. Ed. **11**, 0545 (1939).
[20] B. R. Jennings and K. Parslow, Proc. R. Soc. Lond. Ser. A-Math. Phys. Eng. Sci. **419**, 137 (1988).
[21] F. Puel, G. Fevotte, and J. P. Klein, Chem. Eng. Sci. **58**, 3715 (2003).
[22] C. Lindenberg, M. Kraettli, J. Cornel, M. Mazzotti, and J. Brozio, Cryst. Growth Des. **9**, 1124 (2009).
[23] C. B. B. Costa, M. R. W. Maciel, and R. Maciel, Comput. Chem. Eng. **31**, 206 (2007).
[24] A. Alamdari and E. Tabkhi, Chem. Eng. Process. **43**, 803 (2004).
[25] A. Mersmann, B. Braun, and M. Loffelmann, Chem. Eng. Sci. **57**, 4267 (2002).
[26] D. L. Marchisio and R. O. Fox, J. Aerosol Sci. **36**, 43 (2005).
[27] D. L. Marchisio, R. D. Vigil, and R. O. Fox, J. Coll. Interf. Sci. **258**, 322 (2003).
[28] E. Gavi, L. Rivautella, D. L. Marchisio, M. Vanni, A. A. Barresi, and G. Baldi, Chem. Eng. Res. Des. **85**, 735 (2007).
[29] E. Bayraktar, O. Mierka, F. Platte, D. Kuzmin, and S. Turek, Comput. Chem. Eng. **35**, 2204 (2011).
[30] J. C. Cheng, C. Yang, and Z. S. Mao, Chem. Eng. Sci. **68**, 469 (2012).
[31] R. D, Population Balances: Theory and Applications to Particulate Systems in Engineering (Academic Press, London, 2000).

CRYSTAL Research & Technology

Original Paper

[32] A. Mersmann, Crystallization Technology Handbook (Dekker, New York, 1995).
[33] A. B. Mersmann, K. Braun, B. Heyer, and A. H., and Christiane, (Wiley-VCH Verlag GmbH, Chemie Ingenieur Technik, 2000).
[34] R. David, P. Marchal, and B. Marcant, Chem. Eng. Technol. **18**, 302 (1995).
[35] P. Taboada-Serrano, C. J. Chin, S. Yiacoumi, and C. Tsouris, Curr. Opin. Coll. Interf. Sci. **10**, 123 (2005).
[36] R. David, P. Marchal, J. P. Klein, and J. Villermaux, Chem. Eng. Sci. **46**, 205 (1991).
[37] R. David, A. M. Paulaime, F. Espitalier, and L. Rouleau, Powder Technol. **130**, 338 (2003).
[38] A. Eitzlmayr, C. Petschacher, S. Radl, D. Suzzi, A. Zimmer, and J. G. Khinast, Soft. Matter. **7**, 9484 (2011).
[39] R. D, Population Balances: Theory and Applications to Particulate Systems in Engineering. *2000, Academic Press, London* (Academic Press, London, 2000).
[40] E. J. W. Verwey, J. Phys. Coll. Chem. **51**, 631 (1947).
[41] B. W. Ninham, Adv. Coll. Interf. Sci. **83**, 1 (1999).
[42] H. C. Schwarzer and W. Peukert, Chem. Eng. Sci. **60**, 11 (2005).
[43] M. Vanni, J. Coll. Interf. Sci. **221**, 143 (2000).
[44] J. Abrahamson, Chem. Eng. Sci. **30**, 1371 (1975).
[45] F. E. Kruis and K. A. Kusters, Chem. Eng. Commun. **158**, 201 (1997).
[46] N. S. Tavare, M. B. Shah, and J. Garside, Powder Technol. **44**, 13 (1985).
[47] H. Qunwu, Y. Hasegawa, and N. Kasagi, Int. J. Heat Fluid Flow **31** (2010).
[48] S. Qamar, A. Ashfaq, I. Angelov, M. P. Elsner, G. Warnecke, and A. Seidel-Morgenstern, Chem. Eng. Sci. **63**, 1342 (2008).
[49] S. Kumar and D. Ramkrishna, Chem. Eng. Sci. **51**, 1311 (1996).
[50] S. Kumar and D. Ramkrishna, Chem. Eng. Sci. **51**, 1333 (1996).
[51] G. D. Maia and M. Giulietti, J. Chem. Eng. Data **53**, 256 (2008).
[52] A. Hodzic, M. Llusa, S. D. Fraser, O. Scheibelhofer, D. M. Koller, F. Reiter, P. Laggner, and J. G. Khinast, Int. J. Pharm. **428**, 91 (2012).
[53] P. Vishweshwar, J. A. McMahon, M. Oliveira, M. L. Peterson, and M. J. Zaworotko, J. Am. Chem. Soc. **127**, 16802 (2005).
[54] C. G. Kontoyannis and M. Orkoula, Talanta **41**, 1981 (1994).
[55] A. Mersmann, Chem. Eng. Process. **38** (1999).
[56] B. S. O'Sullivan, Benjamin. Baramidze, Georgiy (Mettler-Toledo AutoChem, Inc., 2012).

3. Continuous API-crystal coating via coacervation in a tubular reactor

M. O. Besenhard, A. Thurnberger, R. Hohl, E. Faulhammer, J. Rattenberger, and J. G. Khinast, *Int. J. Pharm.*, vol. 475, no. 1–2, pp. 198–207, Aug. 2014

International Journal of Pharmaceutics 475 (2014) e198–e207

Contents lists available at ScienceDirect

International Journal of Pharmaceutics

journal homepage: www.elsevier.com/locate/ijpharm

Continuous API-crystal coating via coacervation in a tubular reactor

M.O. Besenhard [a,b], A. Thurnberger [a,c], R. Hohl [a], E. Faulhammer [a], J. Rattenberger [d], J.G. Khinast [a,e,*]

[a] Research Center Pharmaceutical Engineering (RCPE) GmbH, Graz 8010, Austria
[b] Siemens AG, Corporate Technology, Graz 8054, Austria
[c] Microinnova Engineering GmbH, Allerheiligen/Wildon 8412, Austria
[d] Graz University of Technology, Institute for Electron Microscopy and Nanoanalysis, Graz 8010, Austria
[e] Graz University of Technology, Institute for Process and Particle Engineering, Graz 8010, Austria

ARTICLE INFO

Article history:
Received 6 June 2014
Received in revised form 4 August 2014
Accepted 5 August 2014
Available online 7 August 2014

Keywords:
Continuous coating
Coacervation
HPMCP
Eudragit
Enteric coating
Tubular reactor

ABSTRACT

We present a proof-of-concept study of a continuous coating process of single API crystals in a tubular reactor using coacervation as a microencapsulation technique. Continuous API crystal coating can have several advantages, as in a single step (following crystallization) individual crystals can be prepared with a functional coating, either to change the release behavior, to protect the API from gastric juice or to modify the surface energetics of the API (i.e., to tailor the hydrophobic/hydrophilic characteristics, flowability or agglomeration tendency, etc.). The coating process was developed for the microencapsulation of a lipophilic core material (ibuprofen crystals of 20 μm- to 100 μm-size), with either hypromellose phthalate (HPMCP) or Eudragit L100-55. The core material was suspended in an aqueous solution containing one of these enteric polymers, fed into the tubing and mixed continuously with a sodium sulfate solution as an antisolvent to induce coacervation. A subsequent temperature treatment was applied to optimize the microencapsulation of crystals via the polymer-rich coacervate phase. Cross-linking of the coating shell was achieved by mixing the processed material with an acidic solution (pH < 3). Flow rates, temperature profiles and polymer-to-antisolvent ratios had to be tightly controlled to avoid excessive aggregation, leading to pipe plugging. This work demonstrates the potential of a tubular reactor design for continuous coating applications and is the basis for future work, combining continuous crystallization and coating.

1. Introduction

In pharmaceutical manufacturing, batch processing has significant advantages: single batches can be accepted or rejected as a part of a quality system and existing, (seemingly) well-understood equipment can be reused for a wide variety of different campaigns. Moreover, due to the inherent flexibility, batch processes with multi-purpose equipment are conceived to be more profitable for small-scale products than dedicated continuous plants (Plumb, 2005; Goršek and Glavič, 1997). However, batch manufacturing also has disadvantages: scale-up from small-sized laboratory equipment used in the early phase of development to the industrial scale is often highly complex and can pose serious problems, including regulatory issues due to the extensive validation required (Qiu et al., 2009; Närhi and Nordström, 2005). The design of large-scale equipment based solely on geometrical similarity is not sufficient (Montante et al., 2003; Leuenberger, 2001; Klinzing and Bell, 2005). For example, large-scale systems are more likely to create inhomogeneous process conditions with a noticeable impact on product quality. In addition to the scale-up problem, long throughput times, lower equipment usage and extensive equipment maintenance are daily reality in a batch-manufacturing environment. As a result, the development and implementation of innovative processing technologies, including continuous manufacturing has created significant interest. Moreover, this trend is supported by the regulatory authorities (FDA, 2014).

Together with crystallization, filtration (Lawton et al., 2009) and wet granulation (Vervaet and Remon, 2005), coating processes are still considered a bottleneck for an end-to-end continuous manufacturing process. Innovations in continuous functional coating (e.g., enteric coating) focus primarily on the improvement of pan coaters (Ferrero, 1993; O'Hara and Marjeram, 2006; Cunningham et al., 2010; Suzzi et al., 2012), fluidized bed (Liborius,

* Corresponding author. Tel.: +43 316 873 30400; fax: +43 316 873 30402.
E-mail address: khinast@tugraz.at (J.G. Khinast).

http://dx.doi.org/10.1016/j.ijpharm.2014.08.009
0378-5173/

1993; Rümpler et al., 2006; Teunou and Poncelet, 2002) and spouted bed reactors (Jacob et al., 2006; Innovations in Coating Technology, 2008). These technologies are most suitable for processing tablets and pellets. However, functional coatings can also be applied to the crystals themselves, obviating the need to coat pellets or tablets. Among the many microencapsulation techniques (Jyothi et al., 2010; Elkharraz et al., 2011; Im and Sah, 2009; Hirech et al., 2003; Dalmoro et al., 2012; Gouin, 2004; Ghosh, 2006; Kröber and Teipel, 2005), spray drying (Kondo et al., 2014) and solvent evaporation (Li et al., 2008; Lyons and Wright, 2001) are most frequently described. Another important microencapsulation technique relevant for the food and pharmaceutical industry is coacervation (Weiß et al., 1995a; Ganderton et al., 1995; Nakagawa and Nagao, 2012). The term was introduced by Bungenberg de Jong and Kruyt in 1926 (Bungenberg et al., 1929) to describe the formation of polymer-rich coacervate droplets. Coacervation can be induced by adding either an anti-solvent to the polymer (simple coacervation) or an oppositely charged polymer (complex coacervation). The concept of microencapsulation via coacervation involves the deposition of a newly-formed coacervate phase around core particles suspended or emulsified in the same reaction media. The formed shell can then be cross linked, i.e., hardened, for example, by adding an appropriate chemical cross linker or via temperature treatment (Gouin, 2004; Weiß et al., 1995b). Recently, coacervate microcapsules have also been used in the formulation of multilayer oral dosage forms (Feng et al., 2014; Salaün et al., 2009; Pommersheimer, 2005). However, coacervation has mainly done in a batch reactor, stirred-tank environment.

Tubular reactors (including micro-reactors) are increasingly used in research and industry (Roberge et al., 2005; Roberge et al., 2008; Mascia et al., 2013), e.g., for generating nano- and micro-particles (Kawase and Miura, 2007; Yadav et al., 2012; Petschacher et al., 2013; Alvarez and Myerson, 2010; Jiang et al., 2014; Kang et al., 2014) and for chemical synthesis (Kopetzki et al., 2013; Lévesque and Seeberger, 2011; Wahab et al., 2010; Michel and Greaney, 2014; Malet-Sanz and Susanne, 2012; He and Jamison, 2014; Wu et al., 2014). The high surface-to-volume ratio facilitates rapid heat exchange and therefore an accurate temperature control of the processed medium (Tabeling, 2005). These are the desirable conditions when dealing with temperature-dependent phase separation processes, such as coacervation.

The purpose of this work was to investigate the principle of continuous coating of single crystals in a long tubular reactor applying simple coacervation. Two enteric polymers of industrial relevance (HPMCP and Eudragit® L100-55) were used. The outline of the present study is as follows: first, the applied analytical methods are described and the proposed continuous coating process is illustrated. Next, in Section 3 the results of our study are presented. Finally, Section 4 provides a summary, together with a novel coacervation concept that may be highly practical for applications in a tubular reactor.

2. Materials and methods

The API used was ibuprofen (ibuprofen 25) – BASF, Germany. Its cumulative volume density distribution is shown in Fig. 1. Coatings used were hydroxy propyl methyl cellulose phthalate (HPMCP – hypromellose phrhalate, NF; HP-55, nominal phthalyl content: 31%) – Shin-Etsu Chemical Co. Ltd., Japan; Eudragit L100-55 (methacrylic acid–ethyl acrylate copolymer (1:1) Type A Ph. Eur.) – Carl Roth GmbH + Co. KG, Germany. (Anti-) solvents: Ethanol denaturized (≥99.8% with about 1% MEK) – Carl Roth GmbH + Co. KG, Germany; disodium hydrogen phosphate dihydrate (≥99.5%) – Carl Roth GmbH + Co. KG, Germany; sodium sulfate (≥99%) – Carl Roth GmbH + Co. KG, Karlsruhr. Acids: hydrochloric acid (1 N) – Carl Roth GmbH + KG Germany; acetic acid (100%) – Carl Roth GmbH + Co. KG, Germany.

2.2. Process equipment

Three peristaltic pumps (PI–III) were utilized in the coating experiments: PI: ISMATEK Type ISM 831C; PII: ISMATEK Reglo Model ISM 829 B and PIII: Heidolph Pumpdrive Type PD5106. Polysiloxane tubings with an inner diameter (d_{in}) of 2.0 mm and an outer diameter (d_{out}) of 4.0 mm and Y-fittings (PTFE, d_{in} = 2.0 mm) were used to assemble the tubular reactor. Temperature control was performed using two thermostatic bathes: BI (LAUSA Type E 111 Ecoline Staredition) and BII (LAUDA A 24). Agitation and temperature control of suspensions and solutions were carried out with two magnetic stirrers SI (VWR Advanced VMS-C4) and SII (IKAMAG RCT).

2.3. Dissolution studies

Dissolution studies were carried out in order to examine the coating quality according to a method described by Weiß (1991). The method is based on the different solubilities of ibuprofen and the coating polymers at pH = 4. Since ibuprofen crystals dissolve quickly if not coated, the dissolution profile reflects the coating quality. Powder dissolution was performed using an Erweka DT820 dissolution tester with a stirring paddle (Erweka GmbH, Germany). The stirring speed was 100 rpm and the vessels were filled with 900 mL of a dissolution medium that was kept at 37 °C ± 0.5 °C. The phosphate buffer, serving as the dissolution medium, was prepared by dissolving 6.8 g of potassium dihydrogen orthophosphate in deionized water and filled up to 1000 g. The pH value (determined using a FiveEasy from Mettler Toledo) was adjusted to pH 4 by less than 1 mL of phosphoric acid (85%). Adding 0.5 g of a wetting agent (Tween® 20) was sufficient to guarantee good wettability of the suspended particles. 1 g was used in the original method (Weiß, 1991). Since the maximum solubility of ibuprofen in the phosphate buffer medium is 71.4 mg/L at 37 °C (Weiß, 1991), 60 mg of uncoated ibuprofen crystals or the mass equivalent of coated material (see Section 2.4) were suspended in the dissolution vessel. Only sieved powder samples were measured (RETSCH vibratory sieve shake AS200 control, sieving time 5 min mesh size 50–100 μm) to ensure comparability of the dissolution profiles. The quantification of the dissolved ibuprofen concentration was carried out via UV/Vis-spectroscopy at 264 nm (Lambda 950 UV/Vis/NIR

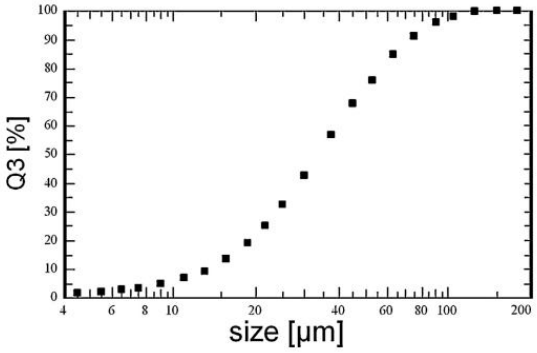

Fig. 1. Cumulative volume density distributions (Q3) of ibuprofen 25 determined by laser diffraction (HELOS/KR, Sympatec GmbH, Clausthal-Zellerfeld, Germany).

spectrophotometer, PerkinElmer). At this wavelength, the spectra do not interfere with other substances used during the coating process (i.e., hydrochloric acid, sodium sulfate, acetic acid). Every sample was analyzed in triplicate.

2.4. Ibuprofen quantification in microcapsules

During dissolution tests, a defined amount of ibuprofen needs to be introduced to the dissolution medium. Thus, the ibuprofen content of the previously-sieved coated material needs to be determined. As before, only sieved powder samples were measured. The quantification was performed similar to the method described in Weiß (1991) utilizing the high solubility of ibuprofen in ethanol. 0.025 g of coated material was dissolved in 25 mL of ethanol (≥99.8% under ultrasonic irradiation for 30 min. Since, unlike Eudragit L100-55, HPMCP is not soluble in ethanol, the ultrasonic irradiation was required to break the HPMCP shell material. After centrifugation for 5 min at 5000 rpm (Hettich Universal 320R), the supernatant was passed through a syringe filter and analyzed via a UV/vis spectrophotometer as described above.

2.5. Scanning electron microscopy (SEM)

SEM micrographs were recorded with a Zeiss Ultra 55 (Carl Zeiss, Germany) using an acceleration voltage of 5 kV and a secondary electron detector for imaging (in-lens detector). Samples were fixed on the SEM stub with conductive double-sided adhesive carbon tape and sputtered with a platinum palladium alloy (50/50, about 8 nm thick) for electrical conductivity.

2.6. Continuous HPMCP coating process

The method presented by Weiß et al. (1995a) served as basis for the development of our continuous HPMCP coating process. Micrographs showing the temperature-dependent encapsulation behavior during our preliminary batch-coating process are shown in Appendix.

Similar to (Weiß et al., 1995a), the HPMCP coating suspension (HPMCP susp.) was prepared by dissolving 9.5 g of disodium phosphate dehydrate in 372 g of demineralized water before adding 20 g of HPMCP. After stirring for 10 h, a clear solution with a pH-value of 5.45 ± 0.05 was obtained. Ibuprofen, i.e., the core material, was suspended in the solution with a ratio 10 (w/w)% at 20 °C and at a stirring rate of 300 rpm at least 20 min prior to the experiments. A 20 (w/w)% sodium sulfate solution (Na_2SO_4 sol.), i.e., the antisolvent, was used to induce the coacervation process. The sodium sulfate solution was prepared at 50 °C and at a stirring rate of 100 rpm. A 7.5 (w/w)% acetic acid solution (CH_3COOH sol.) at 20 °C was used to harden the microcapsules in the tubular reactor. Temperatures and stirring speeds remained the same throughout the experiment.

Fig. 2 presents a schematic of the continuous HPMCP coating process. The parameter settings are listed in Table 1. The HPMCP coating suspension was fed to the tubular reactor (PII : $\dot{V}_{HPMC\ susp.} = 12$ mL/min) and via two Y-fittings (PII : $\dot{V}_{Na_2SO_4\ sol.} = 2 \times 2$ mL/min) mixed with the sodium sulfate solution in a thermostatic bath (BI: 21.5 °C) to induce coacervation. Subsequently, the tubing was heated (BII: 50 °C) to prompt further phase separation and to pre-harden the HPMCP coacervate envelopes. After the temperature treatment, the processed suspension was mixed with the acetic acid solution in a Y-fitting (PIII : $\dot{V}_{CH_3COOH\ sol.} = 34$ mL/min) and filtrated. At six positions along the reactor (denoted by an (X) in Fig. 2) two thin wire spirals were inserted into the tubing to avoid agglomeration of the slurry.

In addition, experiments were performed in which the hardening step was conducted outside of the tubing (hereinafter referred to as 'external hardening'). In this case, the processed slurry was decanted and rinsed with a 5 (w/w)% acetic acid solution 30 min before filtration.

2.7. Continuous Eudragit L100-55 coating process

Based on a method presented by Weiss et al. (Weiß et al., 1993), a continuous Eudragit coating process was developed. The Eudragit coating suspension (Eudragit susp.) was prepared by dissolving 10 g of Eudragit L100-55 in 472.5 g of demineralized water and 17.5 g of an 1 N sodium hydroxide solution which was stirred for 5 h until a clear solution with a pH-value of 5.85 ± 0.05 was obtained. Subsequently, 153 g of isopropyl alcohol were added.

Ibuprofen, i.e., the core material, was suspended with a ratio of 2 (w/w)% at 20 °C and stirred at a rate of 300 rpm at least 15 min prior to the experiments. A 20 (w/w)% sodium sulfate solution (Na_2SO_4 sol.) prepared at 50 °C and stirred at 100 rpm was the

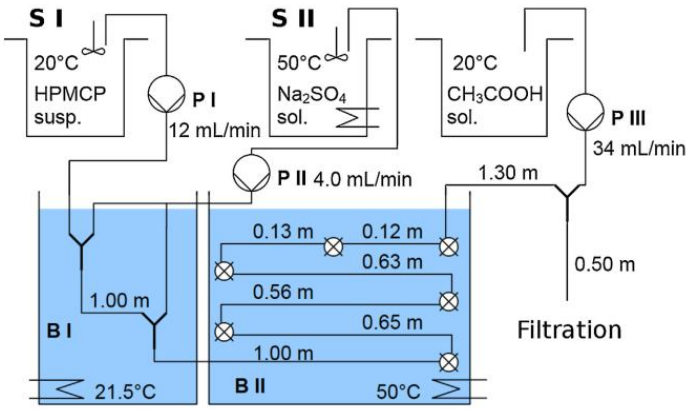

Fig. 2. Schematic of the continuous HPMCP crystal coating process.

Table 1
Parameters and process settings for the continuous coating processes

	Cont. HPMCP coating process		Cont. Eudragit coating process	
Coating suspension	20 g	HPMCP	10 g	Eudragit
	9.5 g	Disodium phosphate dehydrate	17.5 g	1 N sodium hydroxide solution
			153 g	Isopropyl alcohol
	372 g	Demineralized water	472.5 g	Demineralized water
	10 (w/w)%	Ibuprofen (≈40 g)	2 (w/w)%	Ibuprofen (≈10 g)
	20 °C	Temperature	20 °C	Temperature
	12 mL/min	Flow rate	8.7 mL/min	Flow rate
Anti-solvent solution	20 (w/w)%	Sodium sulfate/demineralized water	20 (w/w)%	Sodium sulfate/demineralized water
	50 °C	Temperature	50 °C	Temperature
	4 mL/min	Flow rate	1.3 mL/min	Flow rate
–				
Acid solution	7.5 (w/w)%	Acetic acid/demineralized water	0.001 N	Hydrochloric acid solution
			1 N	Hydrochloric acid solution
	20 °C	Temperature	20 °C	Temperature
	34 mL/min	Flow rate	73.2 mL/min, 8.7 mL/min	Flow rates (0.001 N and 1 N)
Tubular reactor	21.5 °C	Temperature (mixing suspension and solution)	25 °C	Temperature (mixing suspension & solution)
	50 °C	Temperature (after mixing suspension and solution)	25 °C	Temperature (after mixing suspension & solution)
	3 m	Tube length (after mixing suspension and solution)	3 m	Tube length (after mixing suspension & solution)

antisolvent. 1 N and 0.001 N hydrochloric acid solutions (HCl sol. 1, HCl sol. 2), both at 20 °C were used to harden the microcapsules in the tubular reactor.

Fig. 3 provides a schematic drawing of the continuous Eudragit L100-55 crystal coating process. The process settings are listed in Table 1. The Eudragit coating suspension was fed into the tubular reactor ($PI: \dot{V}_{Eudragit\ susp.} = 8.7\,mL/min$) and mixed with the antisolvent tempered at 50 °C via two Y-fittings ($PII: \dot{V}_{Na_2SO_4\ sol.} = 2 \times 0.65\,mL/min$). The tube was temperature-controlled (BI: 25 °C) throughout the entire process. The hardening step was performed by mixing the processed suspension with the hydrochloric acid solutions using two Y-fitting ($PIII: \dot{V}_{HCl\ sol.1} = 73.2\ mL/min$,$PI: \dot{V}_{HCl\ sol.2} = 8.7\ mL/min$) before filtration. Again six wires were placed into the tubing to avoid clumping.

Again, experiments were performed excluding the hardening step from the tubular reactor, i.e., external hardening. Here, the processed slurry was decanted and suspended in a 0.1 N hydrochloric acid solution for 30 min before filtration.

3. Results and discussion

The temperature profile along the tube was the main difference between the two different continuous microencapsulation processes (see Figs. 2 and 3). The reason is that the HPMCP and Eudragit exhibit opposed coacervation temperature dependencies. In contrast to most polymers used for coacervation processes (including Eudragit L100-55), HPMCP tends to form gels at higher temperatures due to the hydration of the methyl and hydroxypropyl substituents (Weiß et al., 1995b). However, aggregation of microparticles during coacervate formation is a typical problem commonly encountered in simple and complex coacervation (Dong and Bodmeier, 2006) not only for galantine coatings (Phares and Sperandio, 1964; Shimokawa et al., 2013). Thus, minimizing aggregation is a major concern during the development of the continuous coating processes. In our case, excessive aggregation caused pipe plugging in some cases. Generally speaking, the longer the tube the more aggregation occurred, due to the longer residence times in the reactor. Nevertheless, the tube between the

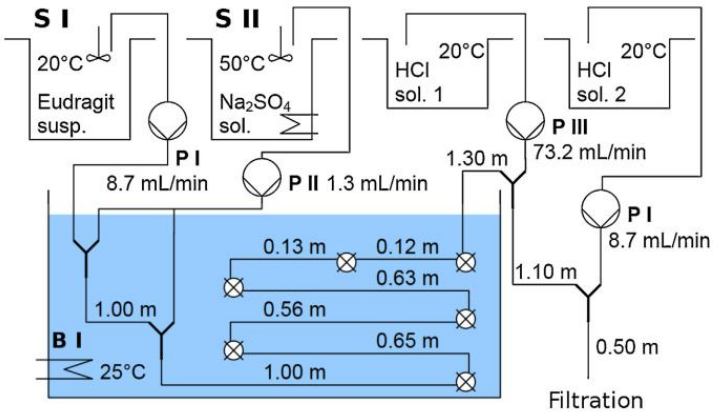

Fig. 3. Schematic of the continuous Eudragit L100-55 crystal coating process.

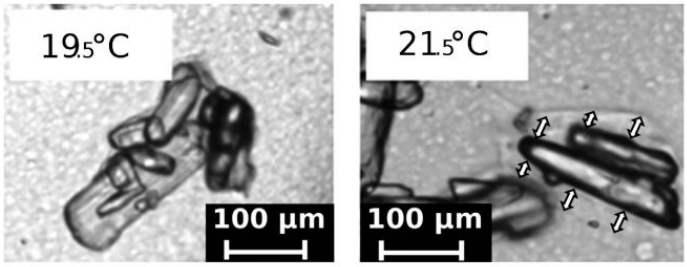

Fig. 4. Micrographs of ibuprofen crystals sampled right after the second Y-fitting (i.e., antisolvent addition) during the continuous HPMCP coating process (see Fig. 2) at different temperatures in B I. A 2 °C temperature increase yields considerably thicker coating layers (highlighted by the arrows) right after the coacervation onset. A further increase in temperature was shown to be disadvantageous for the encapsulation uniformity.

anti-solvent and the acid solution feed never led to pipe plugging. Clearly, the properties of the coating layer strongly impact aggregation and plugging. Especially, the coating layer stickiness depends on the temperature in the tubing and the coating suspension-to-anti-solvent ratio, due to the varying polymer contents in the coating layer (Weiß et al., 1995b). Hence, the aggregation frequency, i.e., the number of aggregation events per time unit, and the encapsulation behavior can vary considerably with even slight changes in the temperature. The latter applies particularly to HPMC encapsulation (see Fig. 4). In addition, the aggregation frequency is known to depend strongly on the flow field (Reinhold and Briesen, 2012; Taboadaserrano et al., 2005). Thus, flow rates (i.e., the coating suspension-to-anti-solvent ratio and their absolute values), temperatures and tube lengths of the processes described above were selected to allow encapsulation of the core material while minimizing aggregation. In the case of the HPMC coating process the anti-solvent flow rate was used to fine-tune the process whereas the temperature of the thermostatic bath controlling the tube temperature (see BI in Fig. 3) was used for the Eudragit coating process.

However, it was not possible to prevent some form of aggregation during the filtration and drying procedure. Thus, automated methods for particle size analysis could not be used.

A uniform encapsulation of crystals is of particular importance for enteric coatings. The complex film forming behavior at the solid surface depends strongly on the interplay between (i) polymer, (ii) solvent and (iii) the solid surface. Moreover, the viscosity of the coacervate phase, the size of coacervate droplets in relation to the core material's dimension and the coalescence among droplets strongly influence the morphology of the final microcapsules. For the HPMCP and Eudragit coating processes, the core material is already present at the coacervation onset. Assuming that the slurry is adequately mixed after the anti-solvent addition, gradual surface deposition (and not the formation of large coacervate droplets followed by bulk encapsulation) is expected to be the dominant microencapsulation mechanism (Arshady, 1990). Hence, the film-forming process at the solid surface and the viscosity of the coacervate phase are the critical factors for the coating uniformity.

The final API content of the HPMCP and Eudragit coated material depends primarily on the ratio of dispersed API and the extent of coacervation during the process, i.e., the quantity of the polymer-rich coacervate phase. Therefore, the quantified ibuprofen content of HPCM coated material (external hardening) is similar to that of Eudragit coated material, even if the amount of suspended core material deviates by almost one order of magnitude (see Table 1).

3.1. Continuous HPMCP coating process

Fig. 5 and 6 show optical and SEM micrographs of ibuprofen crystals microencapsulated with HPMCP using the continuous coating process described above and uncoated crystals for comparison. Both the optical and the SEM micrographs indicate a good encapsulation of the core material, i.e., the ibuprofen crystals. The SEM micrographs of microcapsules processed entirely inside the tubing show a higher amount of fines (mainly $<20\,\mu m$) than those processed via the external hardening step (compare Fig. 6c and e). Since the latter process involves decantation, the fine

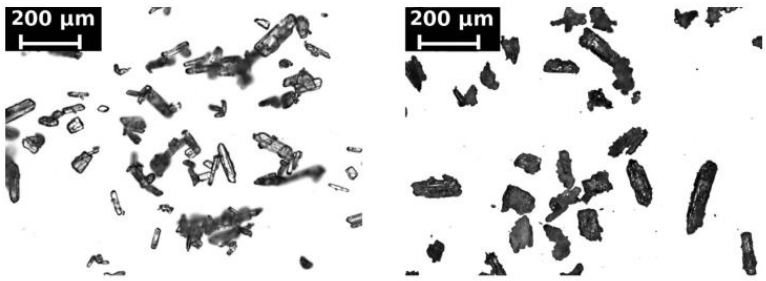

Fig. 5. (a) Micrographs of uncoated ibuprofen crystals and (b) crystals coated continuously with HPMCP using the process described in Section 2.

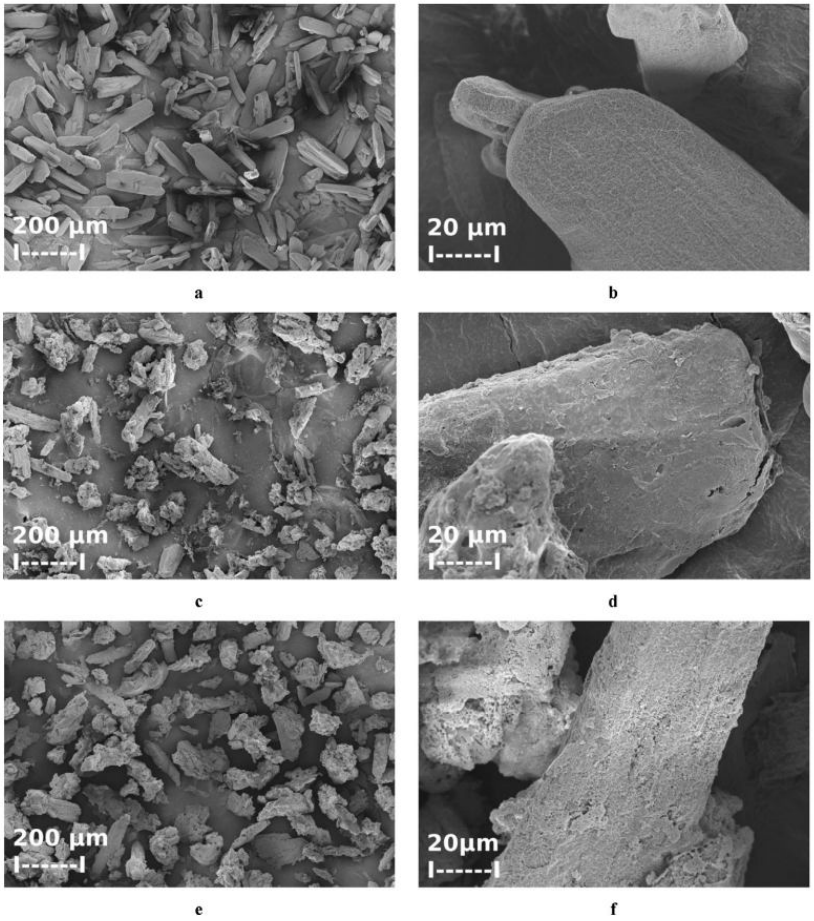

Fig. 6. (a, b) SEM micrographs of ibuprofen crystals, i.e., the core material. (c, d) crystals coated continuously with HPMCP, processed as shown in Fig. 2 and (e, f) via external hardening.

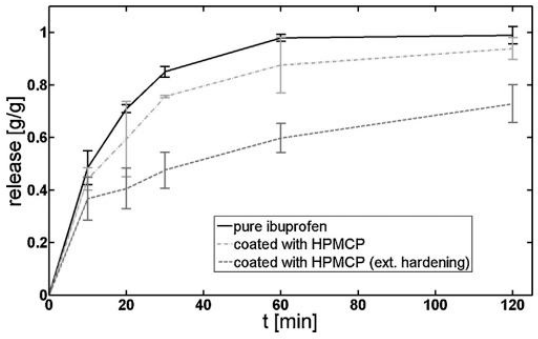

Fig. 7. Dissolution profiles of ibuprofen crystals at pH = 4 continuously coated with HPMCP and uncoated crystals for comparison. Each dissolution study has been performed in triplicate. The error bars account for the release standard deviation.

fraction of empty hardened coacervation droplets that did not contain crystalline material was removed before filtration.

Prior to the dissolution studies, the ibuprofen content in the processed material was quantified. The quantification (see above) yielded 53.8 ± 2.0 (w/w)% API for microcapsules processed entirely inside the tubing and 75.4 ± 4.2 (w/w)% API for those hardened externally. A thicker coating layer of crystals microencapsulated via internal hardening may be the reason for this difference. Another reason might be the presence of empty hardened coacervation droplets, which had a higher likelihood of being removed during the decantation step during the external hardening procedure due to their lower density.

Fig. 7 shows the dissolution profiles of the processed particles. Although the micrographs suggest a good microencapsulation of the core material with internal hardening, the dissolution profiles indicate only little retardation of the ibuprofen release. Only microcapsules hardened externally exhibit a significant retardation effect, although the quantity of HPMCP was higher (=lower ibuprofen content) in the case of internally hardened microcapsules. The poor dissolution results of the internally

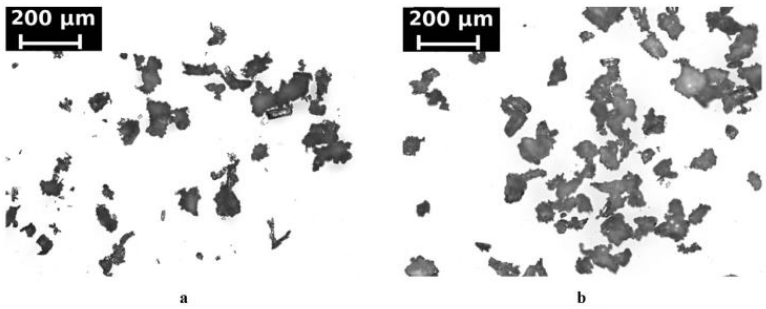

Fig. 8. Optical micrographs of ibuprofen crystals coated continuously with Eudragit L100-55. (a) Processed as shown in Fig. 3 and (b) via external hardening. See Fig. 5(a) for comparison with optical micrographs of the core material, i.e., the ibuprofen crystals.

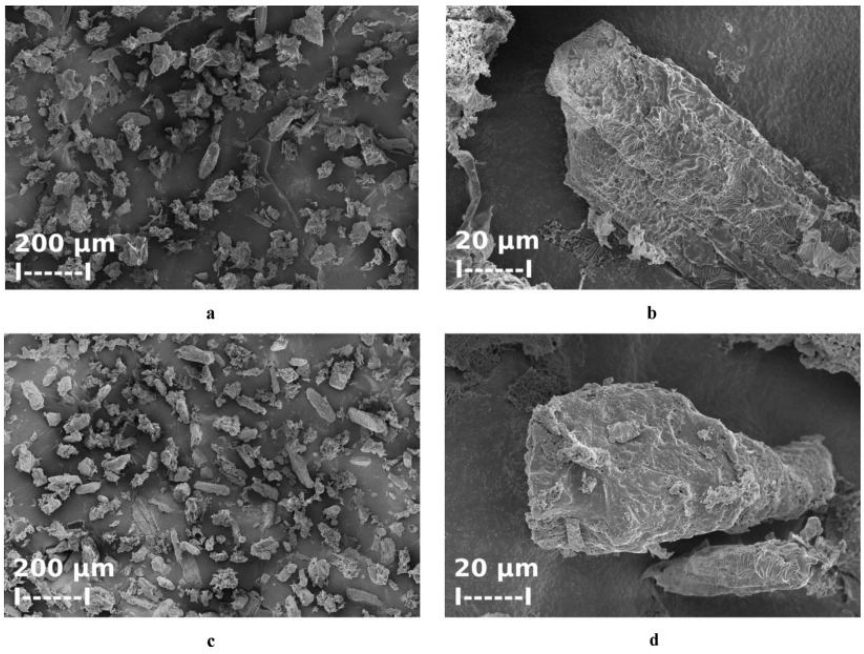

Fig. 9. (a, b) SEM micrographs of ibuprofen crystals coated continuously with Eudragit L100-55, processed as shown in Fig. 3 and (c, d) via external hardening. See Fig. 6(a, b) for comparison with uncoated ibuprofen crystals.

hardened material may be due to a poor coating uniformity, i.e., varying coating thickness or cavities, or a different solubility of the hardened material at pH 4 originating from an incomplete hardening step. The acetic acid concentrations are comparable during the internal and external hardening procedure. Therefore, the different hardening times are expected to cause the poor dissolution results of the internally hardened material. In the case of external hardening, encapsulated particles were suspended around 10–100 times longer in the acid solution than during the internal hardening in the tube.

The limited pH resistance of both HPMCP coatings (hardened internally and externally) might be explained by a partly insufficient polymer content of the polymer-rich coacervation phase for encapsulating the ibuprofen crystals. In the case of HPMCP, an increase in the mixing temperature (BI, see Fig. 2) should yield higher polymer concentrations in the polymer rich phase (Weiß, 1991). Hence, operating the tubular reactor at higher temperatures could increase the quality attributes of the processed microcapsules. As discussed above, longer residence times in the tube after feeding the acid solution may improve the internal hardening procedure.

3.2. Continuous Eudragit L100-55 coating process

Figs. 8 and 9 show micrographs of ibuprofen crystals micro-encapsulated with Eudragit L100-55 using our continuous coating

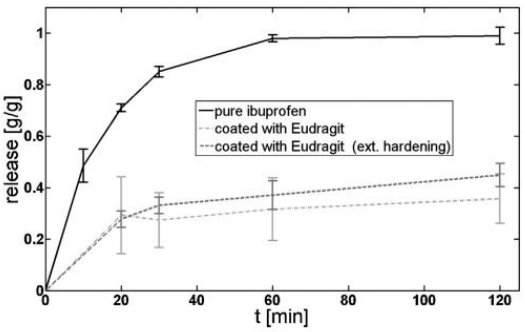

Fig. 10. Dissolution profiles at pH 4 of ibuprofen crystals continuously coated with Eudragit L100-55 and uncoated crystals for comparison. Each dissolution study has been performed in triplicate. The error bars account for the release standard deviation.

process. Both the optical and the SEM micrographs indicate excellent encapsulation of ibuprofen crystals.

As before, the ibuprofen content in the microcapsules had to be quantified prior to the dissolution studies. For Eudragit L100-55 coated particles, the API content was determined to be 79.0 ± 1.2 (w/w)% and 84.3 ± 1.8 (w/w)% for internal and external hardening, respectively. In contrast to the HPMCP coated particles, these values were rather similar.

Fig. 10 shows the dissolution profiles of Eudragit L100-55 microcapsules. The dissolution profiles indicate a significant retardation of the ibuprofen release. Microcapsules hardened internally and externally had an approximately equal retardation effect. These results suggest that both the encapsulation of the core material and the hardening of the coacervation layer can be performed continuously in the tubular reactor.

Although ibuprofen is practically insoluble in the Eudragit coating process, some of the suspended ibuprofen dissolves in the coating suspension due to the presence of isopropyl alcohol. However, this amount is negligible since the solubility of ibuprofen in the Eudragit coating suspension (153 g – isopropyl alcohol/471.5 g water) is ≈1.5 g/kg at 20 °C (Filippa and Gasull, 2013). The increase in temperature due to the thermostatic bath controlling the tube temperature (20 °C → 25 °C) is only expected to increase the solubility of ibuprofen in the slurry (Wang et al., 2010; Gracin and Rasmuson, 2002). Hence, recrystallization of ibuprofen during the coating process was not observed

4. Conclusion and outlook

This work presents a proof-of-concept study of a continuous coating process in a tubular reactor using coacervation as a microencapsulation technique. Continuous coating can have several advantages, as in a single step following crystallization, individual crystals can be prepared with a functional coating, either to change the release behavior, to protect the API from gastric juice, or to modify the surface energetics of the API (i.e., to tailor the hydrophobic/hydrophilic characteristics, flowability or agglomeration tendency, etc.).

Our initial results suggest that a coacervation processes for microencapsulating hydrophobic drugs, such as ibuprofen with the polymers HPMCP or Eudragit L100-55, are promising in a continuous operation mode. Both polymers are frequently applied in pharmaceutical manufacturing, mostly for enteric coating systems. The results of our work can be summarized as follows:

- Micrographs of HPMCP-coated material showed a good micro-encapsulation of the core material, i.e., the ibuprofen crystals. Nevertheless, the dissolution studies indicated only sufficient retardation when the hardening step was performed externally. Thus, the continuous HPMCP coating process, and especially the hardening step, have to be further be optimized to ensure sufficient enteric coating of the core material.
- Eudragit L100-55 coated material clearly showed a delayed ibuprofen release, also for particles coated inside the reactor. Thus, this process is robust and can be utilized in manufacturing.
- Compared to the batch methods, the tubular rector design considerably reduces the processing time. Estimated based on the mean residence time of particles in the tubing, the duration of the process for HPMC encapsulation was reduced from 75 min to 2 min. The overall duration of the Eudragit L100-55 coating process, i.e., encapsulation and hardening, was reduced from 50 min to ≈2 min.

In summary, the results of our study demonstrate the potential of a continuous coating processes based on a coacervation technique in a tubular reactor.

The tubular reactor used in this study resembles designs that have been applied previously for continuous crystallization process (Eder et al., 2010; Eder et al., 2011; Eder et al., 2012; Besenhard et al., 2014). This underlines the possibility of combining continuous crystallization and microencapsulating in a single process. For example, Dong and Bodmeier presented a novel microencapsulation method for APIs using complex coacervation (Dong and Bodmeier, 2006). Unlike during classical coacervation microencapsulation, the API is initially dissolved, rather than dispersed, in the polymer solution prior to adding the non-solvent. Furthermore, ultrasound-induced crystallization in a tubular reactor design, which was demonstrated recently (Eder et al., 2012), could be utilized. The combination of these concepts, i.e., ultrasound-induced nucleation of APIs in a polymer solution undergoing coacervation, may be an effective way to crystallize and encapsulate materials in a single continuous step. This will be a subject of future research.

Acknowledgements

Research Center Pharmaceutical Engineering is funded by the Austrian COMET Program under the auspices of the Austrian Federal Ministry of Transport, Innovation and Technology (BMVIT), the Austrian Federal Ministry of Economy, Family and Youth (BMWFJ) and by the Province of Styria (Styrian Business Promotion Agency, SFG). COMET is managed by the Austrian Research Promotion Agency, FFG. Furthermore, we would like to thank Marielies Reiter, Sharareh Salar-Behzadi and Mario Hainschitz, for their technical support of the experimental

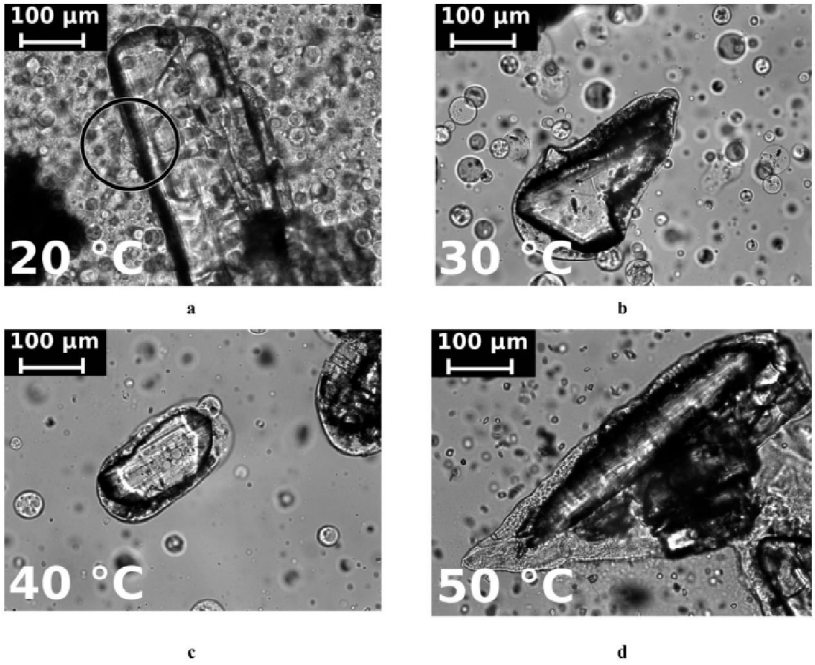

Fig. A1. Micrographs of the microencapsulating behavior of ibuprofen crystals by HPMCP during the method described in (Weiß et al., 1995a). (a) Right after the onset of coacervation. The highlighted area shows the initial covering of a crystal. (b) An initial increase in temperature. Crystals became now enclosed completely; (c, d) further increase in temperature to provoke further phase separation and preharden the HPMCP coacervate envelopes. A change in the appearance of the coacervate is obvious.

studies presented in this work. We also would like to thank Gerd Weiß for his dicussion.

Appendix.

Fig. A1 shows micrographs recoded during a HPMCP microencapsulation batch process as described in (Weiß et al., 1995a).

References

Alvarez, A.J., Myerson, A.S., 2010. Continuous plug flow crystallization of pharmaceutical compounds. Am. Chem. Soc.

Arshady, R., 1990. Microspheres and microcapsules, a survey of manufacturing techniques. Part II: coacervation. Polym. Eng. Sci. 30, 905–914.

Besenhard, M.O., Hohl, R., Hodzic, A., Eder, R.J.P., Khinast, J.G., 2014. Modeling a seeded continuous crystallizer for the production of active pharmaceutical ingredients. Cryst. Res. Technol. 49, 92–108.

Bungenberg, H.G., Jong, D., Kruyt, H.R., 1929. .

Cunningham, J., Nuneviller, F., Rajabi-Siahboomi, A.R., 2010. Evaluation of recent advances in continuous film coating processes. Drug Dev. Ind. Pharm. 36, 227–233.

Dalmoro, A., Barba, A.A., Lamberti, G., d'Amore, M., 2012. Intensifying the microencapsulation process: ultrasonic atomization as an innovative approach. Eur. J. Pharm. Biopharm. 80, 471–477.

Dong, W., Bodmeier, R., 2006. Encapsulation of lipophilic drugs within enteric microparticles by a novel coacervation method. Int. J. Pharm. 326, 128–138.

Eder, R.J.P., Radl, S., Schmitt, E., Innerhofer, S., Maier, M., Gruber-Woelfler, H., Khinast, J.G., 2010. Continuously seeded, continuously operated tubular crystallizer for the production of active pharmaceutical ingredients. Cryst. Growth Des. 10, 2247–2257.

Eder, R.J.P., Schmitt, E.K., Grill, J., Radl, S., Gruber-Woelfler, H., Khinast, J.G., 2011. Seed loading effects on the mean crystal size of acetylsalicylic acid in a continuous-flow crystallization device. Cryst. Res. Technol. 46, 227–237.

Eder, R.J.P., Schrank, S., Besenhard, M.O., Roblegg, E., Gruber-Woelfler, H., Khinast, J.G., 2012. Continuous sonocrystallization of acetylsalicylic acid (ASA): control of crystal size. Cryst. Growth Des. 12, 4733–4738.

Elkharraz, K., Ahmed, A.R., Dashevsky, A., Bodmeier, R., 2011. Encapsulation of water-soluble drugs by an o/o/o-solvent extraction microencapsulation method. Int. J. Pharm. 409, 89–95.

FDA, 2014. Guidance for Industry: PAT—A Framework for Innovative Pharmaceutical Development, Manufacturing, and Quality Assurance. Pharmaceutical CGMPs.

Feng, C., Song, R., Sun, G., Kong, M., Bao, Z., Li, Y., Cheng, X., Cha, D., Park, H., Chen, X., 2014. Immobilization of coacervate microcapsules in multilayer sodium alginate beads for efficient oral anticancer drug delivery. Biomacromolecules 15, 985–986.

P. Ferrero, 1993. Patent, EP0545065.

Filippa, M.A., Gasull, E.I., 2013. Ibuprofen solubility in pure organic solvents and aqueous mixtures of cosolvents: interactions and thermodynamic parameters relating to the solvation process. Fluid Phase Equilib. 354, 185–190.

Ganderton, D., Jones, T., McGinity, J., Nairm, J.G., 1995. 3 Coacervation-phase separation technology. Adv. Pharm. Sci. 7, 93–219.

Ghosh, S.K., 2006. Functional Coatings. FRG: Wiley-VCH Verlag GmbH & Co., KGaA, Weinheim.

Goršek, A., Glavič, P., 1997. Design of batch versus continuous processes. Chem. Eng. Res. Des. 75, 718–723.

Gouin, S., 2004. Microencapsulation. Trends Food Sci. Technol. 15, 330–347.

Gracin, S., Rasmuson, Å.C., 2002. Solubility of phenylacetic acid, *p*-hydroxyphenylacetic acid, *p*-aminophenylacetic acid, *p*-hydroxybenzoic acid, and ibuprofen in pure solvents. J. Chem. Eng. Data 47, 1379–1383.

He, Z., Jamison, T.F., 2014. Continuous-flow synthesis of functionalized phenols by aerobic oxidation of Grignard reagents. Angew. Chem. Int. Ed. Engl. 53, 3353–3357.

Hirech, K., Payan, S., Carnelle, G., Brujes, L., Legrand, J., 2003. Microencapsulation of an insecticide by interfacial polymerisation. Powder Technol. 130, 324–330.

Im, H.-Y., Sah, H., 2009. Ammonolysis-based microencapsulation technique using isopropyl formate as dispersed solvent. Int. J. Pharm. 382, 130–138.

P. Tabeling, Innovations in coating technology, 2008. Recent Patents Drug Deliv Formul., 2, 209-230.

M. Jacob, K. Rümpler, M. Waskow, 2006. Patent US2006228661.

Jiang, M., Zhu, Z., Jimenez, E., Papageorgiou, C.D., Waetzig, J., Hardy, A., Langston, M., Braatz, R.D., 2014. Continuous-flow tubular crystallization in slugs spontaneously induced by hydrodynamics. Cryst. Growth Des. 14, 851–860.

Jyothi, N.V.N., Prasanna, P.M., Sakarkar, S.N., Prabha, K.S., Ramaiah, P.S., Srawan, G.Y., 2010. Microencapsulation techniques, factors influencing encapsulation efficiency. J. Microencapsul. 27, 187–197.

Kang, H.W., Leem, J., Yoon, S.Y., Sung, H.J., 2014. Continuous synthesis of zinc oxide nanoparticles in a microfluidic system for photovoltaic application. Nanoscale 6, 2840–2846.
Kawase, M., Miura, K., 2007. Fine particle synthesis by continuous precipitation using a tubular reactor. Adv. Powder Technol. 18, 725–738.
Klinzing, G., Bell, T.A., 2005. Challenges in the scale-up of particulate processes—an industrial perspective. Powder Technol. 150, 60–71.
Kondo, K., Niwa, T., Danjo, K., 2014. Preparation of sustained-release coated particles by novel microencapsulation method using three-fluid nozzle spray drying technique. Eur. J. Pharm. Sci. 51, 11–19.
Kopetzki, D., Lévesque, F., Seeberger, P.H., 2013. A continuous-flow process for the synthesis of artemisinin. Chemistry 19, 5450–5456.
Kröber, H., Teipel, U., 2005. Microencapsulation of particles using supercritical carbon dioxide. Chem. Eng. Process. Process Intensif. 44, 215–219.
Lévesque, F., Seeberger, P.H., 2011. Highly efficient continuous flow reactions using singlet oxygen as a 'green' reagent. Org. Lett. 13, 5008–5011.
Lawton, S.C., Steele, G., Shering, P., Zhao, L., Laird, I., Ni, X.-W., 2009. Continuous crystallization of pharmaceuticals using a continuous oscillatory baffled crystallizer. Org. Proc. Res. Dev. 13, 1357–1363.
Leuenberger, H., 2001. New trends in the production of pharmaceutical granules: batch versus continuous processing. Eur. J. Pharm. Biopharm. 52, 289–296.
Li, M., Rouaud, O., Poncelet, D., 2008. Microencapsulation by solvent evaporation: state of the art for process engineering approaches. Int. J. Pharm. 363, 26–39.
R. Liborius, 1993. Patent US5648118.
L.S. Lyons, S.G. Wright, 2001. Patent US6331317.
Malet-Sanz, L., Susanne, F., 2012. Continuous flow synthesis. A pharma perspective. J. Med. Chem. 55, 4062–4098.
Mascia, S., Heider, P.L., Zhang, H., Lakerveld, R., Benyahia, B., Barton, P.I., Braatz, R.D., Cooney, C.L., Evans, J.M.B., Jamison, T.F., Jensen, K.F., Myerson, A.S., Trout, B.L., 2013. End-to-end continuous manufacturing of pharmaceuticals: integrated synthesis, purification, and final dosage formation. Angew. Chem. Int. Ed. Engl. 52, 12359–12363.
Michel, B., Greaney, M.F., 2014. Continuous-flow synthesis of trimethylsilylphenyl perfluorosulfonate benzyne precursors. Org. Lett. 16, 2684–2687.
Montante, G., Pinelli, D., Magelli, F., 2003. Scale-up criteria for the solids distribution in slurry reactors stirred with multiple impellers. Chem. Eng. Sci. 58, 5363–5372.
Närhi, M., Nordström, K., 2005. Manufacturing, regulatory and commercial challenges of biopharmaceuticals production: a Finnish perspective. Eur. J. Pharm. Biopharm. 59, 397–405.
Nakagawa, K., Nagao, H., 2012. Microencapsulation of oil droplets using freezing-induced gelatin–acacia complex coacervation. Colloids Surf. A Physicochem. Eng. Asp. 411, 129–139.
D. O'Hara, J. Marjeram, 2006. Patent WO06108280.
Petschacher, C., Eitzlmayr, A., Besenhard, M., Wagner, J., Barthelmes, J., Bernkop-Schnürch, A., Khinast, J.G., Zimmer, A., 2013. Thinking continuously: a microreactor for the production and scale-up of biodegradable, self-assembled nanoparticles. Polym. Chem. 4, 2342.
Phares, R.E., Sperandio, G.J., 1964. Coating pharmaceuticals by coacervation. J. Pharm. Sci. 53, 515–518.
Plumb, K., 2005. Continuous processing in the pharmaceutical industry. Chem. Eng. Res. Des. 83, 730–738.
R. Pommersheimer, 2005. Patent WO2005094980 A1.
Qiu, Y., Chen, Y., Zhang, G.G.Z., Liu, L., Porter, W.R., Strong, J., 2009. Scale-up of pharmaceutical manufacturing operations of solid dosage forms. Developing Solid Oral Dosage Forms 615–636.
K. Rümpler, M. Jacob, M. Waskow, 2006. Patent US2006035022.
Reinhold, A., Briesen, H., 2012. Numerical behavior of a multiscale aggregation model—coupling population balances and discrete element models. Chem. Eng. Sci. 70, 165–175.
Roberge, D.M., Ducry, L., Bieler, N., Cretton, P., Zimmermann, B., 2005. Microreactor technology: a revolution for the fine chemical and pharmaceutical industries? Chem. Eng. Technol. 28, 318–323.
Roberge, D.M., Bieler, N., Mathier, M., Eyholzer, M., Zimmermann, B., Barthe, P., Guermeur, C., Lobet, O., Moreno, M., Woehl, P., 2008. Development of an industrial multi-injection microreactor for fast and exothermic reactions – Part II. Chem. Eng. Technol. 31, 1155–1161.
Salaün, F., Vroman, I., Aubry, C., 2009. Preparation of double layered shell microparticles containing an acid dye by a melt dispersion–coacervation technique. Powder Technol. 192, 375–383.
Shimokawa, K., Saegusa, K., Wada, Y., Ishii, F., 2013. Physicochemical properties and controlled drug release of microcapsules prepared by simple coacervation. Colloids Surf. B 104, 1–4.
Suzzi, D., Toschkoff, G., Radl, S., Machold, D., Fraser, S.D., Glasser, B.J., Khinast, J.G., 2012. DEM simulation of continuous tablet coating: effects of tablet shape and fill level on inter-tablet coating variability. Chem. Eng. Sci. 69, 107–121.
Tabeling, P., 2005. Introduction to Microfluids.
Taboadaserrano, P., Chin, C., Yiacoumi, S., Tsouris, C., 2005. Modeling aggregation of colloidal particles. Curr. Opin. Colloid Interface Sci. 10, 123–132.
Teunou, E., Poncelet, D., 2002. Batch and continuous fluid bed coating–review and state of the art. J. Food Eng. 4, 325–340.
Vervaet, C., Remon, J.P., 2005. Continuous granulation in the pharmaceutical industry. Chem. Eng. Sci. 60, 3949–3957.
Wahab, B., Ellames, G., Passey, S., Watts, P., 2010. Synthesis of substituted indoles using continuous flow micro reactors. Tetrahedron 66, 3861–3865.
Wang, S., Song, Z., Wang, J., Dong, Y., Wu, M., 2010. Solubilities of ibuprofen in different pure solvents. J. Chem. Eng. Data 55, 5283–5285.
Weiß, G., Knoch, A., Laicher, A., Stanislaus, F., Daniels, R., 1993. Microencapsulation of ibuprofen by a coacervation process using Eudragit L100-55 as an enteric polymer. Drug Dev. Ind. Pharm. 19, 2751–2764.
Weiß, G., Knoch, A., Laicher, A., Stanislaus, F., Daniels, R., 1995a. Simple coacervation of hydroxypropyl methylcellulose phthalate (HPMCP) I. Temperature and pH dependency of coacervate formation. Int. J. Pharm. 124, 87–96.
Weiß, G., Knoch, A., Stanislaus, F., Daniels, R., 1995b. Simple coacervation of hydroxypropyl methylcellulose phthalate (HPMCP) II. Microencapsulation of ibuprofen. J. Pharm. 124, 97–105.
Weiß, G., 1991. Mikroverkapselung von Ibuprofen mit Magensaftresistenten Polymeren Durch Einfache Koazervation. Universität Regensburg.
Wu, J., Kozak, J.A., Simeon, F., Hatton, T.A., Jamison, T.F., 2014. Mechanism-guided design of flow systems for multicomponent reactions: conversion of CO_2 and olefins to cyclic carbonates. Chem. Sci. 5, 1227.
Yadav, A.K., Barandiaran, M.J., de la Cal, J.C., 2012. Synthesis of water-borne polymer nanoparticles in a continuous microreactor. Chem. Eng. J. 198, 191–200.

4. Crystal Size Tuning via a Feedback Controlled Tubular Crystallizer [2]

M. O. Besenhard[1,2], P.Neugebauer[3], C. D. Ho[3], J. G. Khinast[1,3*]

1 Research Center Pharmaceutical Engineering (RCPE) GmbH, 8010 Graz, Austria

2 Siemens AG, Corporate Technology, Graz, 8054 Graz, Austria

3 Graz University of Technology, Institute for Process and Particle Engineering, 8010 Graz, Austria

* Corresponding author. Tel.: +43 (316) 873 – 30400; Fax: +43 (0) 316 /873-30402; E-mail address: khinast@tugraz.at

Abstract:

This paper describes a simple model-free control strategy for crystal size tuning in a continuously operated tubular crystallizer. The crystallizer is designed for a seeded cooling crystallization process and acetylsalicylic acid crystallization from an ethanol solution was used as model system. Using a crystal size distribution (CSD) analyzer and minor initial studies, we developed a feedback controller that accurately tuned the mean crystal size within the range of $90 - 140 \mu m$. In addition, we created a cleaning concept for long-term runs based on a consistency study, which demonstrated that the CSD of the products remained robust when process settings were kept constant. To ensure seed crystals with a narrow size distribution we used ultrasound irradiation for seed generation.

Keywords:

Crystallization, continuous crystallization, crystal size tuning, online CSD determination, feed-back control, tubular reactor

[2] This chapter is formatted as it is, since it is primed for a submission to a peer reviewed journal.

4.1 Introduction

The purity of organic materials is an essential quality parameter in many manufacturing processes, including the food, fine-chemical and pharmaceutical industries [1][2]. Due to its efficiency and the relatively low capital and operating costs, crystallization from solution is a common unit operation for the purification of solid particles via phase separation [3][4]. In pharmaceutical manufacturing polymorphism and crystal size/ shape control during crystallization are critical as well, since they affect downstream operations (such as flowability [5], filtration [6], segregation phenomena [7][8], blending [9], capsule filling [10], tabletability [11]) and the dissolution[12] and disintegration rate in the body [13][14]. Hence, significant efforts have been devoted to crystal engineering and the associated crystallization processes. In addition, control of crystallization processes has become increasingly important [15]. In this respect, major advances in solution crystallization control were made due to *in situ* real-time sensor technologies [16][17], faster computers and better control hardware [18].

The objective of most control strategies for crystallizers is to optimize the crystal size distribution (CSD) or the crystal shape and size distribution (CSSD) [15][19][20], to minimize the variability and the yield [21][22] and to maximize the polymorphic purity [23][24][25]. For controlling the CSSD, the most common control variables are temperature trajectories [26][27][24][28][29] (including temperature cycling [30][23]), seeding strategies [31][32] and anti-solvent addition rates or combinations thereof [33][34]. Recently, the addition of crystal growth modifiers was used to achieve the desired crystal shape [35].

Since crystallization processes are highly nonlinear and complex, linear controllers do not provide sufficient control. Thus, model-based control systems are of interest. As a general framework for crystallization modeling, population balance equations (PBE) are frequently applied in nonlinear control methodologies. By coupling these hyperbolic partial differential equations with mass and energy balances, PBEs predict either the CSD (if univariate [36][37]) or the CSSD (if multivariate [29][38][39]). Nevertheless, PBE require parameters for crystal growth, as well as nuclea-

tion/aggregation and breakage rates. These parameters need to be estimated from experimental data [40].

Several model-free approaches have been proposed for crystallization control. The most common ones are direct nucleation control (DNC) [41][30] and concentration feedback control (CFC) [43][44][34]. The idea of DNC is to keep the number of crystals at a constant value during the process such that the product crystal size can be tuned via the number of crystals: the lower the number, the larger the product crystals. CFC is feasible when an accurate *in situ* concentration analyzer, e.g., an IR spectrometer equipped with an attenuated total reflection (ATR) probe, is available. The concept of CFC is to adjust the manipulated variable in order to follow a target supersaturation (frequently fixed at a constant value), which requires knowledge of the metastable zone. CFC is a robust control strategy and is particularly applicable to polymorphic crystallization processes [20].

Tubular crystallization reactors have attracted significant interest in the crystallization field since they can eliminate problems such as inhomogeneous mixing. Moreover, they eliminate the need for rapid stirring, and thus, high shear rates. The high surface-to-volume ratio (compared to stirred-tank crystallizers) facilitates rapid heat exchange and provides accurate control of the temperature of processed medium [46] and the super-saturation profile [44] [45] [47]. Furthermore, tubular reactors are designed for continuous processing which follows the trend of continuous manufacturing [48].A well-known tubular reactor design is the continuous oscillatory baffled crystallizer (OBC) with a piston to agitate the crystal slurry in a long pipe with baffles [49][50][51]. Other tubular crystallizers are designed for seeded [52], self-seeded [53], laminar [54][55][56][57] or plug flow [29][58][59][52], which is commonly achieved via segmenting the slurry into liquid slugs by adding an immiscible fluid

This paper presents a simple but efficient control strategy that facilitates accurate tuning of crystal sizes in seeded tubular crystallizers equipped with a CSD analyzer. Flexible tuning of the mean crystal size within a broad range was shown on the basis of a seeded cooling crystallization process of acetylsalicylic acid (ASA) from an ethanol (EtOH) solution performed in a laminar flow tubular crystallizer (LFTC). It was shown that manipulating the feed rate of the seed suspension is sufficient to tune the

CSD via a model-free feedback controller, developed based on marginal experimental studies. By virtue of a cleaning concept it was possible to perform long-term runs and proof that the product CSD remains robust when process settings are kept constant.

4.2 Materials and methods

4.2.1 Materials

G. L. Pharma GmbH provided acetylsalicylic acid (Rhodine 3020, pharmaceutical grade, M = 180.16 g/mol). Ethanol (96 % denaturized with 1 % methyl ethyl ketone, M = 46.07 g/mol) was purchased from Roth (Lactan). Polysiloxane tubings with an inner diameter (d_{in}) of 2.0 mm and an outer diameter (d_{out}) of 4.0 mm were used for the tubular reactor. Straight and Y-fittings (PTFE, $d_{in} = 2.0$ mm) were used to assemble the tubular reactor. Filtration was performed via filter cycles with pore sizes of $> 4\ \mu m$ (Carl Roth – MN 616).

4.2.2 Process equipment

Three peristaltic pumps, P I (Ismatec Reglo MS 2/6V 1.13C; tubing: PHARMED$^{(R)}$ $d_{in} = 2.8$ mm, $d_{out} = 5.0$ mm) P II (Reglo Digital MS-2/6V 1.13C; tubing: PHARMED$^{(R)}$ $d_{in} = 2.8$ mm, $d_{out} = 5.0$ mm) and P III (Heidolf Pumpdrive 5106; tubing: con $d_{in} = 1.6$ mm, $d_{out} = 4.8$ mm), and a gear pump P IV (Ismatec MCP-Z Process IP65) were used in the tubular reactor and the CSD analyzer. Magnetic (m&m international; 8250 24/DC) and tube pitch (Fluid Concept; Sirai S105) valves were used to switch between process-, measuring- or cleaning-modes. Temperatures were controlled via six thermostatic bathes: B I – B VI (LAUSA Type E 111, Ecoline Star edition and four LAUDA A 24). Sonication was performed in an ultrasonic bath (Elma Transonic 460; 35 kHz). The pressure within the tubing was recorded with the aid of a piezoelectric probe (Hygrosens, DRTR-AL-10V-R1B6). During the process, the CSD was analyzed using the Particle counter TCC$^{(R)}$ (Markus Klotz GmbH) equipped with a $1\ mm^3$ measuring chamber that operated by extinction of (laser) light caused by single particles passing the chamber, as described in detail in [60]. Process control and monitoring (i.e., switching valves, analyzing CSD, computing pump rates, adjusting pump settings, displaying the current pressure) were achieved via the process control software SIPAT (Siemens AG), using Matlab (Mathworks UK)

functions. Communication with the pressure probe and valves was enabled through a USB board (Arduino; Arduino Uno).

4.2.3 Generating the seed suspension

An ultrasound-assisted seed generation method was used to produce sufficiently small seed crystals with a low fraction of fines ($< 10\ \mu m$). A schematic representation of the method and an image of the generated crystals are shown in Figure . ASA was dispersed in EtOH at a ratio of $c_{seed\ susp.} = 0.3\ {}^{g_{ASA}}/_{g_{EtOH}}$ and dissolved in a round bottom flask at $\approx 40°C$ in $500\ mL$. Subsequently, the solution was cooled to $20\ °C$ before starting ultrasound irradiation at $35\ kHz$. At this temperature, the solution had a level of supersaturation of $S \equiv c/c^* = 1.4$. The ultrasound irradiation was stopped $60 - 70\ s$ after the first signs of precipitates appearing (i.e., when the solution became slightly milky). Longer irradiation times yielded smaller seed crystals. Each seed generation run is hereinafter referred to as a seed batch.

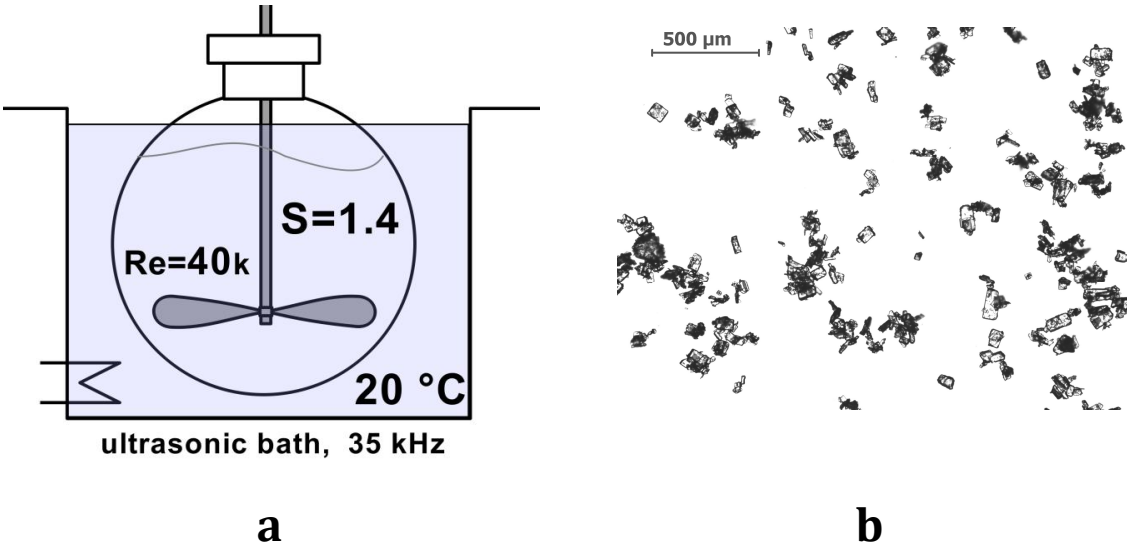

Figure 1: (a) Schematic of the seed generation procedure via sonocrystallization. (b) Image of seed crystals

4.2.4 Setup

A schematic of the tubular crystallizer setup is shown in Figure 2. The process settings of the described setup are listed in Table 1. The design of the tubular reactor was similar to the one presented in previous studies [44][45]. This paper also describes a seeded cooling crystallization process of ASA from an EtOH solution.

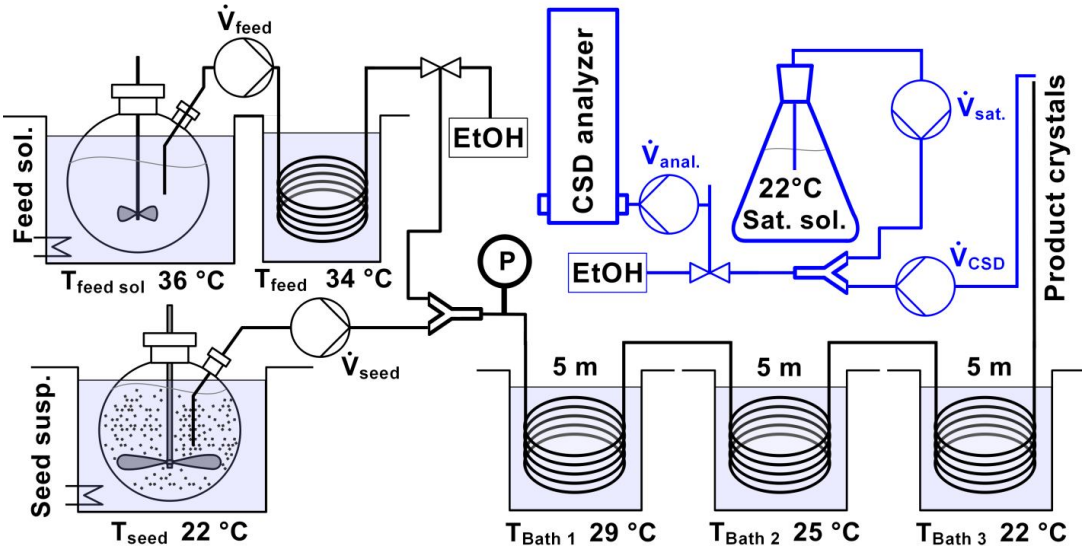

Figure 2: Schematic process representation of the tubular crystallizer (black) including the implementation of the online CSD-analyzer (blue)

To ensure complete dissolution of ASA, an ASA-EtOH feed solution (*Feed sol.*) with a concentration of $c_{feed\ sol.} = 0.4\ {}^{g_{ASA}}/_{g_{EtOH}}$ was kept at $T_{feed\ sol} = 36 \pm 0.2$ °C (B I)in a storage vessel. The ASA-EtOH seed suspension (*Seed susp.*), which was produced as described in Section 2.3, was stirred at $T_{seed} = 22 \pm 0.2$ °C (B II). Peristaltic pumps introduced the feed solution (P I) and the seed suspension (P II) into the crystallizer via a Y-fitting. Before entering the Y-fitting, a thermostatic bath was used to bring the feed solution to $T_{feed} = 34 \pm 0.2$ °C (B III). The tubular crystallizer itself consisted of a $15\,m$ tube subsequently cooled via three thermostatic bathes (B IV: $T_{Bath\,1} = 29\,°C$, B V: $T_{Bath\,2} = 25°C$, B VI: $T_{Bath\,3} = 22\,°C$). The supersaturation level past the Y-fitting was determined based on the feed solution concentrations, feed and seed pump rates $\dot{V}_{feed}$ & $\dot{V}_{seed}$ (yielding the mixture concentration) and tures T_{feed} & T_{seed}. These settings had to be selected such as to introduce slightly su-

persaturated slurry into the crystallizer and thereby prevent nucleation events and the dissolution of seed crystals.

After the product slurry exits the tubular crystallizer samples are withdrawn ($\dot{V}_{CSD}$) for online CSD analysis (see Fig. 2). Before entering the measuring chamber, the withdrawn slurry is diluted with a saturated solution ($\dot{V}_{sat.}$) to avoid multiple particles passing the measuring chamber simultaneously. For each CSD measurement, the diluted product slurry is pumped through the CSD analyzer ($\dot{V}_{anal.}$) for 45 s. Subsequently, the measuring cell is rinsed with EtOH for 45 s. Due to the operating principle of the CSD analyzer, smaller crystals require extreme dilution with a saturated solution. That is why only the product CSD was evaluated.

A pressure probe (labeled **P** in Figure 2) was installed right next to the Y-fitting, i.e., at the entrance of the tubular reactor. Initial experiments with microcrystalline cellulose in water showed that the recorded pressure could indicate the amount of solid material within the tubing and irregularities in the process operation (Figure 3). Regarding the process stability, it is especially important to avoid the insertion of gas bubbles. If air bubbles enter the crystallizer they accumulate solid mass during their transport through the tubing (see insert in Figure 3). Therefore, the insertion of gas bubbles does not only change the residence time distribution and the collision rate of crystals in the crystallizer but tend to result in tube plugging, even in the absence of supersaturation. The incorporation of a gas bubble can easily be monitored via a pressure probe because of the accompanied sharp pressure increase.

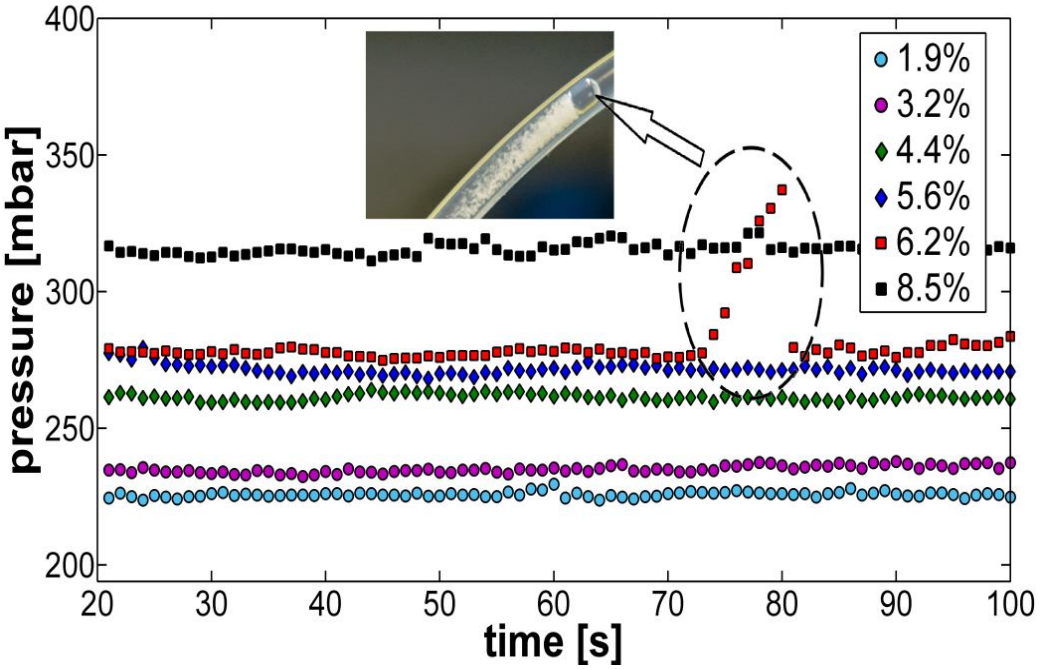

Figure 3: Pressure values recorded while pumping slurries (micro crystalline cellulose in water) of various solid mass fractions ($g_{solid\ material}/g_{slurry}$) through the reactor. The highlighted increase for the solid mass fraction of 6.2 % *originates from an air bubble moving through the tube, as shown in the insert.*

Crusting is another major factor in terms of process stability: crusting on the reactor's wall creates bottle necks that inhibit the transport of particles into the reactor and lead to pipe plugging. To prevent plugging, we rinsed the crystallizer with the solvent (EtOH) at regular intervals ($\approx 10\ min$). The productive time intervals between these cleaning cycles are hereinafter referred to as slots. For each slot, the CSD was determined at least in triplicate.

Table 1: Process settings

Symbol	Description	Value
$c_{feed\ sol.}$	ASA concentration feed solution	0.45 g_{ASA}/g_{EtOH}
$c_{seed\ susp.}$	ASA concentration seed suspension	0.30 g_{ASA}/g_{EtOH}
T_{seed}	Temperature seed suspension	22 °C
T_{feed}	Temperature feed solution	36 °C
$T_{Bath\ 1}, T_{Bath\ 2}, T_{Bath\ 3}$	Temperatures of the thermostatic bathes	29 °C, 25 °C, 22 °C
$\dot{V}_{feed}$	Pump rate feed suspension	22 ml/min
$\dot{V}_{seed}$	Pump rate seed suspension	6 ml/min (if not manipulated)
$\dot{V}_{CSD}$	Pump rate - product slurry withdrawal	6 ml/min
$\dot{V}_{sat}$	Pump rate - saturated solution (ASA in EtOH)	$50 - 60\ ml/min$
$\dot{V}_{anal}$	Pump rate - diluted product slurry for CSD analysis	$22 ml/min$

4.2.5 Feedback control

Several process settings (e.g., feed rated, temperatures, seed loadings, etc.) can be used to control the mean product crystals size L_{mean}. The pump rate of the feed solution and the seed suspension can be the manipulated variables since they can easily be changed. As mentioned above, the supersaturation level past the first Y-fitting, which is determined by the feed solution's and seed suspension's pump rates and temperatures, needs to be kept slightly above one (i.e., supersaturated). Increasing the feed rate of the seed suspension yields a decrease in the temperature past the Y-fitting ($T_{seed} < T_{feed}$). Since the seed suspension is saturated, the concentration of

dissolved ASA in the seed suspension is determined by its temperature. The solubility of ASA in the EtOH (96 %) was known from previous studies [52]. At T_{seed} the saturation concentration is approximately $c^*(22\,°C) = 0.24\ {}^{g_{ASA}}/_{g_{EtOH}}$, which is much lower than the concentration of dissolved ASA in the feed solution (see table 1). An increase in $\dot{V}_{seed}$ caused a decrease in temperature past the Y-fitting and a decrease in the amount of dissolved ASA past the Y-fitting. Due to this compensation, the supersaturation past the first Y-fitting varies only slightly with $\dot{V}_{seed}$, as shown in Figure 4, which makes manipulations of the seed pump rate feasible. This interplay between the temperature and the dissolved ASA applies similarly to the feed solution pump rate $\dot{V}_{feed}$. In the present work we selected $\dot{V}_{seed}$ as the only manipulated variable for crystal size control purposes and the first moment of q_0, i.e., the mean crystal size $L_{mean,q0}$, as the controlled variable.

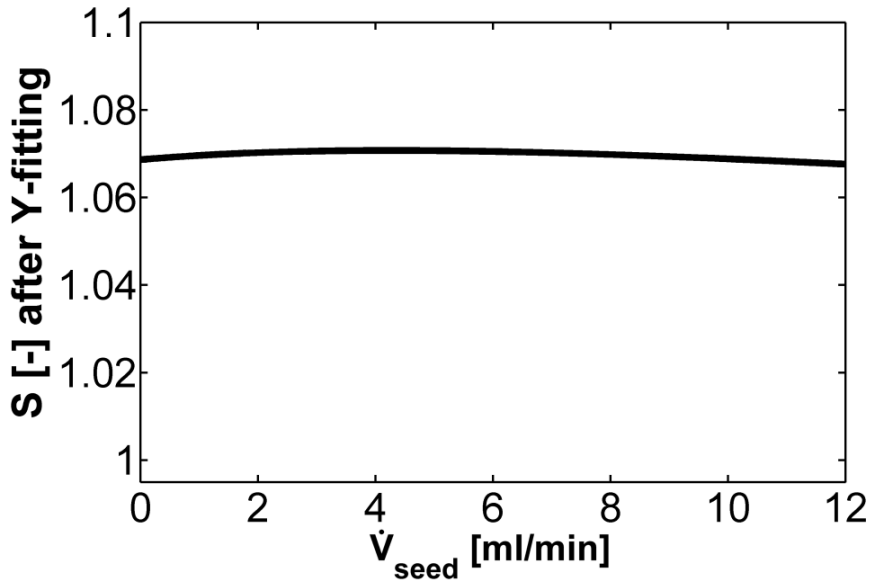

Figure 4: Level of supersaturation after the Y-fitting, depending on the seed solution pump rate.

Initial studies were performed to evaluate the effect of changes in $\dot{V}_{seed}$ on $L_{mean,q0}$. The CSD and $L_{mean,q0}$ were recorded for five seed suspension pump rates using the same seed batch (Figure 5, *Top*). Based on these results, a *generic response function* $\tilde{L}_{mean,q0}(\dot{V}_{seed})$ was defined, as shown in Figure 6, *Bottom*. A control strategy was

developed based on $\tilde{L}_{mean,q0}(\dot{V}_{seed})$ in order to adjust $\dot{V}_{seed}$ according to the difference ε between the target crystal size ($L_{mean,q0\ target}$) and the measured crystal size ($L_{mean,q0\ measured}$).

The control was operated from slot to slot. Hence, the setting of the seed suspension pump rate for the next slot ($i+1$) was updated based on the setting and measured crystal size of the current slot (i). First $\tilde{L}_{mean,q0\ target}$, i.e., the mean crystal size of the generic response function corresponding to an increase by ε, was calculated as stated in Equations 1-2. The new seed suspension pump rate ($\dot{V}_{\text{seed i+1}}$) followed from the value assigned to the response function at $\tilde{L}_{\text{mean,q0 target}}$, see Equation 3.

$$\varepsilon = L_{mean,q0\ target} - L_{mean,q0\ measured} \tag{1}$$

$$\tilde{L}_{mean,q0\ target} = \tilde{L}_{mean,q0}(\dot{V}_{seed\ i}) + \varepsilon \tag{2}$$

$$\tilde{L}_{mean,q0}(\dot{V}_{seed\ i+1}) = \tilde{L}_{mean,q0\ target} \tag{3}$$

$$\rightarrow \dot{V}_{seed\ i+1}$$

The response function was obtained solely from experiments using the same seed batch, which is a simplification since $L_{mean,q0}$ depends on the seed CSSD. Nevertheless, this simple feedback control strategy is effective as long as the mean crystal size response to the seed suspension pump rate shows a monotonic decrease (i.e., higher seed pump rates yield smaller mean crystal sizes).

$L_{mean,q0\ measured}$ was determined by averaging the mean crystal sizes recorded during one slot. New seed suspension pump rates were applied to the next slot, i.e., the feedback control of the tubular crystallizers was operated from slot to slot. In order to screen for erroneous measurements (e.g., due to insufficient dilutions in the measuring chamber), two tests were performed to analyze the CSD measurements.

1. For each CSD measurement at most 30 000 particles were counted (the analysis time was 45 s).
2. A χ^2-test was executed as follows:

$$\chi^2 = \sum_{i_{min}}^{i_{max}} \frac{N_i - n_{0i}}{n_{0i}} \tag{4}$$

For the χ^2-test, the CSD was represented by 20 equally-sized bins between $i_{min} = 35\mu m$ and $i_{max} = 425\mu m$. N_i is the measured number of particles in the i^{th} bin. n_{0i}, i.e., the expected number of particles in the i^{th} bin obtained by fitting a log-normal distribution to the measured CSD. Since the log-normal distribution described most CSDs with sufficient accuracy, Equation 4 was expected to produce higher values in the presence of outliers and faulty measurements. The test was passed if $\chi^2 < 1$. The crystal size was assumed to be "within the control window tuned if $\left|L_{mean,q0\ measured} - L_{mean,q0\ measured}\right| < 3\mu m$.

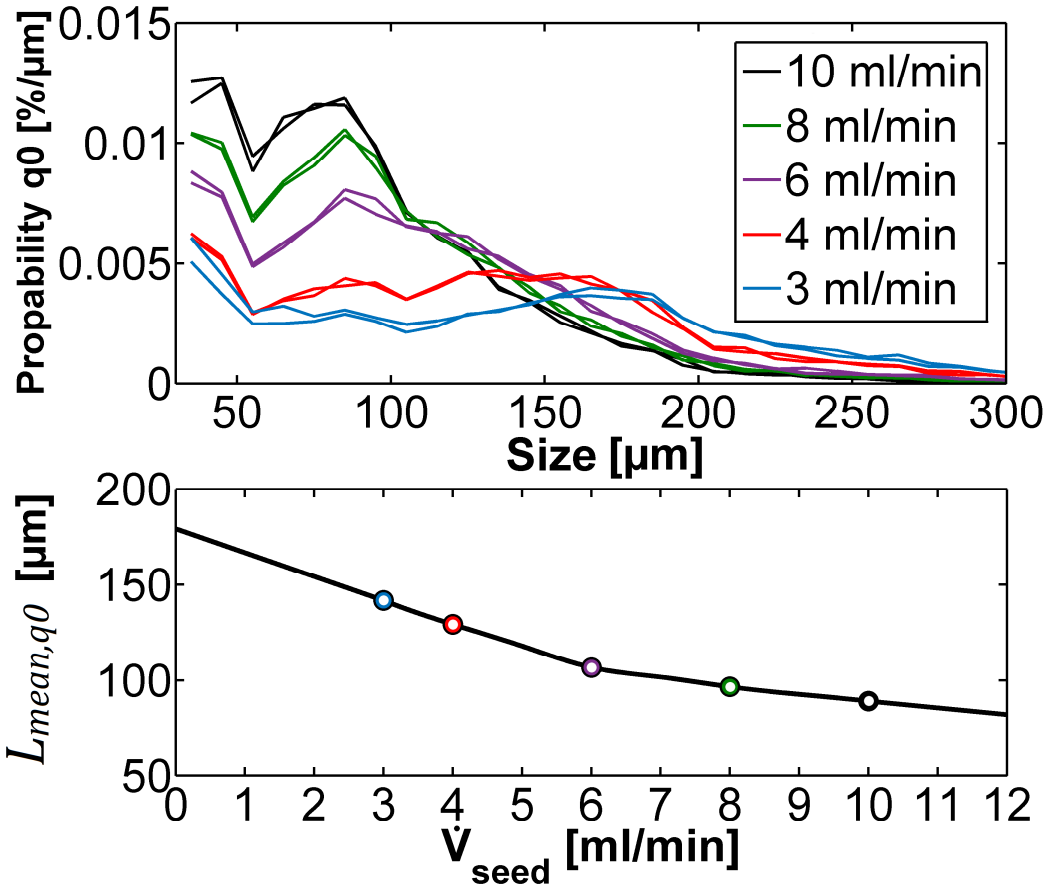

Figure 5: Determination of the response function $\tilde{L}_{mean,q0}(\dot{V}_{seed})$. Top; *CSDs recorded for five seed suspension pump rates (two per setting).* Bottom; *Response function obtained from the linear interpolation and extrapolation between and beyond the (averaged) measured mean crystal sizes.*

4.3 Results and discussion

4.3.1 Consistency of the tubular crystallizer

Before applying feedback control, the process setup was tested for robustness of the product CSD. The tubular crystallizer was operated for one hour, i.e., five slots, with the process settings listed in Table 1 and seeds from a single seed-batch. Figure 6 shows the measured CSDs. The results indicate that the crystallizer produced a robust particle size distribution. Throughout the entire run, deviations in $L_{mean,q0}$ were in the range of 5 μm and the pressure fluctuated only by 3 $mbar$, suggesting that process conditions that affect the CSD (e.g., pump rates, temperatures and the seed loading i.e., the solid mass fraction of the fed seed suspension) varied within an acceptable range. The sensitivity of the CSD analyzer was established by the initial studies of the feedback controller (Figure 5). As such, the presented setup can be assumed suitable for monitoring and controlling the mean crystal size.

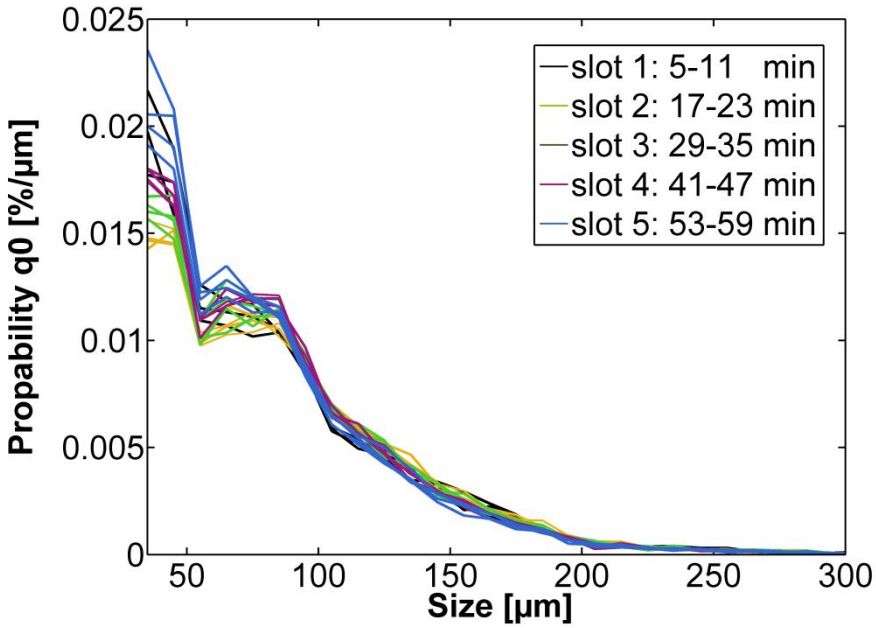

Figure 6: CSD measurements during a crystallization process lasting 1h operated with constant settings (see Table 1). $L_{mean,q0}$ *varied between* 85 μm *and* 80 μm *and the pressure was between* 285 $mbar$ *and* 282 $mbar$.

4.3.2 Tuning the mean crystal size to 140 µm

Figure 7 shows the results of two control experiments using different seed batches with the objective to tune $L_{mean,q0}$ to 140 µm. The pressure varied between $278 - 281\ mbar$ during Experiment 1 (Exp.1) and between $270 - 263\ mbar$ during Experiment 2 (Exp.2).

In both experiments, the tubular crystallizer was initially operated using the settings listed in Table 1, i.e., a seed suspension pump rate of 6 ml/min. With the feedback controller, the target mean crystal size was achieved after one manipulation of $\dot{V}_{seed}$ (one more slot) in Experiment 1 and two manipulations (2 more slots) in Experiment 2.

Slot 1 exhibits the mean crystal size in both experiments using identical process settings. $L_{mean,q0}$ was higher in Experiment 1 and the final seed pump rate (= the pump rate that yielded a $L_{mean,q0}$ value close enough to the target value) was lower in Experiment 2. The discrepancy between the two experiments was caused by different seeds. Ultrasound irradiation was applied for 70 s and 60 s to the seed batches in Experiment 1 and Experiment 2, respectively. As anticipated, for shorter irradiation time seed images indicated (CSD determined via ImageJ) that in Experiment 2 the seeds were bigger and had fewer fines (crystals < 10 µm) than those used in Experiment 1. Hence, Experiment 2 was expected to yield bigger product crystals in slot 1 and require a higher final seed pump rate assuming that the crystal size changes only occur via growth. However, this is in conflict with the experimental observations, indicating the presence of an additional mechanism that altered the CSD. It is known that the likelihood of aggregation (and agglomeration) events is higher if the crystals are smaller [3][61]. Since the experiment with smaller seeds produced larger product crystals, a considerable number of aggregation events seem plausible.

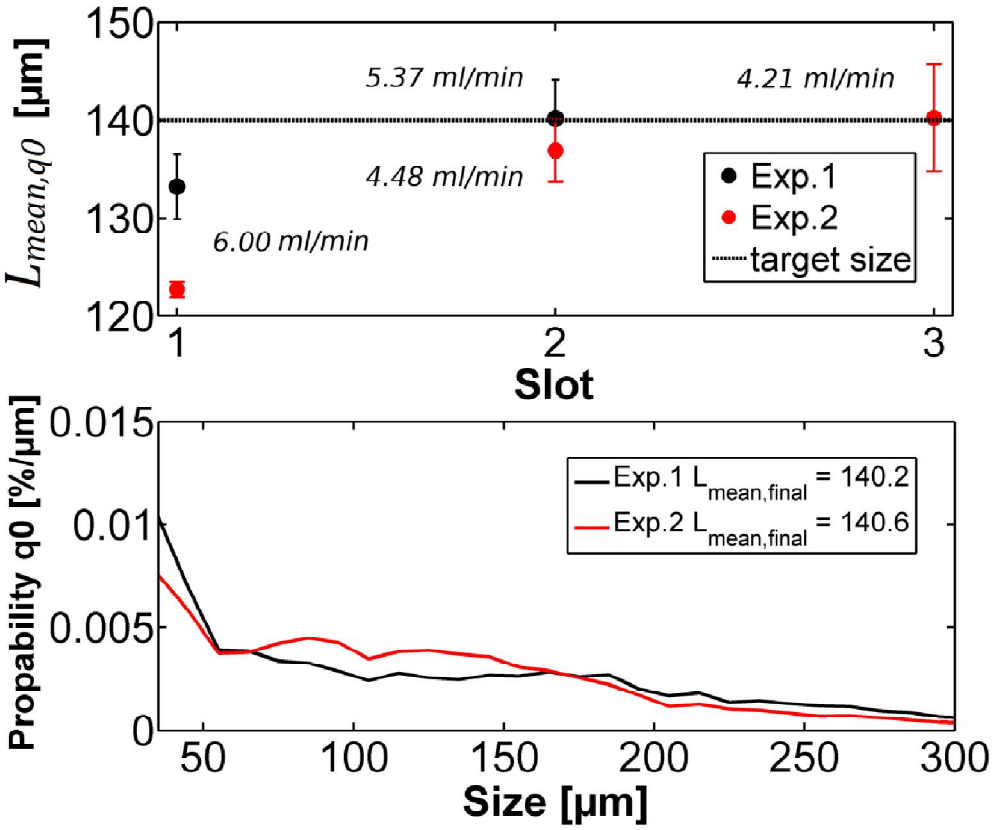

Figure 7: (top) Control of the mean crystal size value with a target value of $L_{mean,q0\ target} = 140\mu m$ *in two experiments.* Top; *Change in mean crystal sizes from slot to slot. The actual seed suspension pump rates are shown as well, and the error bars denote the standard deviations* $\sigma(L_{mean,q0})$ *for a slot; (Bottom) CSDs of the product crystals.*

4.3.3 Stepwise control of the mean crystal size

In order to further examine the feedback controller, the mean crystal size was tuned to five target values, starting at 130 µm and subsequently decreasing by 10 μm (i.e., 130 μm, 120 μm, 110 μm, 100 μm, 90 µm). The CSD of the successfully tuned product crystals and the control history, i.e., changes in $L_{mean,q0}$ from slot to slot, are shown in Figure 8 and Table 2. While achieving the target mean crystal size in the first two steps (130 μm & 120 μm) only required one $\dot{V}_{seed}$ manipulation, the following steps (110 μm & 100 μm) used three slots due to a seed change, since a new seed batch was used from slot 4 on. The last tuning step (100 μm) was again accomplished via a single $\dot{V}_{seed}$ manipulation. Images of the tuned product crystals are shown in Figure 9.

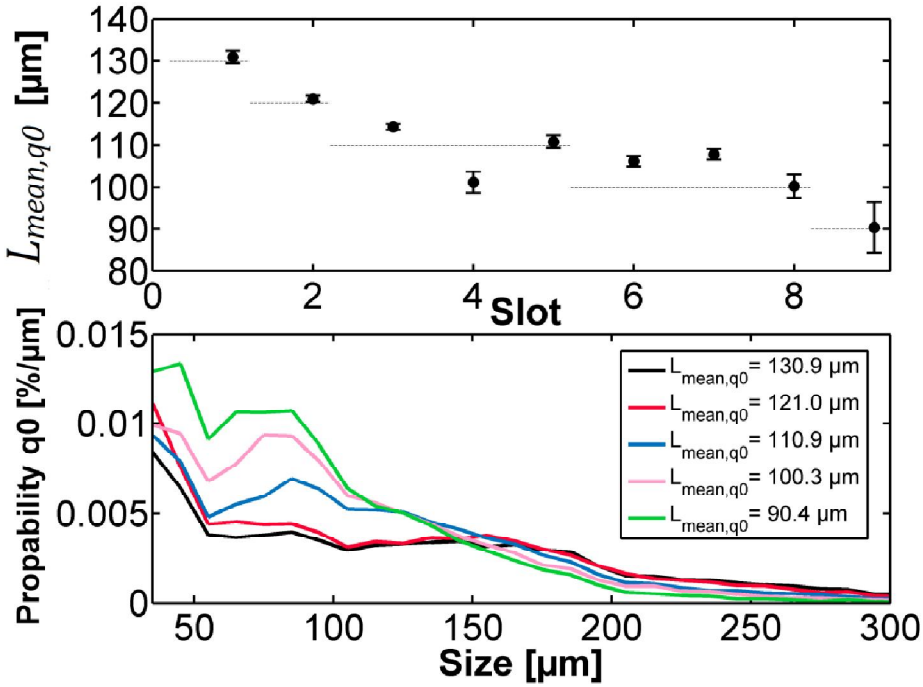

Figure 8: Stepwise control of the CSD, 130 µm → 120 µm → 110 µm → 100 µm → 90 µm. Top; *Change in the mean crystal sizes from slot to slot. The error bars denote the standard deviations* $\sigma(L_{mean,q0})$ *for a slot.* Bottom; *CSDs of the tuned product crystals.*

The pressure in the tube is dependent on the total flow rate ($\dot{V}_{seed} + \dot{V}_{sol}$) and the solid mass fraction (see Figure 3). In the first three slots, the recorded pressure decreased despite an increase in the total flow rate. Even though the solid mass fractions (percentage of solid material in the tubing) were not identical, the results indicated that the pressure rises distinctly when processing larger crystals.

In our previous study [44], we presented a mathematical process model for the cooling crystallization of ASA from EtOH 96% for the same reactor design (but with segmented flow rather than laminar flow in this work). This PBE-based process model was applied to calculate the mean crystal size for all seed pump rates during the stepwise tuning. For all simulations, the seed CSD was assumed to be uniformly distributed between 40 µm and 50 µm, and the solid mass fraction of ASA in the seed suspension was approximated by $g_{ASA\ solid}/mL_{seed\ suspension} = 0.042$ from the solubility of ASA in EtOH (96%) stated in [44]. The simulations only took crystal growth into account (i.e., no nucleation, aggregation or breakage). The obtained mean crystal sizes $L_{mean,q0\ simulated}$ are listed in Table 2. The simulated mean crystal sizes were not expected to match the results obtained during the control history since the pro-

cess model assumed the plug flow (i.e., that all crystals had the same residence time in the reactor) and since no accurate determination of the seed CSDs was available. Nevertheless, the discrepancy between the measured and simulated mean crystal sizes increased as the seed pump rate decreased. The lower $\dot{V}_{seed}$ became, the more the $L_{mean,q0\ simulated}$ underestimated the measured $L_{mean,q0}$. Since the process model only took crystal growth into account, this increasing discrepancy indicated that the CSD was affected by an additional mechanism that gains importance as the seed pump rates decreased. As discussed in Section 3.2, aggregation may play a significant role, especially if the crystals are small. In addition to the crystal size, the level of supersaturation is also known to affect and cause aggregation [62][63][52]. Figure 10 shows the supersaturation profiles obtained by the process model for three seed pump rates. As expected, the simulation results suggested that lower seed pump rates led to higher levels of the supersaturation, especially past the reactor inlet (where the crystals were smallest). Based on this, we assume that aggregation becomes more relevant when the seed pump rates decreased.

Based on the results shown in Figure 7 and Figure 8, the CSD measurements appear more consistent (as indicated by the standard deviations $\sigma(L_{mean,q0})$ within a slot) for smaller crystal sizes (< 130 μm). This was to be expected in the presence of aggregation: since aggregation events are less reproducible, they lead to variations in the CSD.

Table 2: Control settings for the stepwise tuning of the mean crystal size

Slot	$L_{mean,q0\ target}$ [μm]	$L_{mean,q0}$ [μm]	ε [μm]	$\dot{V}_{seed\ i}$ [ml/min]	P [$mbar$]	$L_{mean,q0\ simulated}$ [μm]
1	130	130.96	0.96	4.00	330	111.50
2	120	120.97	0.97	4.99	330	104.04
3	110	114.31	4.31	5.56	325	100.62
4*		101.49	-8.51	5.95	320	98.55
5		110.95	0.95	5.20	340	102.72
6	100	106.27	6.27	6.33	342	95.70
7		107.90	7.90	7.13	340	93.28
8		100.30	0.30	8.21	342	89.43
9	90	90.40	0.40	11.07	343	87.79

*… a new seed-batch was used

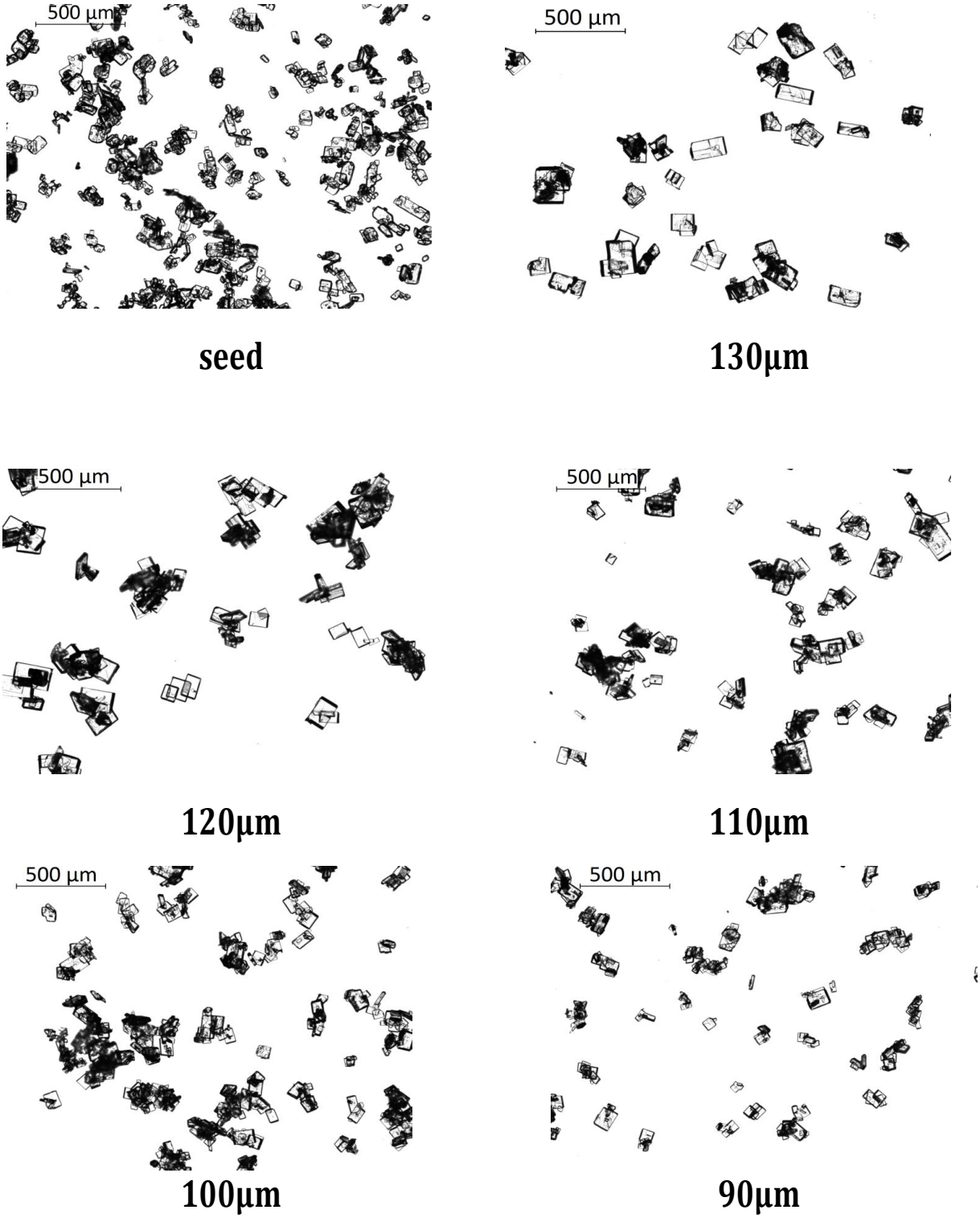

Figure 9: Images of seed and product crystals sampled during the stepwise tuning.

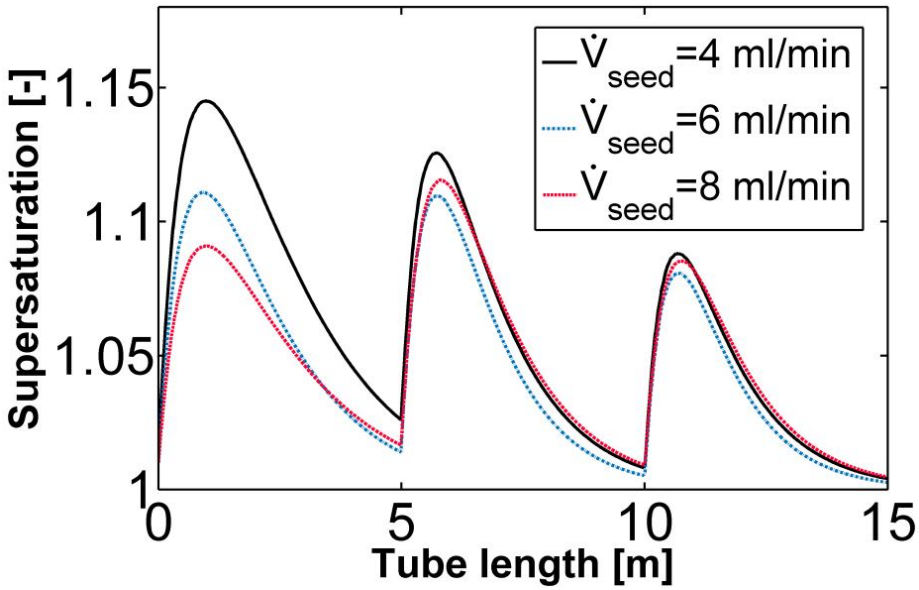

Figure 10: Supersaturation profiles for three seed loadings obtained during the simulations.

4.4 Conclusion and Outlook

This paper presents a model-free control strategy for tuning the number-based mean crystal size in a tubular reactor. The tubular reactor is designed for a seeded cooling-crystallization process. The model substance chosen was acetylsalicylic acid which was crystallized form an ethanolic solution. The mean crystal size of the products was shown to depend on crystal growth and aggregation. Since an increase in both of the effects is associated with a decrease in the seed pump rate, it was possible to develop a feedback controller that manipulates the seed suspension pump rate to tune the mean crystal sizes. Furthermore, since supersaturation levels at the reactor inlet remained unaffected, the seed suspension pump rate proved to be an appropriate manipulating variable.

Beside a proof of concept of the feedback controller, the results of our work can be summarized as follows:

- An ultrasound-assisted seed generation method for producing small seed crystals with a narrow CSD and a low fraction of fines was designed.
- Pressure recordings indicated that the percentage of solid material in the tubing and the particle size could be estimated via a pressure probe.

- A cleaning concept for the tubular crystallizer to enable long term runs was presented. A consistency study demonstrated that the product CSDs was accurately maintained, provided that the process settings were kept constant.
- Aggregation was expected to occur, if the seed pump rate was below a threshold value ($\approx 4.5\ ml/min$ using the process settings in table 1). Although crystal size tuning was also possible in the presence of aggregation, the obtained CSDs are less robust, i.e., featuring higher variations in mean crystal size.

In summary, the results of our study demonstrate the potential for highly accurate crystal size tuning in a tubular crystallizer via a model-free feedback control strategy. Due to the straightforward design of the presented crystallizer, only a few experiments were required to set up a controller.

Acknowledgements

Research Center Pharmaceutical Engineering (RCPE) is funded by the Austrian COMET Program under the auspices of the Austrian Federal Ministry of Transport, Innovation and Technology (BMVIT), the Austrian Federal Ministry of Economy, Family and Youth (BMWFJ) and by the Province of Styria (Styrian Business Promotion Agency, SFG). COMET is managed by the Austrian Research Promotion Agency, FFG. We would like to thank Johannes Österreicher and Martin Joksch (*Siemens AG, Corporate Technology*), Robert Hauser (*Hauser Messtechnik*) and Eva Heider (*RCPE)* for technical support with control and CSD measurements.

References

[1] S. Ahuja, *Handbook of Modern Pharmaceutical Analysis*, vol. 3. Elsevier, 2001, pp. 1–22.

[2] K. Chow, H. H. Y. Tong, S. Lum, and A. H. L. Chow, "Engineering of pharmaceutical materials: an industrial perspective.," *J. Pharm. Sci.*, vol. 97, no. 8, pp. 2855–77, Aug. 2008.

[3] D. J. Kirwan and C. J. Orella, *Handbook of Industrial Crystallization*. Elsevier, 2002, pp. 249–266.

[4] J. Ulrich, "Solution Crystallization– Developments and New Trends," *Chem. Eng. Technol.*, vol. 26, no. 8, pp. 832–835, Aug. 2003.

[5] L. X. Liu, I. Marziano, A. C. Bentham, J. D. Litster, E. T. White, and T. Howes, "Effect of particle properties on the flowability of ibuprofen powders.," *Int. J. Pharm.*, vol. 362, no. 1–2, pp. 109–17, Oct. 2008.

[6] R. Wakeman, "The influence of particle properties on filtration," *Sep. Purif. Technol.*, vol. 58, no. 2, pp. 234–241, Dec. 2007.

[7] M. Combarros, H. J. Feise, H. Zetzener, and A. Kwade, "Segregation of particulate solids: Experiments and DEM simulations," *Particuology*, vol. 12, pp. 25–32, Feb. 2014.

[8] S. Adam, D. Suzzi, C. Radeke, and J. G. Khinast, "An integrated Quality by Design (QbD) approach towards design space definition of a blending unit operation by Discrete Element Method (DEM) simulation.," *Eur. J. Pharm. Sci.*, vol. 42, no. 1–2, pp. 106–15, Jan. 2011.

[9] M. Sen, A. Rogers, R. Singh, A. Chaudhury, J. John, M. G. Ierapetritou, and R. Ramachandran, "Flowsheet optimization of an integrated continuous purification-processing pharmaceutical manufacturing operation," *Chem. Eng. Sci.*, vol. 102, pp. 56–66, Oct. 2013.

[10] E. Faulhammer, M. Llusa, C. Radeke, O. Scheibelhofer, S. Lawrence, S. Biserni, V. Calzolari, and J. G. Khinast, "The effects of material attributes on capsule fill weight and weight variability in dosator nozzle machines.," *Int. J. Pharm.*, vol. 471, no. 1–2, pp. 332–8, Aug. 2014.

[11] S. Mirza, I. Miroshnyk, J. Heinämäki, O. Antikainen, J. Rantanen, P. Vuorela, H. Vuorela, and J. Yliruusi, "Crystal morphology engineering of pharmaceutical solids: tabletting performance enhancement.," *AAPS PharmSciTech*, vol. 10, no. 1, pp. 113–9, Jan. 2009.

[12] R. C. Snyder and M. F. Doherty, "Faceted crystal shape evolution during dissolution or growth," *AIChE J.*, vol. 53, no. 5, pp. 1337–1348, May 2007.

[13] A. Nokhodchi, O. Amire, and M. Jelvehgari, "Physico-mechanical and dissolution behaviours of ibuprofen crystals crystallized in the presence of various additives.," *Daru*, vol. 18, no. 2, pp. 74–83, Jan. 2010.

[14] R. Rowe, P. Sheskey, and S. Owen, *Handbook of pharmaceutical excipients.*, Fifth. London: Pharmaceutical Press, 2006.

[15] Z. K. Nagy and R. D. Braatz, "Advances and new directions in crystallization control.," *Annu. Rev. Chem. Biomol. Eng.*, vol. 3, pp. 55–75, Jan. 2012.

[16] L. X. Yu, R. A. Lionberger, A. S. Raw, R. D'Costa, H. Wu, and A. S. Hussain, "Applications of process analytical technology to crystallization processes.," *Adv. Drug Deliv. Rev.*, vol. 56, no. 3, pp. 349–69, Feb. 2004.

[17] N. A. F. A. Samad, G. Sin, K. V. Gernaey, and R. Gani, "A systematic framework for design of process monitoring and control (PAT) systems for crystallization processes," *Comput. Chem. Eng.*, vol. 54, pp. 8–23, Jul. 2013.

[18] R. M. Haleem, M. Y. Salem, F. A. Fatahallah, and L. E. Abdelfattah, "Quality in the pharmaceutical industry – A literature review," *Saudi Pharm. J.*, Nov. 2013.

[19] M. Fujiwara, Z. K. Nagy, J. W. Chew, and R. D. Braatz, "First-principles and direct design approaches for the control of pharmaceutical crystallization," *J. Process Control*, vol. 15, no. 5, pp. 493–504, Aug. 2005.

[20] Z. K. Nagy, G. Fevotte, H. Kramer, and L. L. Simon, "Recent advances in the monitoring, modelling and control of crystallization systems," *Chem. Eng. Res. Des.*, vol. 91, no. 10, pp. 1903–1922, Oct. 2013.

[21] A. Mesbah, A. Kalbasenka, A. Huesman, H. Kramer, and P. M. J. Van den Hof, "Real-Time Dynamic Optimization of Batch Crystallization Processes," in *World Congress*, 2008, vol. 17, no. 1, pp. 3246–3251.

[22] A. Chianese and H. J. Kramer, *Industrial Crystallization Process Monitoring and Control*. Wiley, 2012.

[23] M. R. A. Bakar, Z. K. Nagy, and C. D. Rielly, "Seeded Batch Cooling Crystallization with Temperature Cycling for the Control of Size Uniformity and Polymorphic Purity of Sulfathiazole Crystals," *Org. Process Res. Dev.*, vol. 13, no. 6, pp. 1343–1356, Nov. 2009.

[24] N. C. S. Kee, R. B. H. Tan, and R. D. Braatz, "Selective Crystallization of the Metastable α-Form of l -Glutamic Acid using Concentration Feedback Control," *Cryst. Growth Des.*, vol. 9, no. 7, pp. 3044–3051, Jul. 2009.

[25] N. Doki, H. Seki, K. Takano, H. Asatani, M. Yokota, and N. Kubota, "Process Control of Seeded Batch Cooling Crystallization of the Metastable α-Form Glycine Using an In-Situ ATR-FTIR Spectrometer and an In-Situ FBRM Particle Counter," *Cryst. Growth Des.*, vol. 4, no. 5, pp. 949–953, Sep. 2004.

[26] J. J. Liu, Y. D. Hu, and X. Z. Wang, "Optimization and control of crystal shape and size in protein crystallization process," *Comput. Chem. Eng.*, vol. 57, pp. 133–140, Oct. 2013.

[27] U. Vollmer and J. Raisch, "Control of batch crystallization—A system inversion approach," *Chem. Eng. Process. Process Intensif.*, vol. 45, no. 10, pp. 874–885, Oct. 2006.

[28] K. Zhang, M. Nadri, and C.-Z. Xu, "Reachability-based feedback control of crystal size distribution in batch crystallization processes," *J. Process Control*, vol. 22, no. 10, pp. 1856–1864, Dec. 2012.

[29] J. Sang-Il Kwon, M. Nayhouse, G. Orkoulas, and P. D. Christofides, "Crystal shape and size control using a plug flow crystallization configuration," *Chem. Eng. Sci.*, vol. 119, pp. 30–39, Nov. 2014.

[30] A. N. Saleemi, G. Steele, N. I. Pedge, A. Freeman, and Z. K. Nagy, "Enhancing crystalline properties of a cardiovascular active pharmaceutical ingredient using a process analytical technology based crystallization feedback control strategy.," *Int. J. Pharm.*, vol. 430, no. 1–2, pp. 56–64, Jul. 2012.

[31] E. Aamir, Z. K. Nagy, and C. D. Rielly, "Optimal seed recipe design for crystal size distribution control for batch cooling crystallisation processes," *Chem. Eng. Sci.*, vol. 65, no. 11, pp. 3602–3614, Jun. 2010.

[32] M. Jiang, M. H. Wong, Z. Zhu, J. Zhang, L. Zhou, K. Wang, A. N. Ford Versypt, T. Si, L. M. Hasenberg, Y.-E. Li, and R. D. Braatz, "Towards achieving a flattop crystal size distribution by continuous seeding and controlled growth," *Chem. Eng. Sci.*, vol. 77, pp. 2–9, Jul. 2012.

[33] S. Ferguson, G. Morris, H. Hao, M. Barrett, and B. Glennon, "Automated self seeding of batch crystallizations via plug flow seed generation," *Chem. Eng. Res. Des.*, Feb. 2014.

[34] Z. K. Nagy, J. W. Chew, M. Fujiwara, and R. D. Braatz, "Comparative performance of concentration and temperature controlled batch crystallizations," *J. Process Control*, vol. 18, no. 3–4, pp. 399–407, Mar. 2008.

[35] A. Majumder and Z. K. Nagy, "Prediction and control of crystal shape distribution in the presence of crystal growth modifiers," *Chem. Eng. Sci.*, vol. 101, pp. 593–602, Sep. 2013.

[36] T. Vetter, C. L. Burcham, and M. F. Doherty, "Regions of attainable particle sizes in continuous and batch crystallization processes," *Chem. Eng. Sci.*, vol. 106, pp. 167–180, Mar. 2014.

[37] W. Paengjuntuek, P. Kittisupakorn, and A. Arpornwichanop, "Optimization and nonlinear control of a batch crystallization process," *J. Chinese Inst. Chem. Eng.*, vol. 39, no. 3, pp. 249–256, May 2008.

[38] J. Chakraborty, M. R. Singh, D. Ramkrishna, C. Borchert, and K. Sundmacher, "Modeling of crystal morphology distributions. Towards crystals with preferred asymmetry," *Chem. Eng. Sci.*, vol. 65, no. 21, pp. 5676–5686, Nov. 2010.

[39] D. L. Ma, D. K. Tafti, and R. D. Braatz, "Optimal control and simulation of multidimensional crystallization processes," *Comput. Chem. Eng.*, vol. 26, no. 7–8, pp. 1103–1116, Aug. 2002.

[40] M. O. Besenhard, A. Chaudhury, T. Vetter, R. Ramachandran, and J. G. Khinast, "Evaluation of Parameter Estimation Methods for Crystallization Processes Modeled via Population Balance Equations," *Chem. Eng. Res. Des.*, Aug. 2014.

[41] M. R. Abu Bakar, Z. K. Nagy, A. N. Saleemi, and C. D. Rielly, "The Impact of Direct Nucleation Control on Crystal Size Distribution in Pharmaceutical Crystallization Processes," *Cryst. Growth Des.*, vol. 9, no. 3, pp. 1378–1384, Mar. 2009.

[42] N. Nonoyama, K. Hanaki, and Y. Yabuki, "Constant Supersaturation Control of Antisolvent-Addition Batch Crystallization," *Org. Process Res. Dev.*, vol. 10, no. 4, pp. 727–732, Jul. 2006.

[43] D. Duffy, M. Barrett, and B. Glennon, "Novel, Calibration-Free Strategies for Supersaturation Control in Antisolvent Crystallization Processes," *Cryst. Growth Des.*, vol. 13, no. 8, pp. 3321–3332, Aug. 2013.

[44] M. O. Besenhard, R. Hohl, A. Hodzic, R. J. P. Eder, and J. G. Khinast, "Modeling a seeded continuous crystallizer for the production of active pharmaceutical ingredients," *Cryst. Res. Technol.*, vol. 49, no. 2–3, pp. 92–108, Mar. 2014.

[45] R. J. P. Eder, E. K. Schmitt, J. Grill, S. Radl, H. Gruber-Woelfler, and J. G. Khinast, "Seed loading effects on the mean crystal size of acetylsalicylic acid in a continuous-flow crystallization device," *Cryst. Res. Technol.*, vol. 46, no. 3, pp. 227–237, Mar. 2011.

[46] P. Tabeling, *Introduction to Microfluidics*, 2nd ed. Oxford University Press, USA, 2006.

[47] R. J. P. Eder, S. Radl, E. Schmitt, S. Innerhofer, M. Maier, H. Gruber-Woelfler, and J. G. Khinast, "Continuously Seeded, Continuously Operated Tubular Crystallizer for the Production of Active Pharmaceutical Ingredients," *Cryst. Growth Des.*, vol. 10, no. 5, pp. 2247–2257, May 2010.

[48] FDA, "Guidance for Industry: PAT—A Framework for Innovative Pharmaceutical Development, Manufacturing, and Quality Assurance. Pharmaceutical CGMPs," 2004.

[49] S. Lawton, G. Steele, P. Shering, L. Zhao, I. Laird, and X.-W. Ni, "Continuous Crystallization of Pharmaceuticals Using a Continuous Oscillatory Baffled Crystallizer," *Org. Process Res. Dev.*, vol. 13, no. 6, pp. 1357–1363, Nov. 2009.

[50] X. Ni and A. Liao, "Effects of mixing, seeding, material of baffles and final temperature on solution crystallization of l-glutamic acid in an oscillatory baffled crystallizer," *Chem. Eng. J.*, vol. 156, no. 1, pp. 226–233, Jan. 2010.

[51] C. J. Brown and X. Ni, "Online Evaluation of Paracetamol Antisolvent Crystallization Growth Rate with Video Imaging in an Oscillatory Baffled Crystallizer," *Cryst. Growth Des.*, vol. 11, no. 3, pp. 719–725, Mar. 2011.

[52] M. O. Besenhard, A. Hodzic, R. J. P. Eder, and J. G. Khinast, "Modeling a seeded continuous crystallizer for the production of active pharmaceutical ingredients," *Cryst. Res. Technol.*, 2014.

[53] R. J. P. Eder, S. Schrank, M. O. Besenhard, E. Roblegg, H. Gruber-Woelfler, and J. G. Khinast, "Continuous Sonocrystallization of Acetylsalicylic Acid (ASA): Control of Crystal Size," *Cryst. Growth Des.*, vol. 12, no. 10, pp. 4733–4738, Oct. 2012.

[54] R. J. P. Eder, S. Radl, E. Schmitt, S. Innerhofer, M. Maier, H. Gruber-Woelfler, and J. G. Khinast, "Continuously Seeded, Continuously Operated Tubular Crystallizer for the

Production of Active Pharmaceutical Ingredients," *Cryst. Growth Des.*, vol. 10, no. 5, pp. 2247–2257, May 2010.

[55] O. Prymak, V. Sokolova, T. Peitsch, and M. Epple, "The Crystallization of Fluoroapatite Dumbbells from Supersaturated Aqueous Solution," *Cryst. Growth Des.*, vol. 6, no. 2, pp. 498–506, Feb. 2006.

[56] J. R. Méndez del Río and R. W. Rousseau, "Batch and Tubular-Batch Crystallization of Paracetamol: Crystal Size Distribution and Polymorph Formation," *Cryst. Growth Des.*, vol. 6, no. 6, pp. 1407–1414, Jun. 2006.

[57] S. Ferguson, G. Morris, H. Hao, M. Barrett, and B. Glennon, "In-situ monitoring and characterization of plug flow crystallizers," *Chem. Eng. Sci.*, vol. 77, pp. 105–111, Jul. 2012.

[58] A. J. Alvarez and A. S. Myerson, "Continuous Plug Flow Crystallization of Pharmaceutical Compounds." American Chemical Society, 01-Mar-2010.

[59] M. Jiang, Z. Zhu, E. Jimenez, C. D. Papageorgiou, J. Waetzig, A. Hardy, M. Langston, and R. D. Braatz, "Continuous-Flow Tubular Crystallization in Slugs Spontaneously Induced by Hydrodynamics," *Cryst. Growth Des.*, vol. 14, no. 2, pp. 851–860, Feb. 2014.

[60] M. Klotz and M. Habenicht, "Lasersensorik in Partikelzählern : Schlüssel zur Optimierung des Partikelmonitoring," *GIT*, vol. 49, no. 9, pp. 774–777.

[61] A. Reinhold and H. Briesen, "Numerical behavior of a multiscale aggregation model—coupling population balances and discrete element models," *Chem. Eng. Sci.*, vol. 70, pp. 165–175, Mar. 2012.

[62] A. Mersmann, Ed., *Crystallization Technology Handbook*, 2nd ed. 2001.

[63] A. Mersmann, K. Bartosch, B. Braun, A. Eble, and C. Heyer, "Möglichkeiten einer vorhersagenden Abschätzung der Kristallisationskinetik," *Chemie Ing. Tech.*, vol. 72, no. 1–2, pp. 17–30, Jan. 2000.

5. Publications

Peer-Refereed Journals

E.-M. Steyskal, M. O. Besenhard, S. Landgraf, Y. Zhong, J. Weissmüller, P. Pölt, M. Albu, and R. Würschum, "Sign-inversion of charging-induced variation of electrical resistance of nanoporous platinum," *J. Appl. Phys.*, vol. 112, no. 7, p. 073703, Oct. 2012.

R. J. P. Eder, S. Schrank, M. O. Besenhard, E. Roblegg, H. Gruber-Woelfler, and J. G. Khinast, "Continuous Sonocrystallization of Acetylsalicylic Acid (ASA): Control of Crystal Size," *Cryst. Growth Des.*, vol. 12, no. 10, pp. 4733–4738, Oct. 2012.

C. Petschacher, A. Eitzlmayr, M.O. Besenhard, J. Wagner, J. Barthelmes, A. Bernkop-Schnürch, J. G. Khinast, and A. Zimmer, "Thinking continuously: a microreactor for the production and scale-up of biodegradable, self-assembled nanoparticles," *Polym. Chem.*, vol. 4, no. 7, p. 2342, 2013.

M. O. Besenhard, A. Hodzic, R. J. P. Eder, and J. G. Khinast, "Modeling a seeded continuous crystallizer for the production of active pharmaceutical ingredients," *Cryst. Res. Technol.*, 2014.

M. O. Besenhard, A. Chaudhury, T. Vetter, R. Ramachandran, and J. G. Khinast, "Evaluation of Parameter Estimation Methods for Crystallization Processes Modeled via Population Balance Equations," *Chem. Eng. Res. Des.*, Aug. 2014.

M. O. Besenhard, A. Thurnberger, R. Hohl, E. Faulhammer, J. Rattenberger, and J. G. Khinast, "Continuous API-crystal coating via coacervation in a tubular reactor.," *Int. J. Pharm.*, vol. 475, no. 1–2, pp. 198–207, Aug. 2014.

M. O. Besenhard, M. Jarzabek, A.O. Farell, J.H.M. Prehn, A.B.Byrne, H.J. Huber, "A new method for in silico predictions of tumor cell proliferation from vascular structure using tissue decomposition into avascular volume elements.," *PLOS one.*, under revision.

Conference proceedings

M. O. Besenhard, A. Eitzlmayr, R.J.P. Eder, D. Suzzi, J.G. Khinast,
"Theory and Application of Population Balance Equations in Chemical Engineering",
7. Minisymposium der Verfahrenstechnik, Graz, Austria, 30.06.-01.07, 2011 (talk)

M. O. Besenhard, R.J.P. Eder, G. Scharrer, J.G. Khinast,
"Control, Design and Applications of a Seeded Continuously Operated Crystallizer for Active Pharmaceutical Ingredients",10th International Workshop on Crystal Growth of Organic Materials, Limerick, Ireland, 25.06.-30.06, 2012 (talk)

M. O. Besenhard, H.J. Huber,
"A new method for in silico predictions of tumor cell", GatsbyMeeting, Dublin, Ireland, .13.01 2012 (talk)

M. O. Besenhard, M. Llusa, J. Gursch, J.G. Khinast
"Continuous Crystallization of Pharmaceuticals in a Tubular Reactor: Applications & Limitations" 9th European Congress of Chemical Engineering, The Hague, Netherlands, 20.04.-24.04, 2013 (talk)

+ Several posters contributions

Scholarships

Marshall Plan Scholarship
Rutgers University, September 2013 – December 2013, New Jersey, USA

Marie Curie Scholarship
Royal College of Surgeons Ireland - February 2013 – June 2013, Dublin, Ireland

Supervised master students

Charlotte Gschnitzner (graduation, September 2012)
Alexandra Thurnberger (graduation, April 2014)
Cheng Da-Ho (graduation, expected soon)

Working experience

Researcher, Biosensors AT, Graz/Vienna, Austria
Siemens Corporate Technology
September 2010 –September 2014

Researcher, Area 1: Modeling and Prediction, AT Graz, Austria
Research Center Pharmaceutical Engineering
Since November 2010

„Wer glaubt, jemand zu sein, hat aufgehört, jemand zu werden.“

Oliver Kahn